Nano Today 19 (2018) 41–83

Contents lists available at ScienceDirect

Nano Today

journal homepage: www.elsevier.com/locate/nanotoday

Graphene/Semiconductor Hybrid Heterostructures for Optoelectronic Device Applications

Chao Xie, Yi Wang, Zhi-Xiang Zhang, Di Wang, Lin-Bao Luo*

School of Electronic Science and Applied Physics and Anhui Provincial Key Laboratory of Advanced Functional Materials and Devices, Hefei University of Technology, Hefei, Anhui 230009, China

ARTICLE INFO

Article history:
Received 17 October 2017
Received in revised form 5 January 2018
Accepted 20 February 2018
Available online 28 February 2018

Keywords:
Hybrid heterostructures
Graphene
Optoelectronic devices
Solar cells
Photodetectors

ABSTRACT

As one of the most appealing two-dimensional materials, graphene (Gr) has attracted tremendous research interest in optoelectronic device applications for its plenty of exceptional electrical and optical properties. The emergence of Gr/semiconductor hybrid heterostructures provides a promising platform for assembling high-performance optoelectronic devices that can overcome intrinsic limitations of Gr. However, although significant achievements have been made, many challenges still exist. Here, we comprehensively review the progress in the development of various optoelectronic devices based on Gr/semiconductor hybrid heterostructures, including /group II-VI nanostructures, /group III-V semiconductors, /group IV semiconductors, /metal oxides and /other semiconductors, in terms of the device design, device performance and physics, processing techniques for performance optimization, *etc*. In the final section, conclusions of the existing techniques are presented and future challenges in optoelectronic applications of Gr/semiconductor hybrid heterostructures are addressed.

Contents

* Corresponding author.
E-mail address: luolb@hfut.edu.cn (L.-B. Luo).

https://doi.org/10.1016/j.nantod.2018.02.009
1748-0132/

Introductions

Graphene (Gr), a single layer of carbon atoms arranged in a closely packed two-dimensional (2D) honeycomb lattice, has attracted explosive research interest from both academia and industry since its discovery in 2004 [1]. Due to its extraordinary structural and physical properties and high specific surface area, Gr has been intensively explored in a wide range of areas, including high-speed electronic and optical devices [2,3], energy conversion and storage [4,5], optoelectronic devices [4,6,7], hybrid materials [8], chemical sensors [9], and also various proof-of-concept devices [10,11]. Among these enormous applications, significant efforts have been devoted to study of optoelectronic devices, including solar cells [12,13], photodetectors [14–16], light emitting diodes (LEDs) [17], lasers [18], *etc.*, thanks to plenty of exceptional electrical and optical characteristics of Gr. From the perspective of solar cells and LEDs, Gr holds a number of distinctive features, such as good electrical conductivity (intrinsic resistivity as low as 30 Ω/sq), high optical transparency (2.3% optical absorption per layer in wavelength range from the near-infrared (NIR) to violet), outstanding thermal stability and chemical inertness, and large-scale, cost-effective processibility, which make it an ideal candidate for next-generation transparent electrode [12,13,19]. In particular, the excellent mechanical robustness with fracture strains of ca. 25% and a Young's modulus of ca. 1 TPa, affords the high suitability of Gr for novel device architectures, such as flexible, stretchable and bendable optoelectronic devices [20]. On the other hand, the gapless and semi-metallic features of Gr allow charge carrier generation by optical absorption over a broad energy spectrum from the ultraviolet (UV) to terahertz (THz) wavelengths, rendering it a promising material for photodetection over a wide spectral range [14–16]. The extremely high carrier mobility (maximum value: 230,000 $cm^2V^{-1}s^{-1}$ at room temperature) of Gr also enables ultrafast conversion of photons or plasmons to electrical signal, which is highly desirable for high-speed photodetection. Furthermore, the tunable electrical and optical properties of Gr, such as carrier densities, band alignments and polarities, *via* chemical or electrostatic doping offer great flexibility for improving the performance of Gr-based optoelectronic devices [21,22]. Another great advantage relies on the compatibility of Gr with the highly mature Si-based technologies, which allows scalable device fabrication and low-cost, large-scale integration of Gr into optoelectronic networks and multipixel complementary metal-oxide-semiconductor (CMOS) read-out-circuits [14].

A large variety of optoelectronic devices based on Gr have been extensively studied and the performances of some devices have already reached a level of competitiveness with conventional semiconductor devices up to now [13,14]. However, there remain grand challenges and the wide applications of Gr-based optoelectronics are still hindered by some issues. For instance, despite the high absorption coefficient, the intrinsic low light absorption of only 2.3% for single-layer Gr, due to the short light-matter interaction length, is insufficient for light-harvesting device applications [16,23]. The ultra-short lifetime of excitons in pure Gr resulting from its gapless nature also leads to fast carrier recombination, which limits the efficient generation of photocurrent or photovoltage [6,24]. To this end, it is therefore necessary to introduce p-n junctions, which are able to effectively separate photocarriers and reduce the possibility of recombination by the built-in potential [25]. Nevertheless, the difficulties in controlled and stable doping

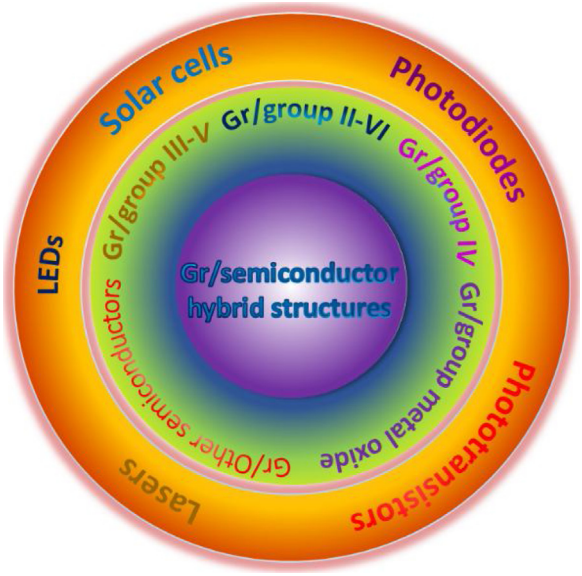

Fig. 1. Schematic illustration of Gr/semiconductor hybrid structure for various optoelectronic device applications.

of Gr have greatly restricted the production of high-quality Gr p-n homojunctions [22]. The emergence of Gr/semiconductors hybrid heterostructures, which was started from the study of the fundamentals of Gr/SiC heterojunction interface in 2009 [26], offers an alternative solution to the above dilemma in that the hybrid structure can take advantage of the synergetic characteristics of both materials. Shortly after this work, Li et al. reported Gr/Si heterojunctions and applied them as solar cells with an initial power conversion efficiency (PCE) of 1.65% in 2010 [27], which is the first demonstration of Gr/semiconductor hybrid heterostructures for optoelectronic device applications. Afterwards, thanks to the rapidly-developed Gr transfer techniques and various effective synthesis methods, diverse and ingenious designs in both functionalities of materials and device geometries have been involved in the investigation of Gr/semiconductor hybrid heterostructures (Fig. 1). Recent studies show that the hybrid heterostructures can not only render interfaces and heterojunctions for effective separation and transport of photocarriers, but also substantially improve optical absorption of the entire system for efficient photocarrier generation with the semiconductors as additional light harvesting media. To date, Gr/semiconductor hybrid heterostructures have found great potential in a series of optoelectronic devices, including solar cells, photodetectors, LEDs and lasers, which usually exhibit much enhanced performance with novel functionalities due to the synergistic effect, as evidenced in many recent papers [28–31]. In spite of the enormous achievements made in this specific field, there are still many challenges that confine future implementation and development for high-performance and large-scale optoelectronic applications. As one of the most explored research field, albeit there has been several review papers concerning the synthesis and applications of Gr/semiconductor hybrid heterostructures [32–35], comprehensive review papers dealing specifically with their various optoelectronic device applications can scarcely be found in recent years. Extensive review of recent advances in this field is helpful for not only bringing about new knowledge of light-matter interaction, but also inspiring unconventional optoelectronic device design in the future.

In this review, we present a comprehensive summary of recent progresses in the development of Gr/semiconductor hybrid heterostructures for optoelectronic device applications. As the synthetic methods for Gr and Gr-based hybrid heterostructures have been extensively discussed in many review papers [36–39], they will not be entertained in this paper. Optoelectronic devices based on a variety of Gr/semiconductor hybrid heterostructures, including /group II-VI nanostructures, /group III-V semiconductors, /group IV semiconductors, /metal oxides and /other semiconductors are systematically reviewed. The critical issues that pertain to the device design, device performance and physics, processing techniques for performance improvement are discussed. Finally, we present summaries of the existing techniques and provide our outlooks with an aim to guide future development of this fast-growing research field.

Properties of Gr, operation mechanisms and performance parameters of devices

Properties of Gr

In the past decade, a large number of appealing properties have been discovered for Gr *via* investigation of pristine Gr. These properties include extremely high charge carrier (electron and hole) mobility (up to 230000 $cm^2V^{-1}s^{-1}$), high visible light absorption of 2.3%, large thermal conductivity of 3000 WmK^{-1}, the highest strength of 130 GPa, the highest theoretical specific surface area (2600 m^2g^{-1}), and half integer quantum Hall effect even at ambient temperature (minimum Hall conductivity ~4 e^2h^{-1}, even at carrier concentration is zero). In this section, we are going to briefly introduce electrical transport and optical properties of Gr that are relevant to the topic of this paper. For a more detailed overview of the properties of Gr, interested readers can refer to other related review papers [34,40–43].

Electrical transport property

Pristine Gr is a naturally zero bandgap material, whose band structure exhibits two bands intersecting at two inequivalent point K and K' in the reciprocal space [41]. Close to these points, electronic dispersion resembles that of the relativistic Dirac electrons, and K and K' are referred as Dirac point where valence and conduction bands are degenerated. One of the most fascinating features of Gr is its highly abnormal nature of charge carriers, which act like massless relativistic particles (Dirac fermions). Due to the unique band structure, electrons in Gr can move with a Fermi velocity in the ballistic transport [34]. This characteristic together with the defect free nature gives remarkable charge carrier mobility and high electronic conductivity in pristine Gr. It has been reported that the mobility of mechanically exfoliated suspended layer of Gr can reach up to 200 000 $cm^2V^{-1}s^{-1}$ [44], without considering the charged impurities and substrate ripples. However, the carrier transport is inevitably limited by some intrinsic and extrinsic sources in practice. The proposed former source includes longitudinal acoustic phonon scatterings [45], the lattice defects and grain boundaries formed during the growth process [46], whereas the latter sources contain surface charge impurity scattering [47], interfacial roughness [48], interfacial phonon scattering [49], and wrinkles or cracks caused during the growth and transfer processes [50].

Another pivotal property of single-layer Gr is its ambipolar electric field effect at room temperature, which means that charge carriers can be tuned between electrons and holes by applying an appropriate gate voltage [1]. The Fermi level of Gr rises above the Dirac point which propels electrons populating into the conduction band in a positive gate bias, while the Fermi level drops below the Dirac point promoting holes in valence band in a negative gate bias.

The zero bandgap nature of Gr even at its charge neutrality point, however, is one of the biggest obstacles for the application of Gr as an electronic material, for example, in field-effect transistors (FETs). Later studies have shown that the modification of the band struc-

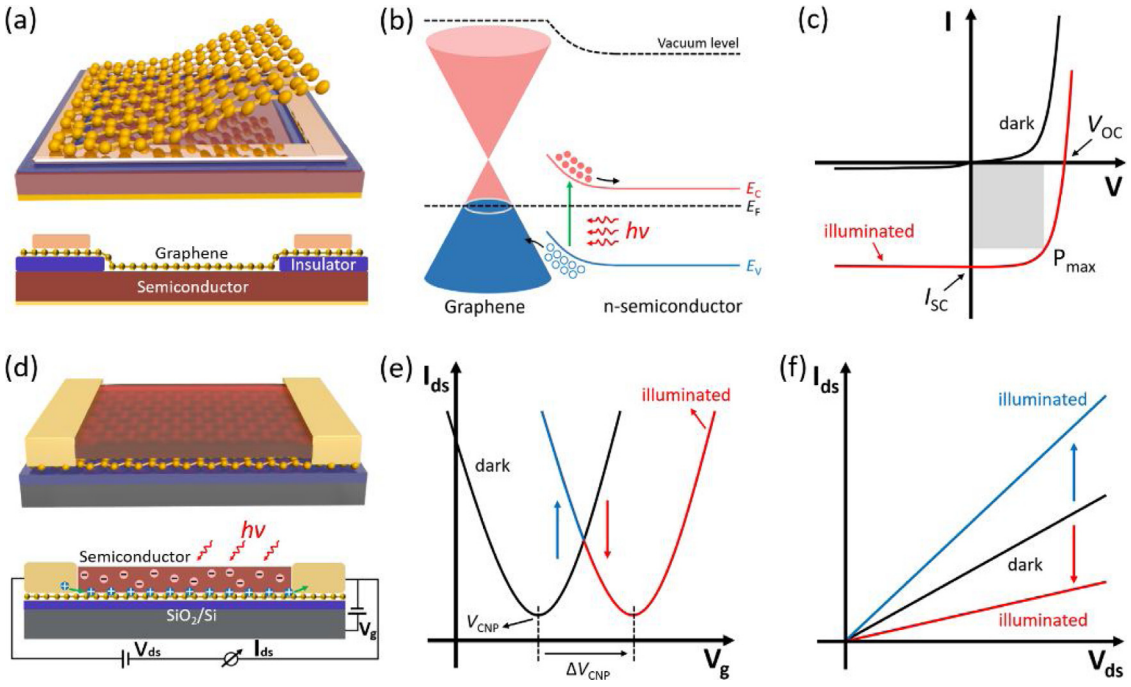

Fig. 2. (a) The schematic structures of a Gr/3D semiconductor hybrid heterojunction. (b) Energy band diagram of a typical Gr/n-semiconductor hybrid heterojunction under illumination. E_F represents the common Fermi energy level for Gr and n-semiconductor, and E_C and E_V are conduction band minimum and valence band maximum for n-semiconductor, respectively. (c) *I-V* curves of a device working with photovoltaic effect in the dark and under illumination. P_{max} represents the point of maximum generated electrical power. (d) The schematic structure and work principle of a Gr/semiconductor hybrid phototransistor. (e) I_{ds}-V_g curves of a device working with photogating effect in the dark and under illumination. V_{CNP} represents the charge neutrality point (the Dirac point) of Gr and ΔV_{CNP} is the shift value of V_{CNP} under illumination. (f) I_{ds}-V_{ds} curves in the dark and under illumination. The photocurrent can be positive or negative values at different V_g regions.

ture of Gr is viable *via* lateral quantum confinement through some techniques such as constraining the Gr in nanoribbons (NBs) [51] or quantum dots (QDs) [52], and biasing bi-layer Gr [53]. For example, the electronic bandgap of bi-layer Gr can be controlled by applying an electric field perpendicular to the plane [54]. The double gated approach can controllably induce an insulating state with large suppression of the conductivity in bi-layer Gr. The size of the bandgap is proportional to the potential drop between the two Gr layers and the value can be as high as 0.1-0.3 eV.

Optical property

Gr can absorb incident light in a wide spectrum from the UV to THz region due to its gapless band structure and semi-metallic nature [55]. Many literatures have confirmed that the absorption of light for single-layer Gr is 2.3% over a broad wavelength range and the value increases linearly with the increase of the number of layers [56]. It has also been reported that the absorption for single-layer Gr is flat from 300-2500 nm and the inter band electronic transition from the unoccupied π^* states causes an absorption peak at ~250 nm in the UV regime [57].

In addition, by significantly changing the Fermi energy *via* electrical gating, the optical transition of Gr can be modified [21]. Photon absorption on the surface induces the generation of electron-hole pairs in Gr, which recombine very quickly on a picosecond time scale depending on the temperature as well as density of electrons and holes [58]. The electrons and holes can be separated, which generates photocurrent, in the presence of an applied external electric field or an internal electric field formed near the Gr and electrode interface. The unique optical properties in conjunction with the exceptional electrical transport characteristics have opened new avenues for various optoelectronic applications of Gr, for example, to be used as ultrafast photodetectors with very high bandwidth (>500 GHz), extremely wide detection spectrum range and good quantum efficiency [59].

Another feature of Gr is photoluminescence (PL). Researches have shown that it is possible to make Gr luminescent by introducing a suitable bandgap through some effective routes including cutting Gr in NBs or QDs, and physical or chemical treatment with various gases to reduce the connectivity of the π electron network [18,60,61]. For example, oxygen plasma treatment of single-layer Gr on substrate can induce strong PL [62].

Operation mechanisms

Gr/semiconductor hybrid heterostructures can be formed by directly combining Gr with various dimensional semiconductors through relatively simple fabrication processes. Solar cells based on these heterostructures work on the photovoltaic effect, while photodetectors can work on either the photovoltaic effect or the photogating effect depending on their device configurations. In this section, we will introduce the main working principle involved in the optoelectronic devices (solar cells and photodetectors) primarily discussed in this paper.

Photovoltaic effect

Fig. 2a shows a schematic illustration of a typical Gr/three-dimensional (3D) semiconductor hybrid heterostructure, where Gr is directly transferred atop the semiconductor and an insulating layer is normally employed to separate the semiconductor from the metal contact to Gr. Due to the disparity in their work functions, charge transfer takes place between the two materials until their Fermi energy levels align. Meanwhile, charge transfer depletes a region of free charges (a space charge region) inside the semiconductor interface and consequently induces a built-in electric field. In most studied hybrid heterostructures (Gr/n-type semiconductor), the withdrawal of partial electrons in the depletion region leaves behind immobile positive charges, which causes energy levels of the semiconductor near the interface to bend upward (Fig. 2b).

At equilibrium state (the Fermi energy levels have aligned), the discontinuity in allowed energy states of the two materials creates the energy barrier, preventing the flow of electrons from the semiconductor to Gr. Therefore, the heterostructures usually present nonlinear current-voltage (*I-V*) characteristics (rectifying behavior) in the dark (Fig. 2c). Upon illumination, photoexcited electron-hole pairs generated predominately in the semiconductor are separated by the built-in electric field and subsequently electrons and holes are propelled towards opposite directions (Fig. 2b). Under zero external bias, the photogenerated carriers flow through the external circuit, which generates a sizeable photocurrent (short-circuit current, I_{SC}). When the device is open-circuited, the accumulation of carriers with opposite types in the distinct part of the device gives rise to a photovoltage (open-circuit voltage, V_{OC}). A solar cell usually work in the region of the *I-V* curve lays in the fourth quadrant (negative current, positive bias) to generate electrical power, as shown in Fig. 2c. A photodetector working on this mechanism is named as a photodiode. The photodiode can work at the zero bias (photovoltaic mode), where it has an improved specific detectivity and maximized linearity and sensitivity thanks to the lowest dark current. However, the responsivity is usually low due to lack of internal gain (*G*). Alternatively, it can operate at reverse bias (photoconductive mode) as well, where a moderate external electric field towards the built-in one increases the separation efficiency of electron-hole pairs and improve the response speed stemming from reduced transit time and lowered diode capacitance. In practice, a photodiode working at photovoltaic mode is more suitable for precise light detection, while the one working at photoconductive mode is better suited for high-speed applications. Under sufficiently large reverse bias, electric field becomes high enough to initiate impact ionization, causing avalanche multiplication or breakdown of the photodiode, and therefore leading to large internal gain.

Photogating effect

A schematic illustration of a representative Gr/semiconductor heterostructure-based hybrid phototransistor is depicted in the top panel of Fig. 2d. The bottom panel illustrates the working mechanism of such phototransistors. Under illumination, electron-hole pairs are generated in the semiconductor, and subsequently one type of carriers is transferred to the Gr, leaving oppositely-charged carriers trapped in the semiconductor. The trapped charges function as a local gate and effectively modulate the Fermi level of Gr *via* capacitive coupling, which induces more carriers and consequently modulates its electrical conductance. Meanwhile, the transferred free carriers can recirculate multiple times in the Gr channel within their lifetimes (τ_{lifetime}), which gives rise to a high photoconductive gain. The gain *G* can be qualitatively expressed as: $= \frac{\tau_{lifetime}}{\tau_{transit}}$, where τ_{transit} is the transit time of photogenerated carriers across the Gr channel. The τ_{transit} is defined as: $\tau_{transit} = \frac{L^2}{\mu V_{ds}}$, where *L* is the channel length, μ is the carrier mobility and V_{ds} is an external bias applied between source/drain electrodes. To obtain a high gain, the carrier transit time should be short while the lifetime of photocarriers is usually optimized to be long. Nevertheless, the response time that is directly related to the carrier recombination processes, is also determined by the lifetime of photocarriers. So high gain will prolong the response time. Usually, a phototransistor can have a much higher responsivity than that of a photodiode, however, at the expense of slower response speed. Due to the effective gate electric field of the trapped carriers, the photogating effect is usually seen as a horizontal shift in the source-drain current-gate voltage (I_{ds}-V_{g}) curve of the Gr transistor upon illumination, as shown in Fig. 2e. The direction of the curve shift indicates the polarity of the trapped carriers. Also, the photogating effect can lead to either positive photocurrent or negative photocurrent determined by the working V_{g} (Fig. 2f).

Performance parameters

Performance parameters of solar cells

Power conversion efficiency (PCE), V_{OC}, I_{SC} (short-circuit current density (J_{SC})), fill factor (*FF*) and external quantum efficiency/internal quantum efficiency (EQE/IQE) are main performance parameters of a solar cell [63]. The definitions of V_{OC} and I_{SC} have been introduced previously. *FF* is defined as the ratio of maximum obtainable power to the product of V_{OC} and I_{SC}:

$$FF = \frac{P_{max}}{V_{OC} * I_{SC}} \tag{1}$$

where P_{max} is the maximum output power of a solar cell. Note that *FF* is always less than unity.

PCE refers to the portion of energy in the form of sunlight that can be converted *via* a solar cell to electricity and is usually expressed as:

$$\text{PCE} = \frac{V_{OC} * I_{SC} * FF}{P_{in}} \tag{2}$$

EQE/IQE is the ratio of the number of charge carriers collected by a solar cell to the number of incident/absorbed photons of a given energy by the device. EQE can be expressed as:

$$EQE = \frac{I_{ph}/e}{P_{in}/h\nu} \tag{3}$$

Where I_{ph} is the photocurrent, e the elementary charge, P_{in} the incident light power, *h* the Planck's constant, and ν the frequency of the incident light. As the absorbed photons can be determined by deducting the photon losses including those due to reflection and transmission from the total number of incident photons, IQE can be inferred by the following equation:

$$IQE = \frac{EQE}{1 - Reflection - Tranmission} \tag{4}$$

In particular, the optical interference effects should be taken into account when estimating *IQE* of a solar cell with an ultrathin active layer.

Performance parameters of photodetectors

Similarly, responsivity (*R*), noise equivalent power (*NEP*), specific detectivity (D^*) and response speed are important performance parameters of a photodetector [23,64]. Responsivity is defined as the output photocurrent or photovoltage to the incident optical power on the active region of a photodetector and is usually expressed as:

$$R = \frac{I_{ph} \text{ or } V_{ph}}{P_{in}} \tag{5}$$

where V_{ph} is the photovoltage.

Noise equivalent power *NEP* is the minimum incident optical power required to achieve a signal-to-noise ratio of unity at 1 Hz and can be defined as:

$$NEP = \frac{\bar{i}_n^{2\,1/2}}{R} \tag{6}$$

where $\bar{i}_n^{2\,1/2}$ (in $AHz^{-1/2}$) is the mean-square noise current measured at the bandwidth of 1 Hz in darkness.

Specific detectivity is a critical parameter that can be used to compare the device performance between photodetectors with different materials and geometries, and is defined as:

$$D^* = \frac{(A\Delta f)^{1/2}}{NEP} \quad (7)$$

where A is the device area and Δf the bandwidth. In shot noise dominated photodetectors, D^* can also be expressed as:

$$D^* \approx \frac{A^{1/2}R}{(2eI_d)^{1/2}} \quad (8)$$

where I_d is the dark current.

Response speed denotes the ability of a photodetector to follow a fast varied optical signal. In the time domain, rising/fall time (t_r/t_f) is usually used to characterize response speed. In most cases, t_r/t_f is defined as the time interval required for the photoresponse to rise/decay from 10/90% to 90/10% of its peak value.

Gr/Group II-VI nanostructures

The discovery of carbon nanotubes (CNTs) in 1990s has intrigued great research interest in exploiting low-dimensional semiconducting nanostructures for potential applications in electronic and optoelectronic devices [65,66]. Among the huge semiconducting nanostructure family, non-oxide group II-VI (*e.g.*, CdS, CdSe, ZnS, ZnSe, CdTe, ZnTe, *etc.*) nanostructures have received considerable attention in recent years due to their unique electrical, optical and optoelectronic properties derived from the significant size/surface effects and quantum confinement effect [67,68]. The prominent properties render these nanomaterials promising candidates for high-performance optoelectronic devices, including solar cells, photodetectors, LEDs, lasers, *etc.* [69–72]. In particular, these materials possess direct bandgaps between 1.5 eV (CdTe) and 3.7 eV (ZnS), which make them ideally suitable for light harvesting or light detection from the UV to the visible range [67,68]. In this section, we will summarize the progress in optoelectronic devices applications based on Gr/non-oxide group II-VI nanostructure hybrid heterostructures.

Gr/Cd chalcogenides (S, Se, Te)

Gr/CdS

Cadmium chalcogenides including CdS, CdSe and CdTe, have direct bandgaps from 1.50 to 2.42 eV [67,73,74]. Among them, CdS, an intrinsically *n*-type semiconductor, possesses versatile and fundamental properties such as a direct bandgap of 2.42 eV, a small exciton binding energy, excellent transport properties, good thermal and chemical stability [75], which render CdS one of the most fascinating materials for optoelectronics. In particular, CdS nanostructures have been widely employed to assemble photovoltaic and photodetection devices, which demonstrate superior performance over counterparts based on CdS thin films/bulks [73,76]. The integration of CdS nanostructures with Gr to form hybrid heterostructures offers an alternative way to further enhance the device performances.

Cao et al. firstly reported the assembly of Gr/CdS QDs hybrid heterostructures through a facile one-step method [77]. Time-resolved fluorescence spectroscopy analysis disclosed ultrafast electron transfer from the excited QDs to Gr on the order of picoseconds, suggesting potential optoelectronic applications of the hybrid structures [78]. Afterwards, such Gr/CdS QDs heterostructures have been employed as layered photoelectrodes in photoelectrochemical cells [79]. Benefiting from the advantages such as uniform distribution, favorable energy levels and ultrafast charge transfer, the optimized device demonstrated performance that is superior to counterparts composed of bare Gr, pure CdS QDs, and single-walled carbon nanotubes (SWCNTs)-CdS QDs heterostructures.

In addition, Gr/one-dimensional (1D) CdS nanostructure hybrids have shown promise in photovoltaics. For example, Dufaux et al. have fabricated a Gr/CdS NW hybrid heterojunction and investigated its photoelectric properties [80]. Fig. 3a shows the optical and atomic force microscopy (AFM) images of a representative heterojunction. The scanning photocurrent microscopy (SPCM) measurement in Fig. 3b revealed obvious photocurrent of hundreds of pA that is localized at the edge of Gr. Through chemical control of the Gr/CdS interface and annealing, the photocurrent can be improved by approximately two orders of magnitude with photoresponse distributed along the entire Gr/CdS interface. The internal PCE (this parameter is calculated by deducting the light absorption losses) reached 0.34%. The PCE of such heterojunction solar cells can be greatly boosted to ~1.65% by employing Au (5 nm)/Gr combined electrodes (Fig. 3c) [81]. In this structure, the Gr has advantages of high conductivity and transparency, while the 5 nm Au layer can form good Schottky contact to the CdS NW. These advantages, together with the unique Gr top-contacted mode (Fig. 3d), facilitate efficient separation and transport of photocarriers, giving rise to prominent photovoltaic performance.

Gr/CdS nanostructure hybrids have demonstrated potential in the realm of photodetection as well [82,83]. Specifically, Gr phototransistors sensitized with CdS nanocrystals (NCs) as the light absorbing media have been reported, which showed a peak responsivity of 3.4×10^4 AW^{-1} and a specific detectivity of 10^{13} Jones at the UV region, respectively [82]. With increasing light power, the transfer curves shifted horizontally towards negative gate voltages while the responsivity decreased gradually (Fig. 3e and f), confirming the photogating effect as the main working mechanism. Photogenerated electrons are readily transferred from NCs to the Gr and continue to transport, contributing to the photocurrent, whereas photogenerated holes are trapped by local trap states at the NCs surface, which leads to a strong photogating effect on the Gr through capacitive coupling. Although suffering from a slow photocurrent decay presumably due to the presence of deep trap states, the device is still capable of detecting fast switching signal up to 2000 Hz.

Gr/CdSe

Another cadmium chalcogenide that has also attracted great interest is CdSe, which has a moderate direct bandgap (1.75 eV) and outstanding optoelectronic properties [84]. Ye et al. demonstrated a Gr/CdSe NB Schottky junction photovoltaic device (Fig. 4a) [85], whose working mechanism resembles that of conventional Schottky solar cells (Fig. 4b). The work function difference between the two materials produce a built-in electric field at Gr/CdSe interface, which drives photogenerated electrons and holes within the depletion region towards CdSe and Gr, respectively. The device exhibited an obvious photovoltaic behavior with a PCE of 1.25%, as depicted in Fig. 4c. Later, Zhang et al reported a similar device, however, with much inferior PCEs of only 0.1%, presumably owing to the large active area and long path that photocarriers need to travel [86]. Flexible solar cells have also been assembled on plastic substrates [87]. After 60 cycles bending tests or at bending angles as large as 105°, the devices showed neglectable performance variation, suggesting excellent performance stability and great promise for next-generation wearable and bendable optoelectronic applications.

Gr/CdSe NB Schottky junctions have been employed as photodetectors with excellent performance as well [88–90]. For instance, Dai's group has fabricated Schottky junctions on rigid or flexible/transparent substrates, which can function as self-powered photodetectors [88,89]. This photodetector is very sensitive to visible light with high photosensitivity over 10^5 and respon-

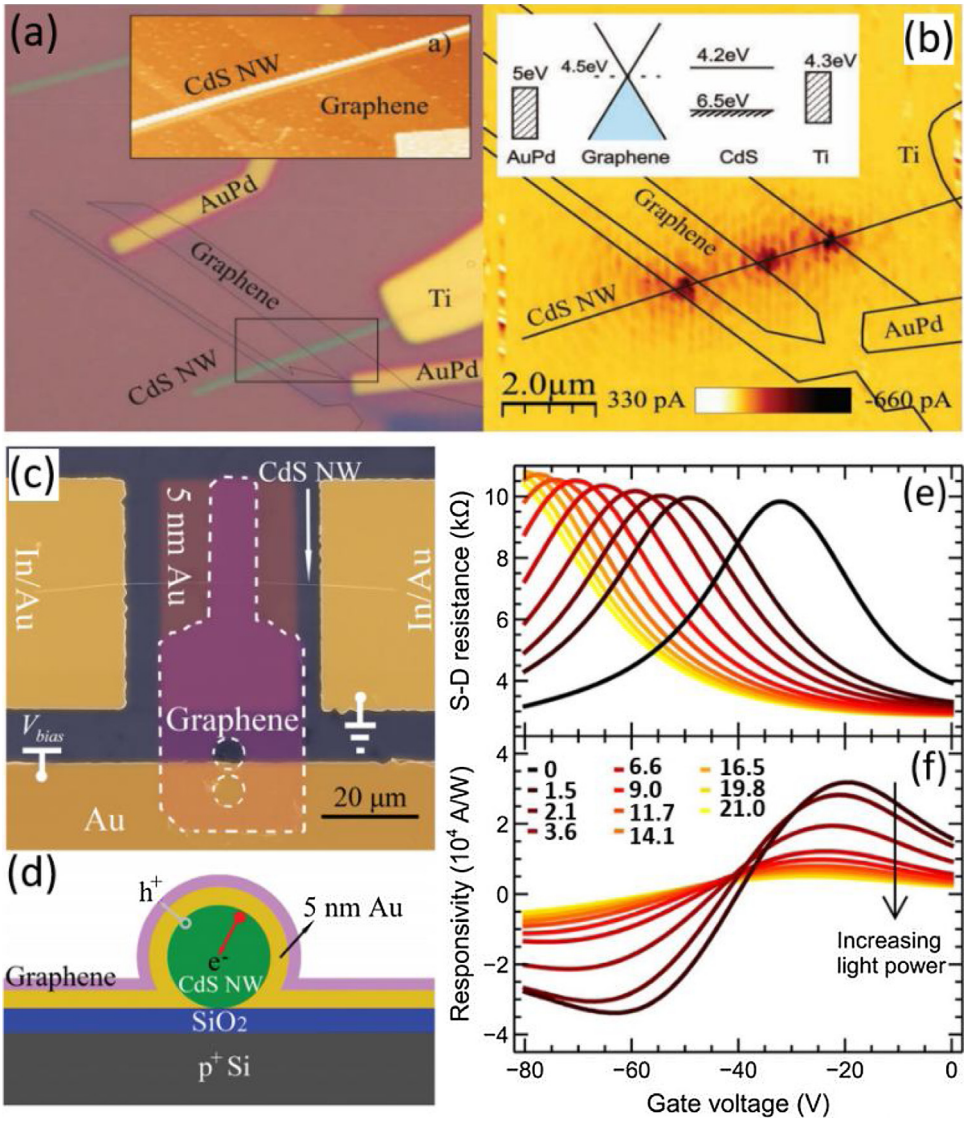

Fig. 3. (a) SEM image of the Gr/CdS NW heterojunction solar cells. (b) Zero-bias SPCM image of the heterojunction device. Reprinted with permission from Wiley-VCH. [80] (c) SEM image of a typical Gr/CdS NW solar cell. (d) Schematic illustration of the heterojunction. Reprinted with permission from American Chemical Society. [81] (e) I_{ds}-V_{ds} curves of the Gr/CdS NCs hybrid phototransistor at different laser intensities. (f) Responsivities at UV light illumination. Reprinted with permission from American Chemical Society. [82]

sivities of ~10 AW^{-1} (Fig. 4d). The response times are tens of microseconds (Fig. 4e and f). In addition to these efforts, reduced Gr oxide (rGO)/CdSe QDs (nanoparticles (NPs)) nanocomposites derived from solution-based methods can also act as photodetectors[91,92]. Such devices typically demonstrated a fast and prominent photoresponse, which is better than their counterparts made of bare rGO, pure CdSe NPs, and the physically mixed rGO/CdSe NPs. The dramatically enhanced photoresponse is attributed to the efficient and separately transfer of the photocarriers from the CdSe NPs to rGO.

Gr/CdTe

In addition, CdTe with a direct bandgap of 1.50 eV, has been integrated with Gr to explore the optoelectronic applications. Li et al. demonstrated a new photovoltaic device that mainly consists of Gr/CdTe thin film Schottky heterostructures [93]. The PCE was greatly increased by ~50% from 2.0 to 3.10%, upon coating a layer of CdSe QDs. The phenomenon is explained by the photo-induced doping originating from the charge generation in the QDs and subsequently hopping into Gr, as evidenced by the coincidence of the PL quenching and improved IQE in the range of 450-850 nm. The photo-induced doping effectively elevates the Fermi level of Gr, which leads to enhanced electron collection ability by Gr and eventually improved photovoltaic performance. Self-aligned microstructured CdTe thin films have been grown selectively on Gr serving as pre-defined seed layer, where defects are introduced intentionally to act as CdTe nucleation sites [94]. The as-prepared heterostructures are very sensitive to UV illumination with good reproducibility, which implies great promise of such Gr/semiconductor hybrid for next-generation optoelectronic systems application.

Gr/Zn chalcogenides (S, Se, Te)

Gr/ZnS

Compared with cadmium chalcogenide, the zinc chalcogenide (ZnS, ZnSe and ZnTe) possesses relatively large direct bandgaps ranging from 2.26 to 3.77 eV. It has found wide application in diverse fields such as flat panel displays, LEDs, injection lasers and UV-visible photodetectors, owing to its excellent photoelectric

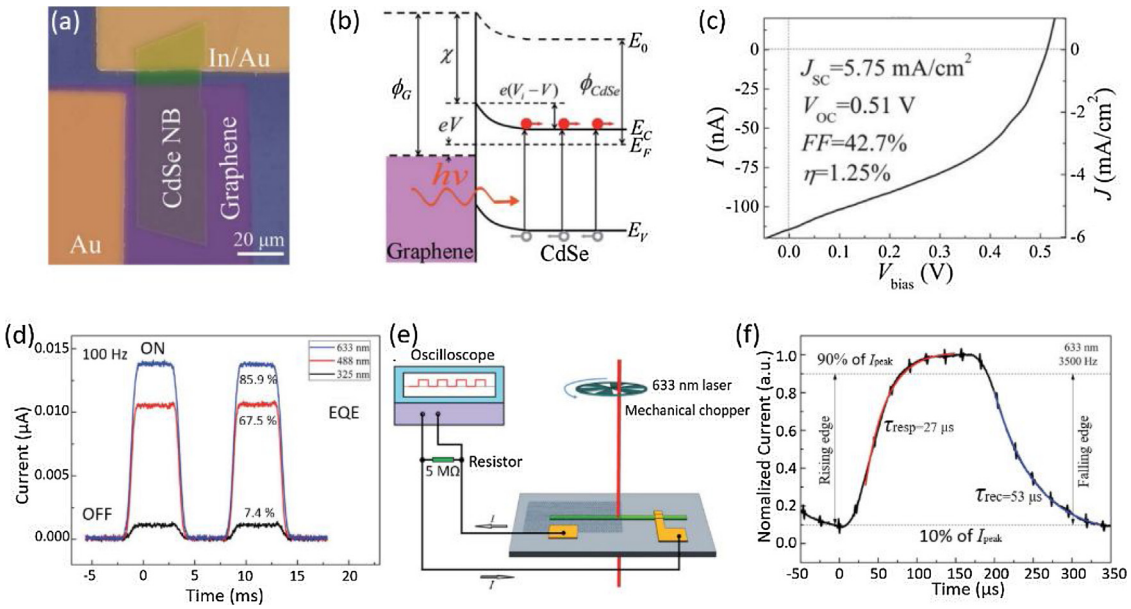

Fig. 4. (a) SEM image of the Gr/CdSe NB solar cell. (b) Energy band diagram of the Schottky junction under light illumination. (c) *I-V* curves of the solar cells under AM 1.5G illumination. Reprinted with permission from the Royal Society of Chemistry. [85] (d) The photoresponse of the Gr/CdS NW photodetector under different wavelengths illumination. (e) Schematic illustration of the setup for measuring response speed. (f) A normalized response cycle for measuring the rising/fall time. Reprinted with permission from the Royal Society of Chemistry. [89]

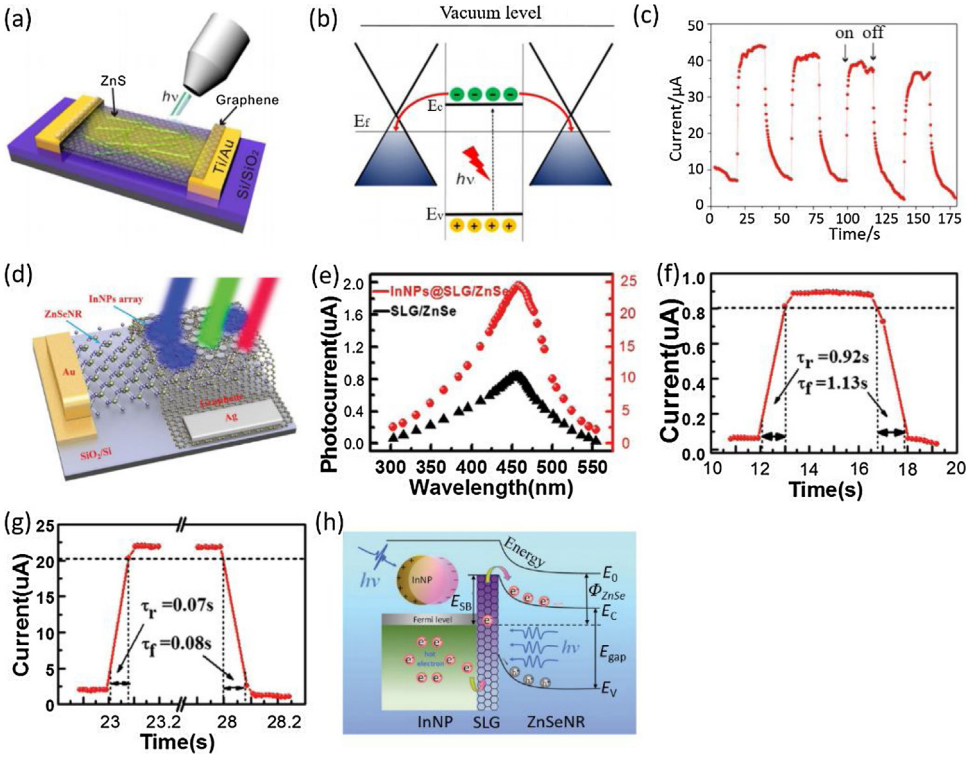

Fig. 5. (a) Schematic of the Gr/ZnS NW hybrid phototransistor. (b) Energy band diagram of the heterojunction under light irradiation. (c) Photoresponse of the device under UV illumination. Reprinted with permission from Nature Publishing Group. [99] (d) Schematic of In NPs enhanced Gr/ZnSe NB heterojunction device. (e) Comparison of the photocurrent without and with plasmonic In NPs. A single magnified photoresponse of the device (f) without and (g) with plasmonic In NPs. (h) Mechanism of the In NPs decorated photodetector. Reprinted with permission from Wiley-VCH. [102]

properties [95–97]. In particular, ZnS with a wide bandgap of 3.77 eV, is a highly promising light absorber for visible-blind UV photodetection [95]. Similar to Gr/CdS QDs (NPs), Gr/ZnS QDs (NPs) hybrids with a high degree of crystallinity and dispersity could be synthesized through solvothermal methods [78,98]. Kim et al. reported an UV photodetectors composed of solution-processed ZnS NBs and CVD-Gr, as shown in Fig. 5a [99]. The effective junction area was expanded by using sandwiched structures and multilayer stacking techniques. In this structure, the ZnS NBs act as the UV light absorber and Gr serves as the fast charge transfer channel. Upon UV illumination, electron-hole pairs are generated in the ZnS, and subsequently photoexcited electrons transfer to Gr spontaneously

because of appropriate band alignment (Fig. 5b). In addition, the charge recombination processes are drastically inhibited due to the high carrier mobility of Gr. It is for these reasons that the as-assembled Gr/ZnS/Gr photodetector displayed a high photocurrent of 37 μA with stable on-off switching and excellent spectral selectively (Fig. 5c). The photocurrent can be further increased to 0.115 mA by using multiple sandwiched Gr and ZnS, which is 10^7 higher than that of pure ZnS NBs.

Conceptually similar structures have also been realized by using ZnS films as absorbing media [100]. The devices demonstrated an ultrahigh responsivity of 1.7×10^7 AW^{-1} and a fast response speed of ~50 ms with good reproducibility. The wavelength of detected light can be distinguished by means of response time in an intelligent device based on Gr/ZnS/CdS hybrids, as later reported by the same group [101]. In their study, the time needed for the transfer of visible light-generated carriers from CdS to Gr through the intermediate ZnS can be tuned by adjusting the thickness of ZnS film.

Gr/Other Zn chalcogenides (ZnSe, ZnTe)

ZnSe holds a direct bandgap of ~2.70 eV and has long been considered as a prospective material for optoelectronics in the near UV-blue region [96]. Wang et al. have proposed a blue light photodetector made of Gr/ZnSe NR hybrid heterojunctions, on which hexagonally packed In NPs were modified to boost the photosensitivity (Fig. 5d) [102]. It is found that upon NPs modification, the devices demonstrated a substantially improved photocurrent by ~20-fold, and much faster response speeds, as shown in Fig. 5e–g. As a result, the responsivity increased from 26.5 to 647 AW^{-1}. This increase in responsivity is ascribed to contribution from the In NPs that can increase the optical path inside the device to effectively trap incident light and induce direct electron injection from the NPs to Gr, as manifested by the optical absorption spectrum and theoretical simulations. Upon illumination, the In NPs are capable of trapping incident light and induce localized surface plasmon resonance (LSPR). The resultant hot electrons with relatively high energies inside the NPs can easily transfer to Gr and then migrate towards the Gr/ZnSe interface, where they are separated by the built-in electric field and contribute to photocurrent (Fig. 5h).

ZnTe with a direct bandgap of ~2.26 eV has also shown potential for a number of optoelectronic devices, including green LEDs, electro-optic detectors, and solar cells [97]. Luo et al. have recently reported a Gr/ZnTe NW heterostructure for visible light detection [103]. They found that the device was very sensitive to light illumination at reverse bias voltages, with a stable and reproducible I_{light}/I_{dark} ratio of 10^2, which is believed to originate from the low dark current due to the enlarged space-charge region at reverse bias. The responsivity and specific detectivity are as high as 4.87×10^5 AW^{-1} and 3.19×10^{13} Jones, respectively.

Gr/2D group II-VI semiconductor heterostructures

2D group II-VI semiconductors are promising candidates that can be integrated with Gr to form van der Waals heterostructures that is capable of decoupling the photogeneration from the transport. However, pure 2D group II-VI semiconductors usually have large exciton binding energy, which strongly prevents efficient charge transfer from them to neighboring layers. A promising solution to this issue is to assemble 2D group II-VI semiconducting heterostructures at the nanoscale [104]. As an example, 2D CdSe nanoplatelets (NPLs) were employed as photoactive media and combined with Gr to construct phototransistors in an electrolytic transistor configuration (Fig. 6a). The Dirac point voltage exhibited an obvious shift towards negative gate voltages upon illumination due to charge transfer, as shown in Fig. 6b. By using colloidal atomic layer deposition (c-ALD) procedures, CdSe-CdS core-shell and CdSe-CdTe core-crown heterostructured NPLs were successfully synthesized. It was found that both heterostructures demonstrated a reduced overlap of electron and hole wave functions, which reduces exciton binding energy and facilitates efficient charge dissociation. On the other hand, the valence band level of the core-crown heterostructure is raised closer to the Gr Fermi level while its conduction band is getting off resonance as a result of the introduction of a CdTe crown, which may lead to a more favorable hole transfer to Gr. As expected, the Dirac point voltage shifted to more negative gate voltages for a core-shell NPLs-based phototransistor than for a CdSe NPLs-only device (Fig. 6c) upon illumination, indicating a more efficient n-type photogating effect. In the case of core-crown NPLs-based device, the Dirac point shifted reversely toward positive gate voltages under illumination higher than 100 mW/cm^2 (Fig. 6d).

In summary of this part, Gr/group II-VI nanostructure hybrid heterostructures have shown great promise in both solar cells and photodetectors. The performance parameters of some representative Gr/group II-VI nanostructure devices are summarized in Table 1. For solar cell applications, from the available data, we found that Gr/group II-VI NW/thin film heterostructures can show the maximum PCE of ~1.65%/~3.10%. Performance improvement is achievable through various techniques, such as interface modification, eliminating interface contaminations, increasing electronic coupling, and photo-induced doping of Gr. On the other hand, phototransistors based on Gr/group II-VI NC (thin film) heterostructures working on photogating effect demonstrated high responsivities (3.4×10^4 to 3.4×10^7 AW^{-1}) and fast response speeds (~50 ms), whereas Gr/group II-VI NW (NB) heterostructure-based photodiodes can show a high I_{light}/I_{dark} ratio of 10^5, a responsivity of ~10 AW^{-1} at zero bias, which can be greatly enhanced to $\sim 3.4 \times 10^5$ AW^{-1} upon a moderate reverse bias. The control of charge transfer and exploiting LSPR effect of metallic NPs have proved to be effective routes for photoresponse improvement. In addition, flexible solar cells and photodetectors have also been assembled on plastic substrates, which usually exhibited good flexibility and excellent bending durability.

Gr/Group III-V semiconductors

Group III-V semiconductors refer to materials comprising group III elements (essentially Al, Ga, In) with group V elements (essentially N, P, As, Sb). The combination can give rise to more than ten possible semiconductors with distinctive electrical and optoelectronic properties. Among this class of semiconductors, GaN, GaAs, InP and InAs, that show strong light absorption/emission characteristics for their appropriate direct bandgaps, are most widely explored materials for optoelectronic applications [105–107]. For example, GaN, with excellent optical and electrical properties including a wide bandgap of 3.4 eV and high electron mobility, is considered as one of the most crucial semiconductors that has found ample applications in a variety of optoelectronic devices such as displays, lasers and detectors [108]. In particular, GaN is extensively studied for short wavelength emitters and solid state lighting applications. On the other hand, the bandgap of GaAs (~1.42 eV) is close to the optimal value (~1.40 eV) for achieving maximum solar energy conversion efficiency in a single p-n junction solar cell under AM 1.5G solar spectrum [105,109]. GaAs and its related compound semiconductors are also highly favorable for infrared light emission and detection using inter-subband transitions. Furthermore, it is feasible to engineer the bandgap as well as other physical properties of the compound semiconductors by alloying them [105]. Undoubtedly, the formation of heterostructures by integrating group III-VI semiconductors with Gr has brought about new device architectures with unique functionalities and charac-

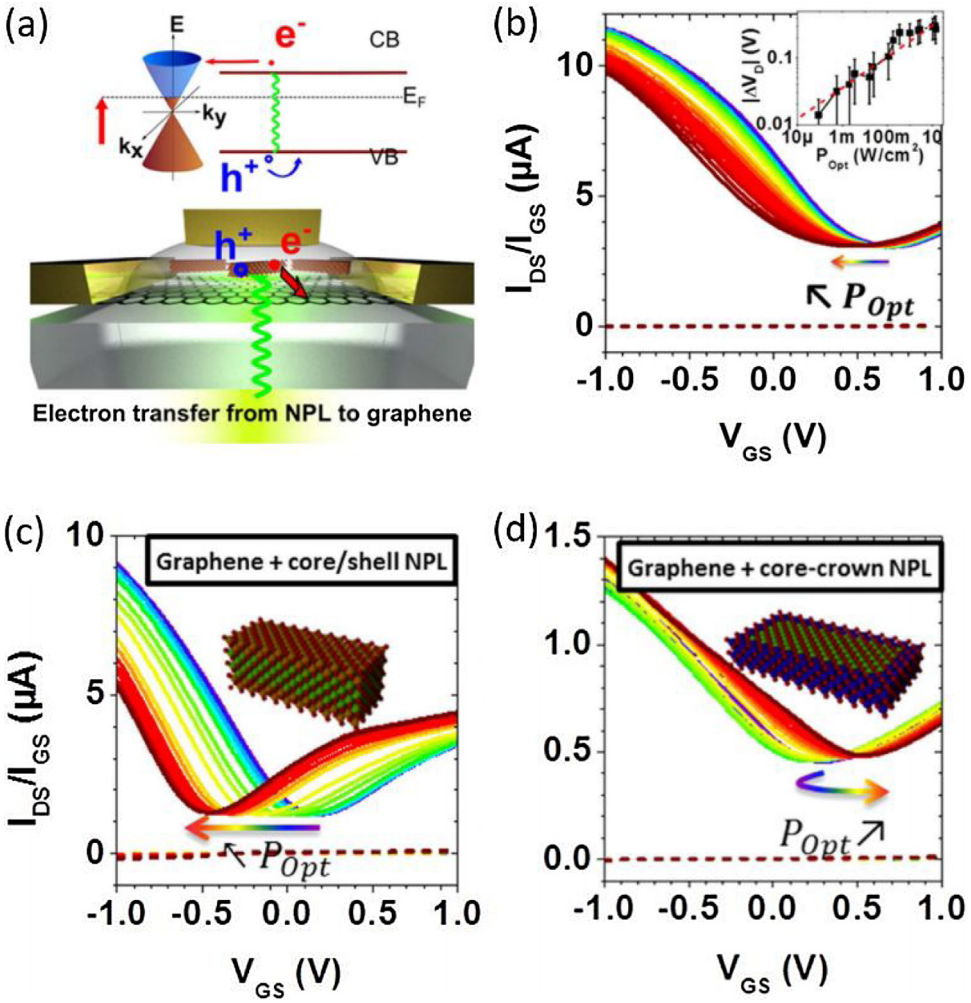

Fig. 6. (a) Schematic illustration of electron transfer from NPL to Gr under light illumination. (b) Transfer curves of the device under increasing light intensities. (c) Transfer curves of the CdSe/CdS core/shell NPL/Gr phototransistor under various light intensities. (d) Transfer curves of the CdSe-CdTe core-crown NPL/Gr phototransistor. Reprinted with permission from Nature Publishing Group. [104]

teristics. In this part, we are going to introduce research advances in Gr/group III-V semiconductor hybrid heterostructure based optoelectronic devices.

Gr/GaN

As discussed above, GaN is a wide direct bandgap semiconductor with distinguished physical properties, such as excellent optical/electrical characteristics and good chemical stability at elevated temperatures, enabling its versatile applications in various optoelectronic devices. In the past decade, Gr has proved to be an ideal candidate to replace transparent conductive electrodes (e.g., ITO) in GaN-based LEDs with aims to improve the device performance and reduce fabrication cost [110,111]. Since this topic has already been systematically discussed in some review papers [17], it will not be covered here. We only focus on several representative studies concerning LEDs application. It has been reported that Gr can form stable Schottky contacts with either *p*-GaN or *n*-GaN substrates due to the difference in Fermi level [112–114]. Taking advantage of the Schottky barrier contacts, Wang et al. have studied the effect of HNO_3 doping on the electrical characteristics of Gr/*p*-(*n*-)GaN junctions [115]. It is found that that acid treatment is beneficial for reducing operating voltage in that the doping will elevate its work function and leads to higher conductivity of Gr. As an example, they assembled and examined GaN-based vertical LEDs incorporating Gr as transparent electrodes. Although the devices with Gr showed slightly degraded *I-V* characteristics, their light output power was increased by ~34%, compared with conventional vertical LEDs without Gr. Upon acid treatment, the value can be further increased by ~19%.

Meanwhile, Chang and co-workers have developed a metal-insulator-semiconductor (MIS) LED structure consisting of a Gr film on p-GaN substrate separated by an ~10 nm insulating SiO_2 layer [116]. The devices exhibited tunable electroluminescence (EL) spectra under forward or reverse bias conditions, which is explained by the carrier tunneling through the thin oxide layer from Gr to the p-GaN. (Fig. 7a–c). The generation of UV emission is attributed to the radiative recombination of the injected electrons with the holes in the acceptor levels of p-GaN, while the tunnel electrons from the conduction band recombine with the holes in the deep acceptor levels and generate the observed weak orange-red emission. On the other hand, under reverse bias, the observed orange-red emission can be related to the recombination of tunnel holes from the deep acceptor levels with electrons in the conduction band, whereas the recombination process of UV emission can be understood by the transition from the conduction band of p-GaN to the acceptor levels when the applied bias is high enough. The work might accelerate the development of economical alternatives to current tunable LEDs and represents a novel application of Gr in MIS-based optoelectronic devices.

Table 1
Summary of performance parameters of some representative Gr-group II-VI nanostructures, /group III-V semiconductors, /group IV semiconductors hybrid heterostructure optoelectronic devices.

Devices	Geometry	Mode	Wavelength	On/Off	*R* (A/W)	Speed/frequency	Ref
PDs	Gr/CdS NCs	Phototransistor	349 nm	/	3.4×10^4	2 kHz	[82]
	Gr/CdS NW	Phototransistor	White light	1.26	0.276	3 kHz	[83]
	Gr/CdSe NB	Photodiode	633 nm	1.0×10^5	3.5×10^5	82/179 μs	[88]
	Gr/CdSe NB	Photodiode	633 nm	1.2×10^5	8.7	70/137 μs	[89]
	Gr/CdSe QDs	Photoconductor	532 nm	17	/	250 μs	[92]
	Gr/CdTe film	Phototransistor	365 nm	2.8	/	10.4 s	[94]
	Gr/ZnS NB/Gr	Photodiode	300 nm	4	1.9×10^3	2.8 s	[99]
	Gr/ZnS film	Photodiode	365 nm	1.25×10^4	1.7×10^7	50 ms	[100]
	Gr/ZnS-CdS	Photodiode	365 nm	/	/	270 ms	[101]
	Gr/ZnSe NR	Photodiode	460 nm	20	26.5	2 s	[102]
	Gr/ZnSe NR:Au	Photodiode	460 nm	5	6.47×10^2	0.1 s	[102]
	Gr/ZnTe NW	Photodiode	532 nm	1.0×10^2	4.17×10^3	/	[103]
	Gr/GaN NW	Photoconductor	357 nm	3	25	/	[117]
PDs	Gr/GaN film	Photodiode	325/514 nm	$10^3/10^3$	/	0.2/1.1 ms	[119]
	Gr/GaAs nanocones	Photodiode	850 nm	10^4	1.73×10^{-3}	72 μs	[128]
	Gr/GaAs	Photodiode	850 nm	10^5	5×10^{-3}	380 ns	[129]
	Gr/h-BN	Photoconductor	1550 nm	/	0.36	42 GHz	[146]
	Gr/InP	Photodiode	980 nm	776	4.61×10^{-2}	441 ns	[134]
	Gr/InAs NW	Photodiode	1000 nm	5×10^2	0.5	250 Hz	[137]
	Gr/CNTs	Photodiode	980 nm	1×10^2	0.209	68/78 μs	[170]
	Gr/CNTs	Phototransistor	650/1550 nm	/	100/40	100 μs	[169]
	Gr/Si	Photodiode	488 nm	10^4	0.435	10-3 s	[240]
	Gr/Si	Phototransistor	1550 nm	/	83	600 ns	[254]
	Gr/Si	Photodiode	890 nm	10^7	0.73	0.32 ms	[249]
	Gr/GeNNs	Photodiode	1550 nm	5×10^4	0.185	450/460 ns	[278]
	Gr/Ge	Photodiode	1550 nm	2×10^4	5.18×10^{-2}	23/108 μs	[277]
	Gr/SiC	Phototransistor	532 nm	/	18	> 10 s	[289]
	Gr/Gr QDs/Gr	Photodiode	800 nm	240	0.5	100 μs	[156]
	Gr/Gr QDs	Phototransistor	325 nm	1.6	4.06×10^9	0.3 s	[154]
	F-Gr/Gr	Phototransistor	255/4290 nm	/	$10^3/10$	80/200 ms	[171]

Devices	Geometry	V_{OC}	J_{SC}	*FF*	PCE	Ref
	Gr/CdS NWs	0.15 V	0.275 nA	40%	1.65%	[81]
	Gr/CdSe NB	0.51 V	5.75 mA/cm^2	42.7%	1.25%	[85]
	Gr/CdSe NB	0.52 V	1 mA/cm^2	23.7%	0.12%	[86]
	Gr/CdSe NB	0.31 V	4.73 mA/cm^2	36.1%	0.53%	[87]
	Gr/CdTe	0.51V	16.4 mA/cm^2	37.1%	3.1%	[93]
Solar cells	Gr/GaAs	0.65 V	10.03 mA/cm^2	30%	1.95%	[122]
	Gr/GaAs	0.96 V	23 mA/cm^2	62.8%	18.5%	[31]
	Gr/GaAs	0.81 V	28.6 mA/cm^2	68.9%	16.2%	[125]
	Gr/InP	0.67 V	23.9 mA/cm^2	35%	5.6%	[133]
	Gr/Si (the first report)	0.48 V	6.5 mA/cm^2	56%	1.65%	[27]
	Gr/Si	0.82 V	25.3 mA/cm^2	63%	8.6%	[197]
	Gr/Si	0.612 V	32.7 mA/cm^2	72%	14.5%	[194]
	Gr/Si (record PCE)	0.595 V	36.7 mA/cm^2	72%	15.6%	[28]
	Gr/Si hole array	0.52 V	31.56 mA/cm^2	63%	10.4%	[199]
	n-Gr/p-Si	0.48 V	34.3 mA/cm^2	63.6%	10.5%	[209]
	Gr/Si (40 μm)	0.54 V	22.86 mA/cm^2	58%	8.26%	[196]
	Gr QDs/Si	0.58 V	33.93 mA/cm^2	63%	12.35%	[236]
	Gr-CNT/Si	0.618 V	31.9 mA/cm^2	75.5%	15.2%	[239]

Another important application of Gr/GaN heterostructures is UV/visible photodetection, normally based on metal-semiconductor-metal (MSM)-type architecture or Gr/GaN Schottky diodes [117–119]. In the former structure, Gr serves as a transparent electrode to replace a metal electrode in one side. Typically, UV sensors employing epitaxial grown GaN layer as the light sensitizer exhibited a pronounced photoresponse to UV illumination with a high I_{light}/I_{dark} ratio of 3.9×10^5 and a UV-to-visible rejection ratio of 1.8×10^3 [118]. In addition, Babichev et al. reported UV detectors composed of vertically standing GaN NW arrays as light absorbing media, on which Gr is transferred to form a large-area continuous transparent electrode [117]. The device was sensitive to UV illumination with a responsivity reaching ~25 AW^{-1} at 357 nm, indicative of potential for optoelectronic devices operated in UV region. In another work, Lin and colleagues presented dual-wavelength photodetection based on Gr/GaN Schottky diodes (Fig. 7d) [119]. The diode with a Schottky barrier height of ~0.49 eV exhibited an obvious rectifying behavior in dark. Moreover, the device was found to be very sensitive to UV and green illuminations under both forward and reverse biases (Fig. 7e and f). The I_{light}/I_{dark} ratio can exceed 10^3 for both illuminations at a reverse bias of -10 V. However, the physical mechanisms of the photoresponse at varied wavelengths are quite different, which can be understood from the energy band diagrams (Fig. 7g–i). The different working mechanisms can be evidenced by the distinct relationships between the photocurrent and the light power at different wavelengths. The device also exhibited fast response speeds for UV and green lights, with response times at the millisecond level.

In fact, Gr has also been employed as transparent conductive electrodes in photovoltaic devices composed of a multi-quantum-well (MQW) structure sandwiched between *p*- and *n*-GaN layers [120]. It was observed that the Au NPs decoration on Gr can significantly enhance the device parameters, such as J_{SC} and V_{OC}.

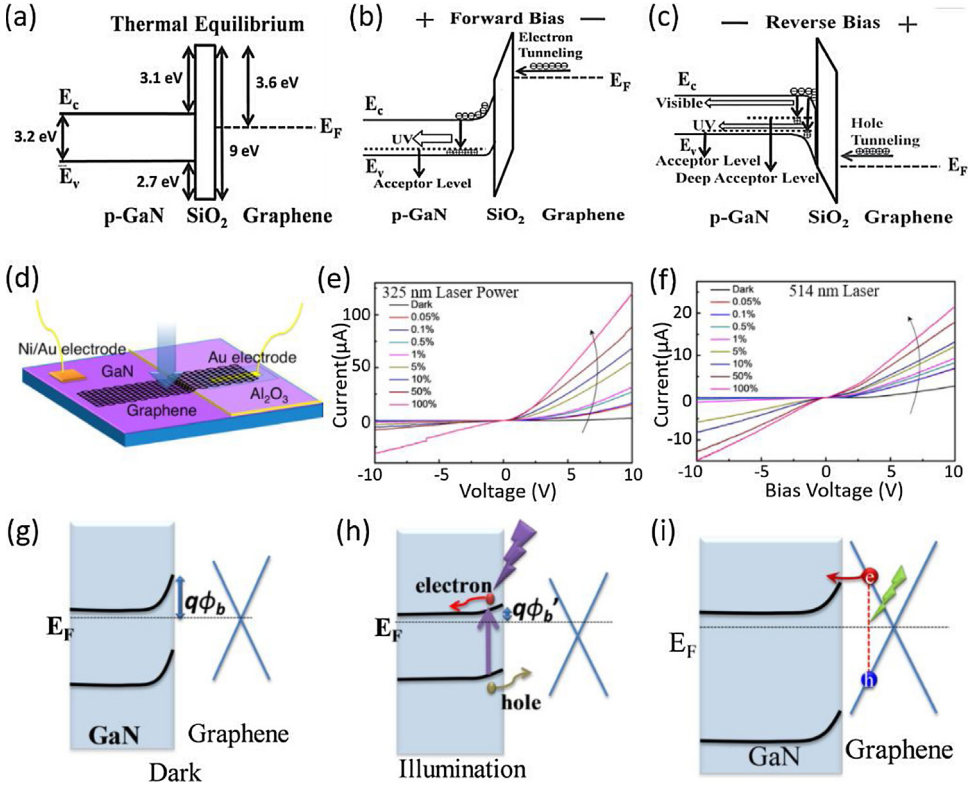

Fig. 7. Energy band diagram of Gr/SiO_2/*p*-GaN MIS-LED (a) under thermal equilibrium, (b) under forward bias voltage, and (c) under reverse bias voltage. Reprinted with permission from Wiley–VCH. [116] (d) Device structure of the Gr/GaN based LED. *I-V* curves of the device shined by (e) 325 nm and (f) 514 nm. Energy band diagram of the device (g) in dark, (h) under UV illumination, and (i) under green illumination. Reprinted with permission from American Institute of Physics. [119]

According to their experimental analysis, the improved electrical conductivity and light absorption through light scattering of Au NPs contribute to the increased J_{SC}, whereas the increase in V_{OC} is related to the optimized band energy alignment, which facilitates the transport of photoexcited holes to the p-contact Gr electrode.

Gr/GaAs

GaAs has long been considered as an ideal candidate material for photovoltaic and NIR photodetection applications due to its striking electrical and optical properties such as high carrier mobility, direct bandgap of ~1.424 eV, and large optical absorption coefficient and so on [105,121]. In 2013, Jie et al. reported a Schottky junction photovoltaic device composed of CVD derived Gr and *n*-GaAs substrate (Fig. 8a and b) [122]. The device exhibited an obvious current rectifying behavior in dark and a remarkable photovoltaic characteristic under illumination. The bi-layer Gr-based device showed a V_{OC} of 0.65 V and a J_{SC} of 10.03 $mAcm^{-2}$, yielding a PCE of 1.95% (Fig. 8c), which is superior to that of mono-layer device. Considering the fact that the device performance of the Gr/GaAs solar cell is influenced by various issues (e.g., doping concentration and carrier mobility of GaAs, thickness of the oxide layer, etc.) [123], many optimization techniques have been adopted to improve the PCE. These techniques include gating or doping of Gr, antireflective layer coating, surface plasmon metallic NPs modification, interface engineering, and so on [31,124–127]. For example, a 10 nm P3HT thin layer has been introduced into a Gr/GaAs solar cells as not only a hole-transport layer but also an electron-blocking layer to suppress the electron recombination at the Gr anode [124]. Device analysis revealed that the both Schottky barrier height and built-in potential at the Gr/GaAs interface are increased, giving rise to increase in V_{OC}. What is more, due to passivation effect of P3HT, the J_{SC} increases as well. As a result, the PCE increases from 4.63 to 6.84%. In fact, the PCE can be further increased to 13.7% by chemical doping of Gr *via* bis(trifluoromethanesulfonyl)-amide (TFSA) and deposition of TiO_2 NPs film as an antireflective layer. Besides the passivation using P3HT layer, the incorporation of large-area 2D hexagonal boron nitride (*h*-BN) proves beneficial for high PCE [127]. It was observed that the inserting 2D *h*-BN can greatly suppress the static charge transfer and increase the barrier height from 0.88 to 1.02 eV. This leads to an increase of PCE from 8.63 to 10.18%.

Later on, Li et al. designed a Gr/dielectric (Al_2O_3 thin layer)/Gr gating structure for improving the efficiency of Gr/GaAs solar cells (Fig. 8d) [31]. As illustrated in Fig. 8e, the V_{OC} increased remarkably with increasing negative gate voltage applied on the top Gr, which is attributed to the higher Schottky barrier height and consequently larger built-in potential at Gr/GaAs interface induced by the down-shifted Gr Fermi level (Fig. 8f). Remarkably, the maximum PCE can reach 18.5% at the gate voltage of -15 V. More recently, surface plasmon Au NPs have been incorporated into Gr/GaAs solar cells as the antenna for light harvesting [125]. Thanks to more efficient separation and collection of the photocarriers near the junctions, this scheme thus leads to remarkably suppressed carrier recombination occurring in the bulk of GaAs. The optimal size of the Au NPs is ~80 nm dominated by the competition of the radiation damping effect and surface plasmon effect. This technique, together with chemical doping of Gr and antireflective layer coating, gave rise to a PCE of 16.2% eventually.

Exploiting the strong photovoltaic effect, Gr/GaAs heterostructures have also been widely studied for photodetection application [127–130]. GaAs nanocones or NW arrays with pronounced light trapping capability have been synthesized by nanospheres lithography assisted chemical etching [128], or Au-catalyzed metal organic CVD method [130]. Heterojunctions composed of these GaAs structures and Gr are sensitive to the visible-NIR illuminations and can work as self-powered detectors with fast response speed.

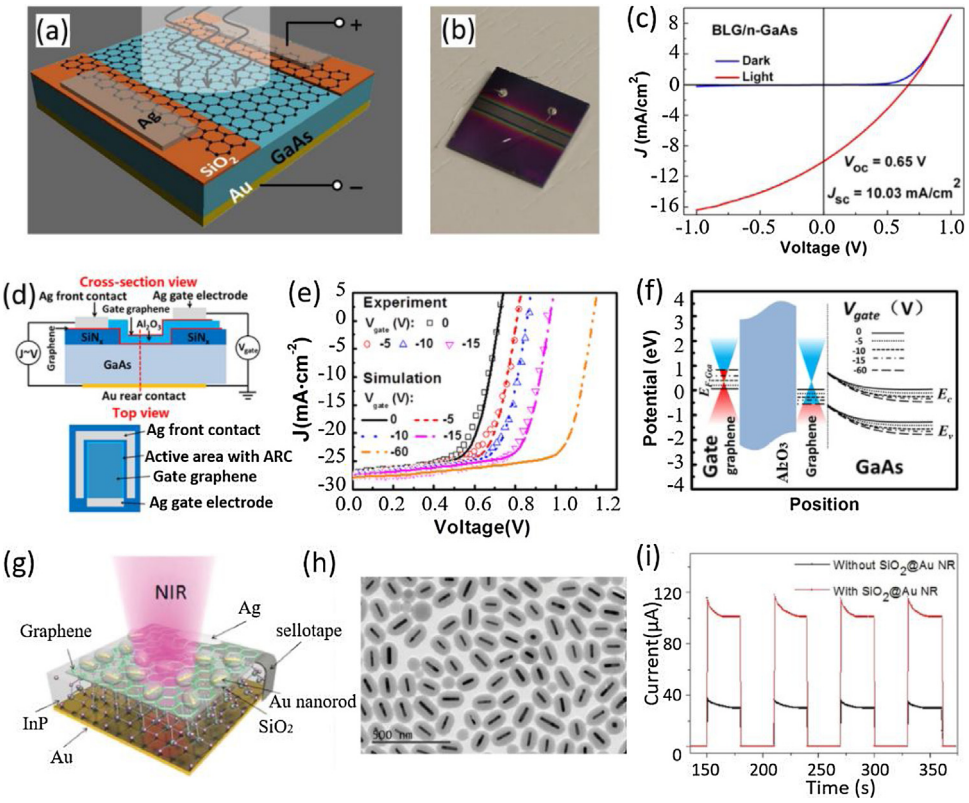

Fig. 8. (a) Illustration of the Gr/GaAs Schottky junction solar cell. (b) Photography of the device. (c) *J-V* curves of the heterojunction in dark and under AM 1.5G illumination. Reprinted with permission from American Institute of Physics. [122] (d) Cross-section view and top-view illustrations of the field-effect enhanced Gr/GaAs solar cell. (e) Both experimental and theoretical *J-V* curves under different gate biases. (f) Energy band diagram of the heterojunction under different gate biases. Reprinted with permission from Elsevier B.V. [31] (g) Schematic of the Au NPs modified Gr/InP NIR photodetector. (h) TEM image of the Au NPs. (i) Photoresponse of the Gr/InP with and without surface modification. Reprinted with permission from Wiley–VCH. [134]

For example, Luo et al. reported a highly sensitive near infrared light photodetector based on Gr/GaAs nanocone arrays Schottky junction [128]. Under 850 nm illumination, the devices exhibited I_{light}/I_{dark} ratio as high as 10^4 with good reproducibility. The responsivity and specific detectivity reached 3.73 mAW^{-1} and 1.83×10^{11} Jones, respectively. The photocurrent depends almost linearly on the illumination across a broad light intensity range, indicating high quality of the junction as well as low density of trap states at the surface of GaAs. More importantly, the detectors demonstrated a fast response speed with rising/fall times of 70/122 μs. The excellent performance is attributed to the GaAs nanocone arrays, which can efficiently trap incident NIR light. In order to optimize the photosensitivity of Gr/GaAs NIR detectors, a AlO_x thin layer was introduced in the device geometry, which serves as not only the surface passivation layer to suppress carrier recombination, but also as a barrier to reduce the current leakage [129]. As a result, AlO_x insertion led to a considerable increase in photocurrent and an obvious decrease in dark current. The responsivity and specific detectivity increased by ~4-folds to 5 mAW^{-1} and 2.88×10^{11} Jones, respectively, as compared to the device without AlO_x layer. The devices also exhibited fast response speed with rise/fall times of 320/380 ns.

Gr/InP, InAs

InP possesses a variety of extraordinary electrical and optical properties, such as high electron mobility, and direct bandgap of 1.34 eV close to the optimal energy range for solar energy conversion, high resistance to space radiation damage [131,132]. For these reasons, InP has been a promising material for high efficiency solar cells towards space applications, and other optoelectronics including NIR photodetectors and laser diodes. Wang et al. have fabricated Gr/p-InP Schottky junction solar cells with a PCE of 3.3% [133]. Through electric field modulation and chemical doping of Gr using a reduced viologen solution, the PCE can be further promoted to 5.6%. In addition to photovoltaic applications, Gr/InP heterostructures have also shown great promise in NIR photodetection. Luo and co-workers have designed a Gr/InP Schottky junction, on which SiO_2 encapsulated plasmonic Au nanorods are placed (Fig. 8g and h) [134]. These Au nanorods act as "optical antenna" that can effectively confine the incident NIR light and enhance the local electric field near the junction due to the strong LSPR effect. On the other hand, the decoration of Au nanorods can increase the barrier height, facilitating efficient separation of photocarriers. As a result, the devices exhibited a considerably enhanced photoresponse with responsivity and specific detectivity increased by several-folds to 139.8 mAW^{-1} and 1.05×10^{11} Jones, respectively (Fig. 8i). What is more, the response speed can reach ~400 ns. InP NCs with high structural quality and excellent optoelectronic properties have been epitaxially grown on Si [135]. The as-formed Gr/InP NCs/Si heterostructures showed an obvious rectifying behavior and promising photodetection characteristics. The high compatibility with Si-CMOS technology suggests that this work opens up a new possibility for the monolithic integration of a variety of group III-V materials and thus various high-performance electronic/optoelectronic devices onto the mainstream Si technology platform.

InAs, as a crucial group III-V compound semiconductor, has been extensively explored for constructing IR detectors at the wavelength range of 1-3.8 μm for its high electron mobility and narrow direct bandgap of 0.354 eV [136]. Miao et al. presented a new type of NIR photodiodes made of Gr/InAs NW vertically stacked het-

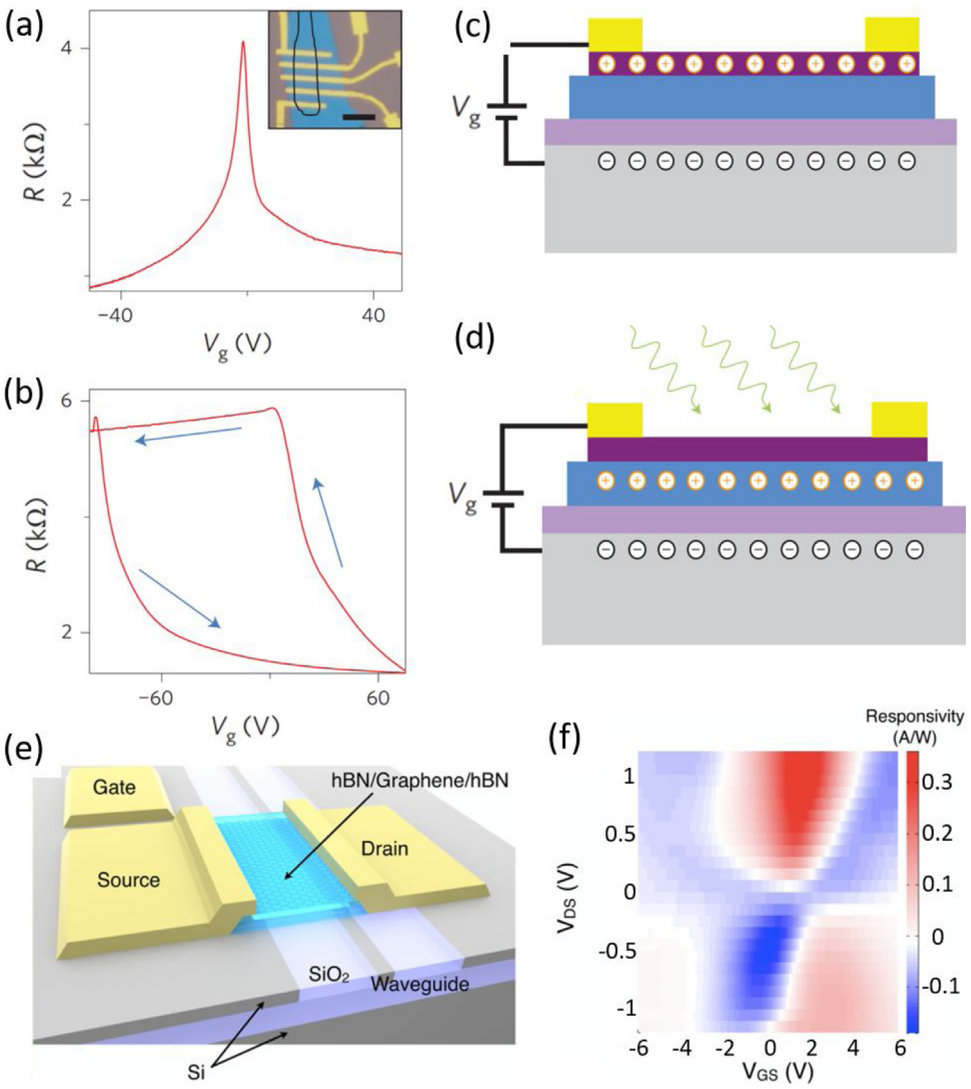

Fig. 9. (a) *I-V* curves of the Gr/*h*-BN heterostrucutre device in dark. (b) Resistance trace as V_g sweep under light illumination. Charge distribution in the Gr/*h*-BN heterostructure (c) in dark, and (d) under illumination. Reprinted with permission from Nature Publishing Group. [144] (e) Illustration of the *h*-BN/Gr/*h*-BN photodetector on a silicon waveguide. (f) Experimental responsivity as a function of V_{gs} and V_{ds}. Reprinted with permission from American Chemical Society. [146].

erojunctions [137]. The as-fabricated heterojunctions exhibited a tunable rectifying behavior in dark. Upon 1 μm NIR illumination, the devices showed a pronounced photoresponse with an I_{light}/I_{dark} ratio of 5×10^2 and a responsivity of 0.5 AW^{-1}, which outperformed those of a pure Gr IR photodetector by several orders of magnitude.

Gr/h-*BN*

Hexagonal boron nitride (*h*-BN) is the most stable crystalline form of boron nitride. This material has been widely used in electronics, for example, as a substrate for semiconductors and as a dielectric in resistive random access memories [138,139], for its wide indirect bandgap of ~6 eV, low dielectric constant, and chemical inertness [140]. Like layered structure of graphite, 2D *h*-BN layer can be exfoliated from bulk crystal or grown *via* CVD approach [141,142]. With its atomically smooth surface that is relatively free of dangling bonds and charge traps, 2D *h*-BN layer has recently emerged as a fundamental building block for van der Waals heterostructures [141,143]. A pronounced photoinduced modulation doping in a Gr/*h*-BN van der Waals heterostructures has been reported [144]. When shined by light illumination, the heterostructure exhibited an abnormal charge transport behavior, which is completely different from what is observed in dark (Fig. 9a and b). Such an intriguing photoinduced response is associated with the microscopically coupled optical and electrical response of the heterojunction (Fig. 9c and d) which includes optical excitation of the defect transitions in the BN, electrical transport in Gr, and charge transfer between BN and Gr. It should be noted that the unique photoinduced modulation doping provides two obvious advantages for novel Gr electronics and optoelectronics. First, this technique offers incredible flexibility for control of doping by optical illumination, that is, different doping concentration and patterns can be easily written using light. They can be generated and erased at will. Second, because the dopants in *h*-BN are separated from the conducting channel (Gr) which prevents charge scattering, this doping mechanism can preserve the extremely high mobility typical of Gr/*h*-BN heterostructures.

Meanwhile, Chen et al. studied the thermoelectric transport characteristics across a Gr/*h*-BN/Gr heterostructure [145]. Through introducing a temperature gradient between the bottom and top Gr layers, a relatively large Seebeck coefficient of -99.3 μV/K was determined for the Gr/*h*-BN/Gr heterostructure. Such a negative Seebeck coefficient is due to the relatively smaller band offsets. This study is useful for understanding the thermoelectric characteristics

in emerging 2D heterostructures as well as for guiding the development of Gr/*h*-BN heterostructures-based optoelectronic devices working on photo-thermoelectric effect. Afterwards, Shiue et al. demonstrated on-chip high-speed photodetectors based on a 2D heterostructure consisting of single-layer Gr encapsulated by high mobility *h*-BN layers (80000 $cm^2V^{-1}s^{-1}$), which is coupled to the optical mode of a Si waveguide (Fig. 9e) [146]. This device exhibited a maximum responsivity of 0.36 AW^{-1} and ultrafast operation with a 3-dB cutoff at 42 GHz. The working mechanism relies mainly on the photo-thermoelectric effect at the metal/Gr junction, which could be concluded from the change of the sign of photocurrent at varied top-gate and source-drain voltages (Fig. 9f). The minimum time resolution was measured to be as low as 3 ps with the lowest required peak power of 67 mW, which is comparable to autocorrelators based on two-photon absorption of Si or III-V compound semiconductors. The fully integrated photodetector and autocorrelator, along with the Si-CMOS compatible fabrication technology, paves an avenue towards compact photonics integrated circuits for ultrafast measurement, mode locking, and other high-speed optoelectronic applications.

In summary, Gr/group III-V semiconductor hybrid heterostructures have found numerous applications in various optoelectronic devices. Table 1 summarizes the performance parameters of some representative Gr/group III-V semiconductors-based optoelectronic devices. Doping of Gr can enhance the light output power of Gr/GaN Schottky junction LEDs. Through a variety of optimizing techniques including gating or doping of Gr, antireflective layer coating, surface plasmon metallic NPs modification, interface engineering, *etc.*, the PCEs of Gr/GaAs Schottky junction solar cells can be significantly improved from the initial value of 1.95% to as high as 18.5%. On the other hand, photodetectors based on Gr/GaN hybrid heterostructures are highly sensitive to UV illumination with a UV-to-visible rejection ratio exceeding 10^3, whereas Gr/GaAs (InP, InAs) Schottky junction photodiodes are useful for NIR photodetection with responsivities typically less than 1 AW^{-1} and rapid response speeds even faster than 1 μs. Some effective strategies to improve photoresponse include using nanostructure arrays, exploiting LSPR effect of metallic NPs, and interface passivation. The ultra-flat and charged impurity-free h-BN surface can afford a high mobility up to 80000 $cm^2V^{-1}s^{-1}$ of *h*-BN encapsulated Gr, which provides a promising platform for implementation of high-speed Gr optoelectronic devices.

Gr/Group IV semiconductors

Elementary group IV semiconductors, in particular Si, are the most important materials in the semiconductor and microelectronics industries that have profoundly changed human's life in the past several decades [63]. Currently, Si is still dominating the commercial electronics and optoelectronics widely used in our daily life [63], while carbon materials, such as Gr and carbon nanotubes (CNTs) have already emerged as promising alternatives for next-generation electronic device applications [10,147]. In recent years, many group IV semiconductors have been integrated with Gr to form hybrid heterostructures, which have found extensive applications in various optoelectronics with novel device architectures and functionalities. In this section, we will review the recent progress in the development of optoelectronic devices based on Gr/group IV semiconductor hybrid heterostructures.

Gr/Other carbon nanomaterials

Low-dimensional carbon nanomaterials (*e.g.*, zero-dimensional (0D): fullerenes, QDs; 1D: CNTs; 2D: Gr) have attracted significant research interest in the past several decades due to their unique structural and physical properties [148,149]. These allotropes of carbon are composed entirely of sp^2 bonded graphitic carbon, whose highly delocalized electronic structure enables high carrier mobility for electronic applications. In addition, due to the reduced dimensions down to nanometer scale, their properties are strongly dependent on the atomic structures and the surrounding materials, which offers multiple degrees of freedom for customizing their electrical and optoelectronic characteristics. For example, it is feasible to tune the bandgap of semiconducting CNTs *via* control of their diameters. By this token, carbon nanomaterials have been considered as potential successors to conventional semiconductors such as Si in various electronic and optoelectronic applications[150]. Recently, benefiting from the rapid advances in synthesis, sorting and assembly techniques [148], different kinds of carbon nanomaterials have been integrated together to from hybrid structures, which usually exhibit superior physical properties than their individual components, and may hold great possibilities in future electronics and optoelectronics [151]. In this part, we provide a discussion on the optoelectronic applications of hybrid structures consisting of Gr and other carbon nanomaterials.

Gr/0D carbon nanomaterials

0D carbon nanomaterials, including graphite QDs, Gr QDs and C_{60}, have been deposited onto Gr through spin-coating or thermal evaporation approaches to form hybrid structures for high-performance phototransistors application [152–155]. For example, Chen et al. demonstrated an all carbon-based photodetector, where graphite QDs serve as the light harvesting material, Gr functions as fast carrier conduction path, and carbon conductive pastes are used as electrodes (Fig. 10a) [152]. Under light illumination, holes are transferred to the Gr, while electrons reside within QDs and act as an effective local gate to modulate the conductance of Gr through capacitive coupling. This led to a shift of the Dirac point voltage of Gr towards higher gate voltages at elevated illumination levels (Fig. 10b). The spatial separation of photocarriers thus effectively inhibits the electron-hole recombination and consequently prolongs their lifetimes. Meanwhile, the recirculation of holes through Gr channel within the lifetime of trapped electrons enables a high photoconductive gain. As a result, the devices exhibited an ultrahigh responsivity of 4×10^7 AW^{-1}, and a photoconductive gain as high as 3.75×10^9 under UV illumination. Afterwards, stretchable photodetectors consisting of Gr hybridized with Gr QDs were fabricated on a rippled PDMS [153]. Such a rippled geometry can overcome the native stretchability limit of Gr. The photoresponse depends highly on the external strain, and the photocurrent decreases gradually with increasing strains due primarily to the reduced optical absorption as a result of fewer multiple reflections of photons within the ripples. The maximum responsivity is ~800 AW^{-1}, which corresponds a photoconductive gain of 2.8×10^3 in the UV region.

Further photoresponse improvement has been achieved by assembling Gr/Gr QDs hybrid phototransistors on piezoelectric lead zirconate titanate [$Pb(Zr_{0.2}Ti_{0.8})O_3$] substrates, which can facilitate the separation and transport of photocarriers by providing a vertical polarization electric field [154]. It was found that this device exhibited an ultrahigh responsivity exceeding 10^9 AW^{-1}, corresponding to a gain of ~10^{10}, and ~10 times faster response speed. In addition, the high responsivity can be maintained over a wide range of illumination power and the value can be as high as 10^7 AW^{-1} even at laser power up to nanowatt level. Obviously, this exceptional good device is understandable considering the detrimental effects that limit the responsivity are suppressed, such as trapping of photocarriers at interfacial trap states and screening of the built-in electric field.

Recently, Gr NRs/C_{60} heterostructures photodetectors operating in mid-infrared (MIR) range (wavelength: 10 μm) at room temper-

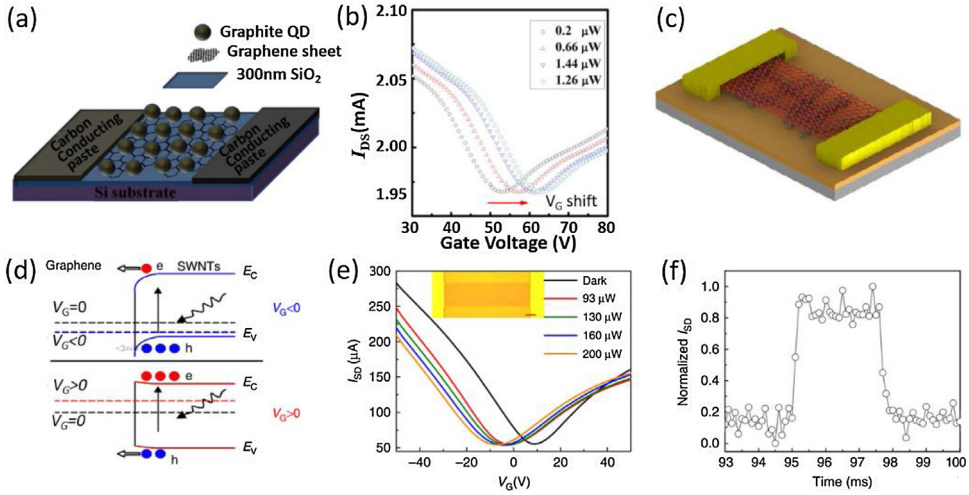

Fig. 10. (a) Structure of the all carbon phototransistor based on Gr/graphite QDs hybrid heterostructure. (b) Transfer characteristics of the device under illumination of various light intensities. Reprinted with permission from Nature Publishing Group. [152] (c) Structure of the Gr/CNTs hybrid phototransistor. (d) Energy band diagram of the phototransistor at various gating voltages. (e) I_{ds} vs V_g curves under different light intensities. (f) Transient photoresponse of the Gr/CNTs photodetector. Reprinted with permission from Nature Publishing Group. [169]

ature have been reported [155]. Unlike the above discussed cases, the 10 nm wide Gr NR with an opened bandgap of ~100 meV served as both the light absorption media and carrier transport channel. What is more, the key role the C_{60} plays is to trap photogenerated electrons at its defect states so as to increase carrier recombination lifetime in Gr and give rise to a higher photocurrent. As a consequence, the devices reached a responsivity of 0.4 AW^{-1}, which represents one order of magnitude improvement over devices made from pure Gr NRs. Besides, multiple-layer Gr QDs have been incorporated into two Gr layers to form a hybrid photodetector working in a broad spectral range from the UV to NIR [156]. The devices exhibited asymmetric and nonlinear *I-V* characteristics that can be ascribed to the tunneling of charge carriers through the available density of states of Gr QDs between the metallic Gr layers. The device demonstrated a pronounced photoresponse with a maximum responsivity of ~0.5 AW^{-1}, a linear dynamic range (LDR) of ~95 dB, and a fast response speed less than 100 μs.

Gr/1D carbon nanotubes

CNTs are novel materials with appealing physical and chemical properties [157,158]. They can be either metallic or semiconducting depending on their individual chiral vector [159]. Metallic CNTs are particularly useful as transparent conductors, while semiconducting CNTs are promising candidates as channel materials in FETs for electronic applications. In addition, CNTs also hold great promise for novel optoelectronic devices due to their unique optical properties, such as direct bandgap depending on the diameter, strong optical absorption and emission, large radiative lifetimes (up to 100 ns) and fluorescence lifetimes (up to 100 ps) at room temperature and so on. Their optical properties are especially sensitive to the environment and external fields because of the single atomic layer structure, which allows for controlled modification of their optical properties [159].

Gr/CNTs hybrids have been successfully produced *via* various methods including CVD techniques, self-assembly or other solution-based methods [160–163]. One of their most important optoelectronic applications is photovoltaic devices, where they usually serve as transparent conducting electrodes for efficient charge collection and sufficient optical transmittance. Since this topic has been extensively discussed in many recent review papers [12,151,164–166], we will not cover it here and only introduce the photodetector application of Gr/CNTs hybrids. In early studies, Gr/CNTs hybrids such as stacked Gr/CNTs (SG/CNTs) and Gr flakes-multiwall CNT mixtures, have been successfully prepared.[167,168] It was observed that individual SG/CNT is very sensitive to 633 nm illumination with a responsivity of ~0.05 mAW^{-1} [167]. On the other hand, Gr flakes-multiwall CNT mixtures often exhibit an improved photoresponse compared with pure CNT films, benefiting from the enhanced exciton dissociation through heterojunctions formed at Gr/CNTs interfaces [168]. The devices demonstrated nearly one order of magnitude increase in responsivity and 5-fold improvement in specific detectivity under NIR light (1-1.3 μm). In order to enhance photoresponse, Liu et al. designed broadband phototransistors consisting of a Gr film onto an ultrathin layer of single-wall CNTs (Fig. 10c) [169]. The working mechanism relies on a pronounced photogating effect. (Fig. 10d). That is, the electrons are transferred to the Gr channel and holes are trapped in the CNTs. The trapped holes effectively modulate the channel conductance, leading to a continuous negative shift of the Dirac point voltage under increasing illumination (Fig. 10e). Moreover, the built-in potential can be effectively tuned by adjusting Gr Fermi level, leading to a tunable photocurrent and responsivity under different back-gate voltages. The responsivities under 650 and 1550 nm are estimated to be ~120 and ~40 AW^{-1} respectively. Furthermore, the device exhibited a fast response speed of ~100 μs (Fig. 10f), and a gain-bandwidth product of ~1×10^9 Hz.

More recently, Luo et al reported a Gr/CNT thin film photodiode [170], whose working mechanism is different from that of the phototransistors discussed above. Upon illumination, photocarriers near the interface are separated by the built-in potential. Electrons and holes are collected by respective electrodes and forms photocurrent in external circuit. The device displays broadband sensitivity from 300-1100 nm. The I_{light}/I_{dark} ratio, responsivity and specific detectivity can reach 240, 209 mAW^{-1} and 4.87×10^{10} Jones, respectively, superior to other CNTs photodetectors. What is more, the devices also exhibited a fast response rate, with rise/fall times of 68/78 μs and a 3dB bandwidth of 5400 Hz. The results presented in these studies suggest that Gr/CNT hybrids hold promising applications in future optoelectronic devices and system, especially in high-performance broadband photodetectors.

Gr/2D carbon materials

Apart from 0D and 1D carbon nanomaterials, also 2D fluorine-functionalized Gr derivative (fluoro-Gr) has been combined with Gr to form hybrid heterostructure phototransistors [171]. The van der

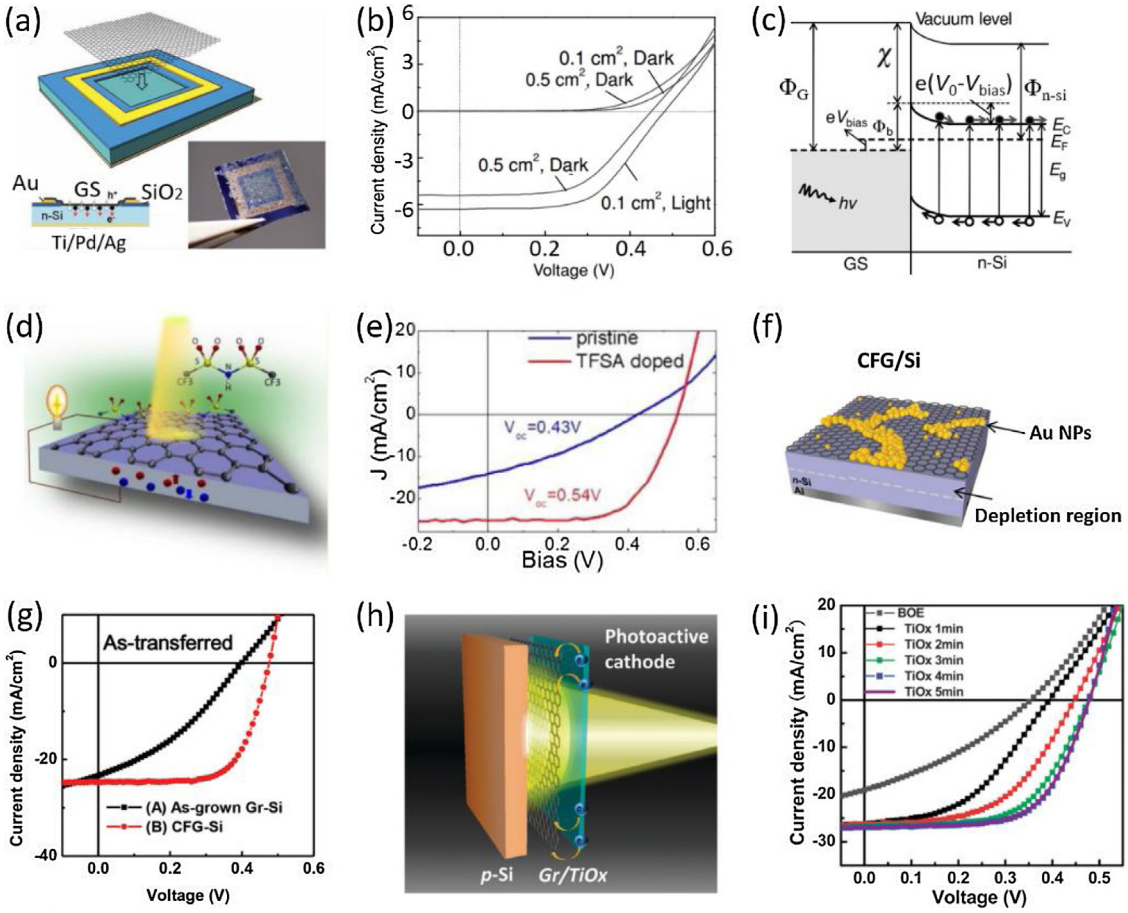

Fig. 11. (a) Schematic illustration of Gr/Si solar cell. Left bottom side: schematic of the cross-section of the device; right bottom side: optical image of the device. (b) *J-V* curves of the device under AM 1.5 G illumination. (c) Energy band diagram of the device under light illumination. Reprinted with permission from Wiley-VCH. [27] (d) Schematic illustration of a Gr/Si solar cell doped by TFSA layer, and the separation of photocarriers in the device. (e) *J-V* curves of the device. Reprinted with permission from American Chemical Society. [197] (f) Schematic of the Au NPs decorated Gr/Si solar cell. The dashed line represents the depletion region at the Gr/Si interface. (g) *J-V* curves of the device. Reprinted with permission from Wiley-VCH. [201] (h) Schematic of the TiO_2/Gr/Si solar cell. (i) *J-V* curves of the device at different illumination times. Reprinted with permission from the Royal Society of Chemistry. [209]

Waals heterostructure of Gr and fluoro-Gr was obtained through fluorinating multilayer Gr. The adsorption of fluorine atoms on Gr surface leads to the rehybridization of the carbon atoms from trigonal sp^2 to tetragonal sp^3 bonds, which opens the bandgap of the fluoro-Gr. When the heterostructure is shined by illumination, the electrons in the π state can be excited to form electron-hole pairs. These electrons are then trapped due to the presence of quantum confinement and localized states in the π-π^* gap, whereas the holes are driven to the Gr channel by the built-in potential at the heterostructure interface, giving rise to the photocurrent. The devices reached a maximum responsivity exceeding 10^3 AW^{-1}, which is more than 3 order of magnitude higher than that of Gr photodetectors. In addition, the heterostructures can realize broadband photodetection from the UV (255 nm) to MIR (4.3 μm). The photoresponse characteristics can be further optimized by controlling the degree of fluorination on the heterostructures, in terms of the nature of sp^3 sites and the size and fraction of sp^3/sp^2 domains.

Gr/Si

Si is the most dominant material for commercial electronics and optoelectronics extensively used in our daily life, due to its a variety of beneficial features [63,172,173], such as the rich abundance, high carrier mobility, high stability and non-toxicity, and so on [174,175]. As the efficiency of traditional Si solar cells has already reach a high level (crystalline Si solar cells: $26.7 \pm 0.5\%$) [176], the development of photovoltaic technologies begins to focus on material use and manufacturing complexity and cost, which set the criteria for commercialization. Because of the indirect bandgap property of single-crystalline Si, Si solar cells need thick material usage (typically hundreds of micrometers) to guarantee sufficient sunlight absorption. In addition, the fabrication of traditional Si solar cells usually requires complex manufacturing processes and expensive equipment. As a result, the cost of Si photovoltaics is still very high at current stage. Recently, the combination of Gr with Si has led to a new type of Schottky junction solar cells with simple device design, easy and cost-effective fabrication processes [13,177,178]. Compared with metal or ITO electrodes normally used in Schottky solar cells, CVD-Gr electrodes possess the remarkable advantages of low cost, easy fabrication, and mechanical flexibility. More importantly, their efficiencies have increased rapidly from the initial value of 1.65% to 15.6% in only 5 years [177]. In this section, we will review the recent advances in the optoelectronic devices of Gr/Si heterostructures, with emphasis on solar cells and photodetectors application.

With the rapid development of high-quality CVD-Gr and inspired by the previous research on carbon/Si heterojunction solar cells [177,179], Li et al. firstly presented Gr/Si Schottky junction solar cells, which exhibited a rectifying behavior in dark and a pronounced photovoltaic effect under illumination (Fig. 11a and b) [27]. Notably, the Gr layer serves as not only a transparent electrode, but also as an active layer for electron-hole separation

and hole transport (Fig. 11c). Without optimization, the PCE is only 1.65%, which is too low to meet the requirement for practical applications. In order to improve the device efficiency, a great deal of efforts in the following aspects have been made [180]. (1) Doping or layer number tuning of Gr that can adjust its work function, sheet resistance, as well as optical transparency. (2) Interface passivation and band engineering schemes to increase the Schottky barrier height and reduce recombination of photocarriers. (3) Light management for enhanced absorption such as using Si nano/microstructure arrays to replace planar Si, antireflective layer, or plasmonic nanostructures. Normally, these schemes are combined together to eventually realize a high-efficiency Gr/Si solar cells. In addition, some novel conceptual devices such as Gr/Si flexible solar cells, Gr QDs/Si solar cells, Gr related hybrids/Si solar cells, have also been adopted.

Doping or layer number tuning of Gr

In Gr/Si solar cells, the built-in electric field is determined by the work function difference between Gr and Si. However, pristine Gr is usually characterized by a low work function (~4.5 eV), which leads to a low Schottky barrier height [181]. In addition, the Gr/Si device has a large series resistance because of the relatively large sheet resistance (normally hundreds of $\Omega \cdot sq^{-1}$) for pristine single-layer Gr [182]. Apparently, both factors are detrimental to conversion of light to electricity. Increasing layer number proved to be an efficient way to increase the work function and conductivity. Normally, an optimal layer number of 3-5 layers is chosen in view of the trade-off between the sheet conductivity and optical transmittance in Gr/Si solar cells [183–186]. In addition, chemical doping is also an equally important approach to increase work function and conductivity of Gr. To date, various dopants have been employed to dope Gr, such as acids [183–185,187–196], polymer [190,197], metallic nanostructures (NWs or NPs) [28,192,198–204], $SOCl_2$ [189,192,193,205], H_2O_2 [193], boron [206], ionic liquid [207], NiO [208], and so on. Among these dopants, HNO_3 is the most widely used for the pronounced doping effect and ease of operation. Xie et al. have studied the HNO_3 doping effect on the photovoltaic performance of Gr/Si solar cells. Once treated with HNO_3, the PCE was observed increased substantially from 4.42 to 9.70% [185]. It should be noted that, although this doping technique proves very efficient, the stability is a big problem. The photovoltaic parameters decrease quickly, even within only a few minutes after removing the HNO_3 vapor. Therefore, stable dopants for Gr doping after which the doping effect can be furthest retained for a long period need to be urgently developed.

Trifloromethanesulfonic acid (TFSA), an organic polymer is ideal dopant for stable doping of Gr due to its non-volatile property (Fig. 11d) [197]. It has been reported that spin-coating TFSA onto pristine Gr/Si junctions can increase the J_{sc}, V_{oc}, and *FF* from 14.2 to 25.3 mA/cm^2, 0.43 to 0.54 V, and 0.32 to 0.63, respectively, boosting the PCE from 1.9 to 8.6% (Fig. 11e). The improvement is mainly attributed to the increased Gr carrier density and enhanced built-in potential of the Schottky junctions. Moreover, solar cells doped with TFSA exhibited a more stable performance improvement, due to the hydrophobic nature of TFSA, as compared with devices doped with volatile acids.

In addition to organic polymers, gold nanostructures formed by reducing $AuCl_3$ with nitromethane are another alternative stable dopants for Gr [199]. The doping can effectively increase the work function and sheet conductivity of Gr, resulting in an increase of PCE from 6.02 to 10.40%. In this case, the photovoltaic performance are more stable than the devices doped with volatile oxides such as HNO_3 and $SOCl_2$. The devices can retain a PCE of 7.42% even after 3 months storage in air without any encapsulation, suggesting great potential of metallic nanostructures doping for realizing long-term, air-stable Gr/Si solar cells. Recently, Ho et al. have proposed a novel approach for doping Gr with Au NPs *via* a simple reduction-oxidation reaction between the Cu substrate and $HAuCl_4$ (Fig. 11f) [201]. The doped Gr films exhibited superior electrical properties in Gr/Si solar cells. This doping method not only remarkably improved the sheet conductivity, but also substantially reduced contact series resistance. Moreover, Au NPs at the cracks can form excellent Schottky junctions with Si, and therefore the depletion region at the Gr/Si interface would become more uniform. As a result, the PCE increased from 3.3 to 7.9% by employing the Au NPs doped Gr electrodes (Fig. 11g), and finally to 12.3% by combing TFSA doping.

Besides chemical doping, photo-induced doping and electric field gating doping of Gr have also been employed to improve the performance of Gr/Si solar cells [209,210]. As an example, Ho and colleagues have developed *n*-Gr/*p*-Si Schottky junction solar cells using a novel "sunlight-activated" Gr/TiO_x-heterostructure transparent electrode (Fig. 11h) [209]. The coating of TiO_x thin film results in the improved built-in potential and decreased series resistance in Gr/Si solar cells. As a consequence, the devices exhibited a continual increase in V_{OC} and *FF* under illumination for up to 4 min, until all the trap states within TiO_x were completely filled (Fig. 11i). Correspondingly, the PCE increased substantially from the initial value of 2.2% to 8.2%, and further to 10.5% with a PMMA antireflective layer coating.

Interface passivation and band engineering

In spite of the achievement of high efficiency through Gr doping techniques mentioned above, the PCE of Gr/Si solar cells is still hampered by high carrier recombination velocity at Gr/Si interface due to not only the presence of a large number of dangling bonds and defect states at the surface of unpassivated Si, but also the relatively low Schottky barrier (~0.6-0.7 eV of the Gr/Si in contrast to ~1.1 eV for Si p-n junctions), which leads to a large current leakage and consequently a low V_{OC}. Conventional Si solar cells usually employ a relatively thick insulating layer such as Si_3N_4, SiO_2, or Al_2O_3 to passivate the surface of Si [211]. Unfortunately, these materials are not suitable for Gr/Si solar cells as the thick insulating layer will prevent the efficient transport of photocarriers. To this end, an methyl (CH_3) group was used to effectively saturate the defect states at Si surface [185]. It was found that the CH_3-modified devices exhibited a much higher photovoltaic performance as compared to control devices made of H-Si and SiO_2-Si, suggesting effective passivation effect of CH_3-modificaiton. In addition to surface passivation, CH_3-modification can greatly affect the surface electron affinity of Si [183]. The offset of surface electron affinity for CH_3-Si can be +0.35 eV, in contrast to -0.12 eV for H-Si, and the value could be further increased to as high as +0.65 eV *via* additional Pt nanodots modification. Recently, Jiao et al tried to grow carbon nanowalls (CNWs) onto the Si surface in an effort to passivate the surface dangling bonds in Gr/Si solar cells [212]. During the growth, the hydrogen plasma can activate the Si surface to release more nucleation sites, and C_xH_y ions combine with unsaturated Si bonds to form SiC and O-Si-C bonds. Device characterization revealed that the solar cells modified with CNWs and an antireflection layer coating had a PCE as high as 8.9%.

In order to minimize current leakage in Gr/Si solar cells, Xie et al. employed an organic P3HT as an interfacial layer in Gr/Si solar cells (Fig. 12a) [185]. The optimal thickness was ~10 nm in light of the trade-off between film coverage, carrier transport and optical loss. This special geometry had a large barrier for electron transport from Si to Gr and therefore minimizes electron recombination due to the large E_C-LUMO offset. Meanwhile, the small E_V-HOMO offset can facilitate efficient transport of holes from Si to Gr (Fig. 12b). Therefore, the introduction of P3HT as an electron blocking layer greatly reduced the current leakage, which gave rise to an enhanced PCE from 4.24 to 9.70% (Fig. 12c). With the assistance of Gr doping and Si surface passivation, a solar cell with PCE as high as 10.56% was finally achieved.

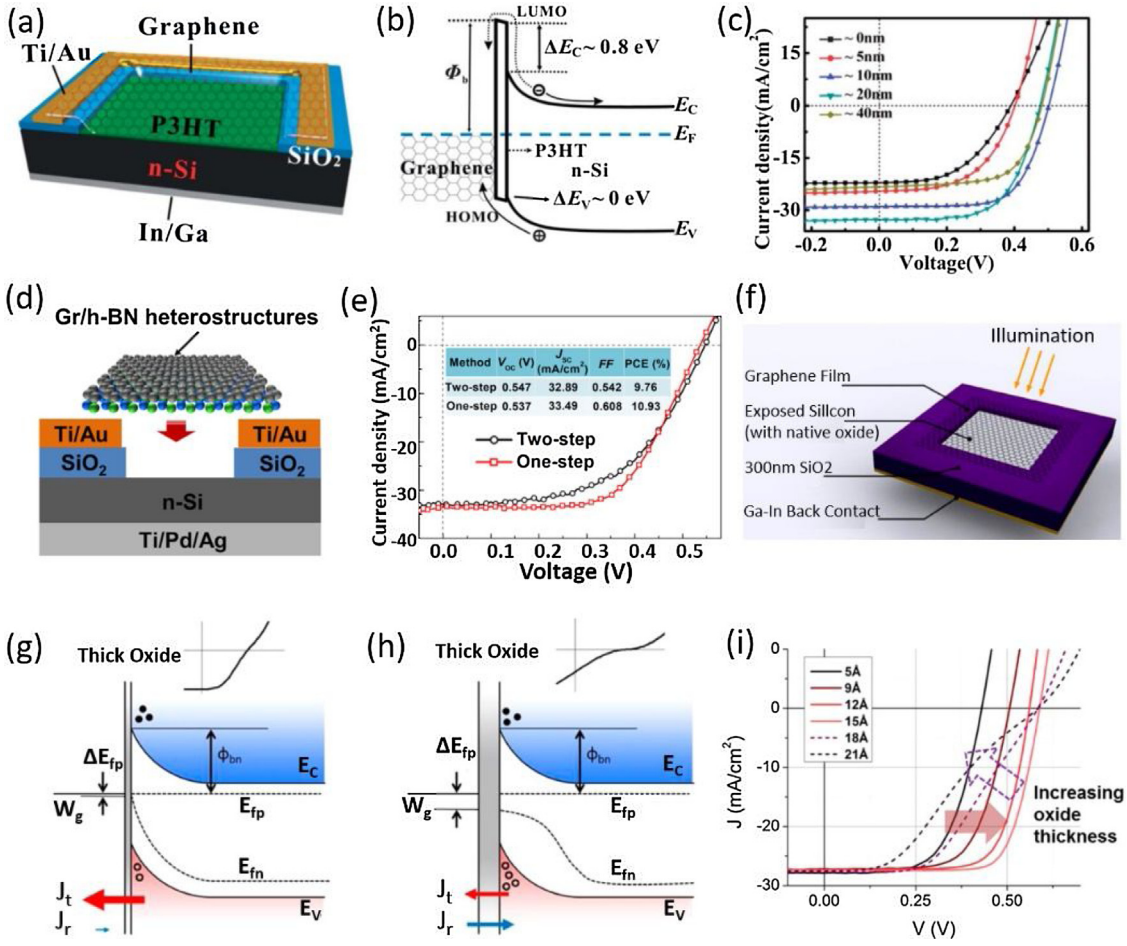

Fig. 12. (a) Schematic of the Gr/Si solar cell with P3HT electron blocking layer. (b) Energy band diagram of the heterojunction with P3HT layer. (c) *J-V* curves of the devices with different P3HT thicknesses. Reprinted with permission from the Royal Society of Chemistry. [185] (d) Schematic of Gr/*h*-BN/Si solar cell by one-step method. (e) Comparison of *J-V* curves of the devices under light illumination. Reprinted with permission from Elsevier B.V. [215] (f) Schematic of the Gr/Si device with interfacial oxide layer. Energy band diagrams of a Gr/Si heterojunction with (g) a thin oxide layer, and (h) a thick oxide layer. (i) *J-V* curves of the solar cells with various oxide thicknesses. Reprinted with permission from American Chemical Society. [28]

Besides organic layers, inorganic Gr oxide (GO), 2D MoS_2, 2D *h*-BN and native oxide have also been incorporated into Gr/Si solar cells [28,195,213–215]. Yang and co-workers have lately studied the effect of the GO thickness on photovoltaic performance [213]. It was revealed that the GO interlayer can effectively increase the V_{OC} because of improved barrier height. Meanwhile, the GO interlayer modifies the electronic states at the Gr/Si interface from deep levels to shallow levels, leading to reduced recombination probability of electrons. Consequently, without other optimization, the PCE increased by 3-4 times to 6.18%. A similar effect was also observed by Jiao et al. [195]. In their work, the authors found that the GO can be regarded as a *p*-doped thin layer, in which holes were efficiently injected and transported, resulting in a dramatic improvement in PCE. Eventually, a high PCE of 12.3% was obtained through chemical doping of Gr and antireflection layer coating.

2D layered materials represent a new class of building blocks for optoelectronic applications with new functionalities [216,217]. Tsuboi and colleagues demonstrated a Gr/Si solar cells with an optimized PCE of 11.1% by inserting MoS_2 as an electron-blocking/hole-transporting layer [214]. The interface carrier recombination is greatly suppressed, leading to a remarkably increased V_{OC}. Moreover, the thin MoS_2 layer can lead to a thicker depletion region in Si, which is also important to the high PCE. Recently, Meng et al. found that few-layer *h*-BN can act as an effective electron-blocking/hole-transporting layer in Gr/Si solar cells as well (Fig. 12d) [215]. The *h*-BN in the device can not only suppress interface carrier recombination, but also reduce the series resistance of the devices. Furthermore, the directly grown Gr/*h*-BN heterostructure can also avoid unfavorable interface defects and contamination. As a consequence, a PCE of 10.93% was demonstrated by further doping of Gr with Au NPs and HNO_3 (Fig. 12e).

Song and co-workers have studied the role of native Si oxide in Gr/Si solar cells (Fig. 12f) [28], in which the photocurrent was determined by a balance between tunneling and recombination. When the native oxide getting thicker, recombination dominates over tunneling, leading to a reduced *FF* (Fig. 12g and h). However, chemical doping of Gr can improve its work function and reduce carrier recombination, giving rise to an improved *FF* for oxide thickness less than 1.5 nm. In addition, when the oxide thickness increases from 0.5 to 1.5 nm, the reverse saturation current decreases by several orders of magnitude, which results in higher V_{OC} for devices with thicker oxides (Fig. 12i). Based on these understandings and the co-optimization of chemical doping of Au NPs and a TiO_2 antireflection layer coating, the authors have achieved a record efficiency of 15.6% for Gr/Si solar cells.

Most recently, Ding et al. have developed a scheme to improve the efficiency of Gr/Si solar cells by introducing a *p*-type MoO_3 layer [218]. Due to the huge contrast in Fermi level, the MoO_3 will induce a *p*-type inversion layer through spontaneous hole injection from the MoO_3 to *n*-Si. Such a *p*-type inversion layer can cause energy band bending near the Si surface, which greatly improves the effective barrier height for efficient separation/transport of

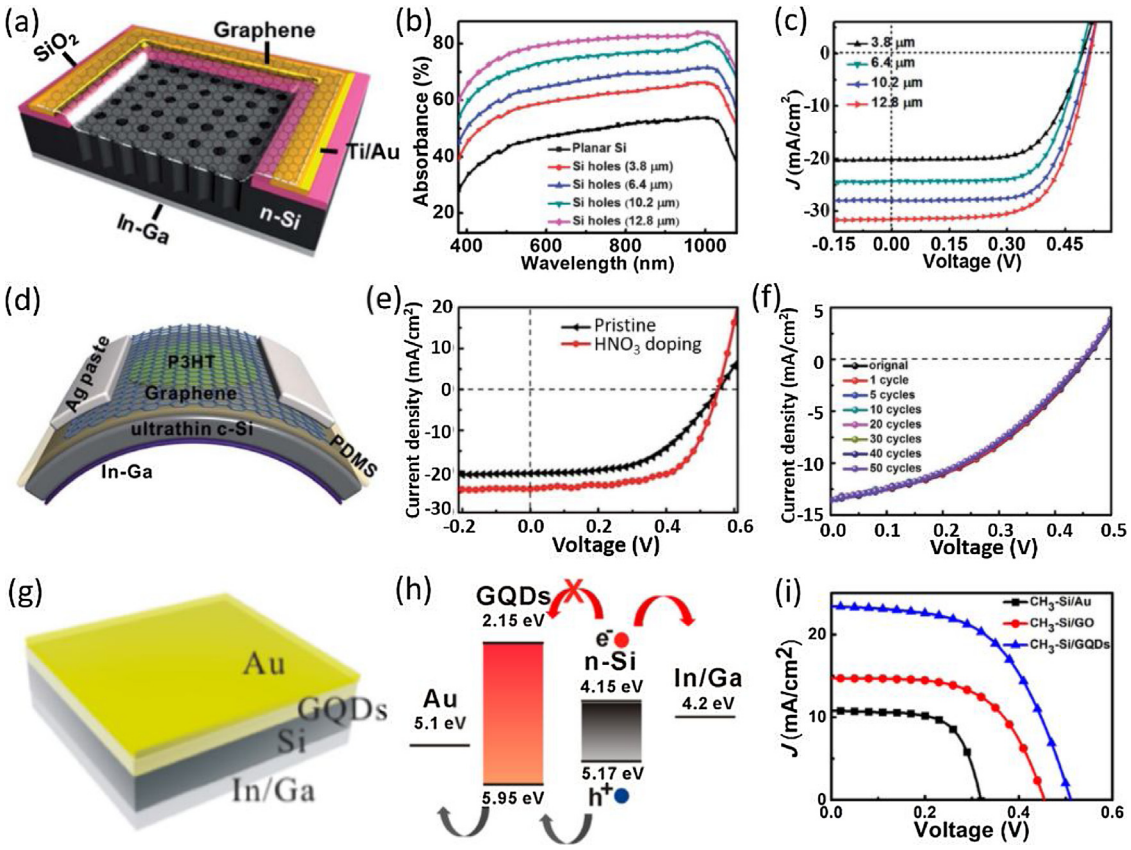

Fig. 13. (a) Geometry of the Gr/SiMH arrays heterojunction solar cell. (b) Absorption of the SiMH arrays with different hole depths. (c) *J-V* curves of the Gr/SiMH arrays solar cell with different hole depths. Reprinted with permission from the Royal Society of Chemistry. [199] (d) Schematic of the flexible Gr/ultrathin Si solar cell. *J-V* curves of the flexible solar cell (e) with and without HNO_3 treatment, and (f) under various bending cycles. Reprinted with permission from the Royal Society of Chemistry. [196] (g) Schematic of the Si/GQDs solar cell. (h) Energy band diagram of the heterojunction. (i) Comparison of *J-V* curves for devices based on Si/Au, Si/GO and Si/GQDs structures. Reprinted with permission from American Chemical Society. [235]

photocarriers, and contributes to the suppression of surface recombination. On the other hand, defect energy levels within the energy band of MoO_3 can allow effective transport of holes through the MoO_3 layer to Gr. The introduction of such a metal oxide, along with the Gr doping and antireflection layer coating, leads to a PCE as high as 12.2%.

Light management in Gr/Si solar cell

Further performance improvement is greatly restricted by the large optical absorption loss since planar Si usually exhibits strong light reflection across the entire UV-Vis-NIR spectrum [172]. Therefore, various nano/microstructure arrays have been widely explored for enhanced light harvesting in various optoelectronic devices [70,219,220]. A solar cell with improved J_{SC} due to enhanced light absorption has been reported by using vertical SiNW array and Gr [188,205]. However, the PCEs are less than expected in the early studies due primarily to the inefficient carrier separation and strong surface recombination. To address this problem, Zhang et al. have optimized Gr/SiNW array solar cells *via* Si surface passivation and interface energy band engineering [183]. In the work, Si nanohole (SiNH) arrays were employed simply because they can guarantee larger effective junction areas and better contact with Gr. Through further chemical doping of Gr, PCEs of 8.71% and 10.30% were achieved for Gr/SiNW and Gr/SiNH arrays solar cells, respectively. In view of the harmful effect of the high surface states density of the SiNH arrays may have on device performance, Si micro-hole (SiMH) arrays with much smoother surface were then adopted for assembling solar cell (Fig. 13a).[199] The light absorption capability can be tuned by adjusting the depth of the SiMH arrays through controlling the etching time, as shown in Fig. 13b. It is also feasible to adjust the diameter and periodicity of the holes by using photolithography masks with different shapes and sizes. Together with further Gr doping utilizing Au NPs, a PCE of 10.40% was obtained for devices made of 12.8 μm thick SiMH array (Fig. 13c). Attempts using other Si nano/microstructures as light harvesting layers have also been reported in Gr/Si solar cells with enhanced performance, such as structured macroporous Si [221], pyramidal Si [222–224], and Si pillar arrays[187,190,192]. In addition, solar cells based on Gr NB/multiple SiNWs junctions have been realized, suggesting great possibility for miniaturization of such solar cells for future nano-optoelectronic applications [225].

Reducing sunlight absorption loss by antireflection layer is an efficient and widely used technique in conventional Si solar cells [226]. Shi et al. have spin-coated a colloidal TiO_2 NPs film (typical thickness: 50-80 nm) onto Gr/Si solar cells as antireflection layer [194]. The optical reflectance of the solar cells drastically decreased from 40% to 10% in the visible region, indicating strong antireflection effect. As a consequence, the J_{SC} increased significantly from 23.9 to 32.5 $mAcm^{-2}$, giving rise to a high PCE of 14.5%. In addition, organic polymers such as PMMA and CYTOP have also been employed as effective antireflection layers in Gr/Si solar cells, as recently reported in some literatures[212,227].

Another important method is to utilize SPR effect of metallic nanostructures, which have proved to be efficient for controlling over light's propagation and absorption in various optoelectronic devices [228]. Luo and colleagues presented improvement in the efficiency of Gr/Si solar cells by decorating Au NPs [204]. Theoretical simulations revealed that Au NPs can induce strong light scattering,

leading to enhanced optical absorption within Si, which accounts for the improved J_{SC}. As a result, the PCE was improved from 6.39 to 10.15%.

Novel conceptual devices

Flexible Gr/Si solar cells have recently attracted increasing attention for their potential application in varied emerging areas such as wearable electronics and artificial eyes.[229] Bendable ultrathin Si films are usually obtained by etching bulk Si wafers in KOH solution [196,230], or *via* a kerf-less exfoliation process from parent bulk Si substrates [231]. Direct transfer of Gr onto these ultrathin Si films can lead to highly flexible solar cell (Fig. 13d). Through various optimization, a PCE of 8.42% was achieved for 40 μm thick Si-based solar cells (Fig. 13e) [196]. In a similar work, Jiao et al. have attained a PCE of 5.09% for 10.6 μm thick Gr/Si solar cells with a PMMA antireflection layer [230]. More importantly, these devices exhibited excellent flexibility and mechanical durability. Their photovoltaic performance is almost invariant of the bending even after tens of cycles of bending (Fig. 13f). More recently, Ahn and colleagues demonstrated flexible solar cells based on Gr/insulator/Si heterojunctions, in which Al_2O_3 interlayer can passivate Si surface and simultaneously acts as a tunneling barrier for holes, reducing the carrier recombination [231]. An optimal PCE of 7.4% was obtained for device made of 35 μm thick Si. It should be noted that the PCEs are much inferior to conventional Gr/Si solar cells, which is probably attributed to the reduced light absorption in thinner Si films [196].

Gr QDs with a size less than 30 nm possess a tunable bandgap which is necessary for efficient photocurrent generation [18,232]. This optoelectronic property, along with the large abundance and non-toxicity nature, renders Gr QDs promising light absorber or carrier transport material for efficient photovoltaic applications [233,234]. Gao et al. presented a new type of solar cell based on Gr QDs/Si heterojunctions (Fig. 13g) [235]. Thanks to the appropriate band alignment, the heterojunction can effectively separate the photocarriers. Meanwhile, the QDs serve as an electron blocking layer for suppressing interface carrier recombination (Fig. 13h). With optimized QDs size and layer thickness, the devices reached a preliminary PCE of 6.63%, superior to control devices without Gr QDs or with a Gr oxide layer (Fig. 13i). Further efficiency improvement is achievable by using a Gr electrode which ensures both efficient light absorption and carrier collection [236]. Upon optimization, a maximum PCE as high as 12.35% can be achieved. In addition, this kind of devices can retain the high performance with only a slight degradation of ~13% after storage in air for 6 months.

Gr related hybrids including Gr-amorphous carbon films [237], Gr woven fabrics (GWFs) [207], and Gr-carbon nanotubes (CNTs) composites [238,239], have also been integrated with Si for high-efficiency solar cells. Except for an early report based on Gr-amorphous carbon films, the majority of the above devices usually exhibited high PCEs exceeding 10%. For example, Li et al. have transferred GWFs onto *n*-Si to form Schottky junctions, where a polyvinyl alcohol (PVA) based solid electrolyte was embedded [207]. Similar to Gr, GWFs also acted as transparent window electrodes for charge transport and collection. It was found that the solid electrolyte served as three roles simultaneously: an antireflection layer, a chemical modification carrier, and a photoelectrochemical channel. By further doping of Gr, a PCE of 11.03% was achieved for this type of solar cells. Recently, Shi and co-workers demonstrated Gr-CNTs composite/Si solar cells, where a bi-continuous structure consisting of an interconnected CNT spider-web uniformly embedded in Gr film was employed as a transparent electrode [239]. The co-existence of both Gr/Si and CNT-Si junctions contributed to the improved photovoltaic performance. Through co-optimization by chemical doping and antireflection layer coating, the devices reached a PCE as high as 15.2%, which represents oen of the highest values among Gr/Si solar cells.

Photodetectors

Taking advantage of the strong photovoltaic effect, Gr/Si heterostructures have also been widely used for photodetection. Similar to Gr/Si solar cells, light absorption mainly takes place in Si, whereas Gr serves as an electrode for efficient carrier transport and collection. Early studies showed that Gr/Si Schottky junctions were very sensitive to a broadband wavelength [240–242]. The devices usually exhibited a high I_{light}/I_{dark} ratio exceeding 10^4, with responsivities approaching tens of to hundreds of mAW^{-1} and response speeds in sub-millisecond scale. For instance, An et al. presented Gr/Si Schottky junction photodetectors, which can operate in both photovoltage and photocurrent modes (Fig. 14a) [240]. It was found that the device can detect very weak signal with a photovoltage responsivity higher than 10^7 VW^{-1} and a noise-equivalent power reaching ~1 $pWHz^{-1/2}$ in photovoltage mode (Fig. 14b). In photocurrent mode, the voltage can effectively adjust the Fermi level of Gr, which controls the number of available states for injection of photogenerated holes from Si under illumination (Fig. 14c). This property allows voltage-tunable responsivity up to 435 mAW^{-1}. In addition, the devices can operate properly over a large dynamic range of six orders of magnitude.

On the other hand, optical absorption can occur in Gr as well, even though single-layer Gr absorbs only ~2.3% of incident light [14]. The gapless and semi-metallic nature of Gr renders it a promising material for broadband photodetection from the THz to UV wavelengths. Due to the fast carrier separation enabled by the presence of a built-in electric field, the Gr/Si Schottky detectors do not suffer from an ultra-short lifetime of photocarriers under 1550 illumination [243]. As a result, the device reached a responsivity of 2.8 mAW^{-1}, corresponding to an internal quantum efficiency (IQE) of 10%, much higher than that of regular Schottky junctions (~1%). It is undeniable that the responsivity is at least 1-2 orders of magnitude lower than the values at visible-NIR region, due to the weak light absorption and relatively short carrier lifetime in Gr.

Enlightened by the various device optimization techniques developed in Gr/Si solar cells, many efforts have been devoted to improving the performance of Gr/Si photodetectors by using plasmonic materials or Si nanostructures array as light absorbing media [244–247]. For instance, Luo et al. reported a high-performance NIR photodetector based on Gr/SiNW arrays decorated with Au NPs [244]. In comparison with planar Si-based detectors, the devices exhibited a much improved photoresponse with a I_{light}/I_{dark} ratio of up to ~10^6, a responsivity of 1.5 AW^{-1} and a specific detectivity of ~10^{14} Jones. The improvement is ascribed to enhanced optical absorption resulting from the strong light trapping effect of SiNWs arrays and surface plasmon polaritons (SPPs) excitation and coupling in the Au NPs. Functionalization of MoO_3 layer on Gr can also induce a significant performance enhancement for Gr/Si photodetectors [248]. Such a surface charge transfer doping will improve the Gr/Si Schottky barrier and reduces the series resistance. Therefore, the separation and collection of photocarriers would be facilitated, giving rise to an improved photoresponse with a responsivity of ~400 mAW^{-1}. By introducing a thin interfacial oxide layer, the dark current can be reduced by two orders of magnitude at zero bias [249]. Consequently, a high specific detectivity of 5.77×10^{13} Jones, along with a high responsivity of 0.73 AW^{-1} and a I_{light}/I_{dark} ratio as high as 10^7 was achieved.

Comparatively, the Gr/Si photodetectors is weakly sensitive to UV light, due to severe absorption and recombination at the front surface. TiO_2 layer [250] and an Al_2O_3 anti-reflection layer [251] have been employed to enhance the photoresponse in UV region. Wan et al. observed that Gr can enhance the UV detection ability of Si Schottky photodetectors due to the long carrier lifetime of hot

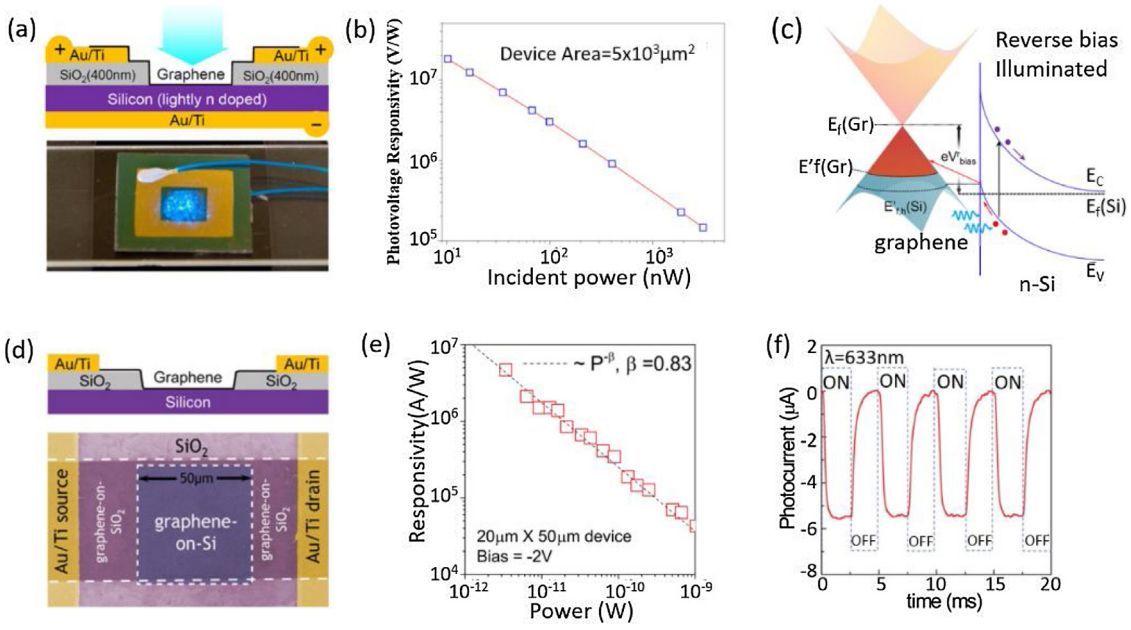

Fig. 14. (a) Schematic and digital photograph of the Gr/Si heterojunction photodiode. (b) Photovoltage responsivity as a function of incident power. (c) Energy band diagram of the Gr/Si heterojunction at reverse bias voltage. Reprinted with permission from American Chemical Society. [240] (d) Schematic illustration and SEM image of the Gr/Si heterojunction in photoconductor mode. (e) Responsivity as a function of light power at 488 nm. (f) Time-dependent photoresponse under 633 nm. Reprinted with permission from American Chemical Society. [252]

carriers in Gr [251]. The ultra-shallow junction at Gr/Si interface, together with the strong built-in electric field, also facilitates rapid separation of photocarriers and reduces surface recombination activity. After further coating with Al_2O_3 antireflection layer, the detectors exhibited superior performance in terms of a responsivity of 0.14 A W^{-1}, a I_{light}/I_{dark} ratio of 1.2×10^6, a specific detectivity of 1.6×10^{13} Jones, and an IQE of 100%.

Gr/Si photodetectors can also operate in photoconductor mode, in which photocarrier collection is accomplished by two metallic electrodes deposited on opposite sides of Gr (Fig. 14d) [252]. The working mechanism relies on the efficient separation of photocarriers by the strong built-in electric field at Gr/Si interface, and electrons are swept into and trapped within Si while holes are swept into Gr. The swept holes can survive much longer than intrinsically photocarriers within Gr, which can overcome the detrimental effect arising from the ultra-short lifetime of photocarriers in Gr that usually results in a low responsivity in Gr-based photodetectors [14]. On the other hand, the high carrier mobility of Gr can cause a high photoconductive gain because of the rapid transport and circulation of holes in the Gr channel. Accordingly, the devices can show a maximum responsivity exceeding 10^6 AW^{-1} and response speed of the order of milliseconds at low light intensity (Fig. 14e and f). In another work, the authors examined the photoresponse under both visible and IR illuminations. The devices have achieved a responsivity of $>10^4$ AW^{-1} at visible light with a fast response speed less than 3 μs, and 0.23 AW^{-1} at 1550 nm [253]. The IR photoresponse can be further boosted by using plasmonic Au nanostructures to realize photon trapping and enhance the IR light absorption [254]. In addition, the response speed can be greatly improved with rising time as low as ~17 ns while retaining the high responsivity ($\sim 3 \times 10^4$ AW^{-1} at visible) through employing an ultrathin MoS_2 interlayer, which acts as a passivation layer to minimize surface states and suppress carrier recombination, and as an carrier tunneling layer to enable carrier transfer *via* ultrafast quantum tunneling effect [255]. It is worth mentioning that the response speed reported in this work is thus far the fastest one for hybrid Gr photoconductors/phototransistors.

Gr nanowalls (GNWs)/Si Schottky junction with a thin oxide interlayer can reduce the reverse leakage current from 10^{-5} to 10^{-8} A, leading to enhanced photovoltage [256]. At photovoltage mode, the devices were capable of detecting weak light with a responsivity exceeding 10^6 VW^{-1}. In addition, the catalyst-free direct growth avoids metal pollution and polymer contamination, which can enable a high quality Schottky junction and is beneficial to photoresponse properties [257]. As a consequence, GNWs/Si junctions exhibited an ultra-low current noise of 3.1 $fAHz^{-1/2}$, with a specific detectivity of 5.88×10^{13} Jones. Moreover, this device exhibits good device performance in terms of a high I_{light}/I_{dark} ratio of up to 2×10^7, a large responsivity of 0.52 AW^{-1}, a fast response speed of 40 μs, and a linear dynamic range of 105 dB.

In addition, rGO/Si heterostructures have attracted a great deal of interest for photodetection applications as well [258–260]. Unlike Gr, rGO possesses a natural energy gap that can be readily adjusted from tens of meV to zero by controlling the degree of GO reduction, which makes it a suitable candidate for MIR or even THz detection [261]. For example, Cao et al. presented ultrabroadband photodetectors based on rGO/SiNW array junctions, which can operate from visible to THz range. At visible to NIR region (<1100 nm), light absorption occurs in both the SiNW array and rGO, whereas light absorption takes place only in rGO at MIR (10.6 μm) to THz (118.8 μm) region. Upon all illumination, the devices can exhibit a pronounced photoresponse with good repeatability, with a maximum responsivity of 9 mAW^{-1} at MIR wavelength region.

Gr/Si heterostructure waveguide photodetectors that can work from visible to MIR spectral range have been reported by several groups respectively (Fig. 15a–c) [262–264]. The parallel propagating evanescent light in the underneath Si waveguides can be absorbed by Gr to generate photocarriers, due to their strong coupling effect. With improved optical absorption, such a device geometry demonstrated responsivity exceeding 0.1 AW^{-1} under 1550 nm NIR or 2750 nm MIR light [262,263]. It was found that the device exhibited an almost uniform photoresponse across all telecommunication windows (from 1310 nm (O band) and 1650 nm (U band)) (Fig. 15d), beyond the operation range of

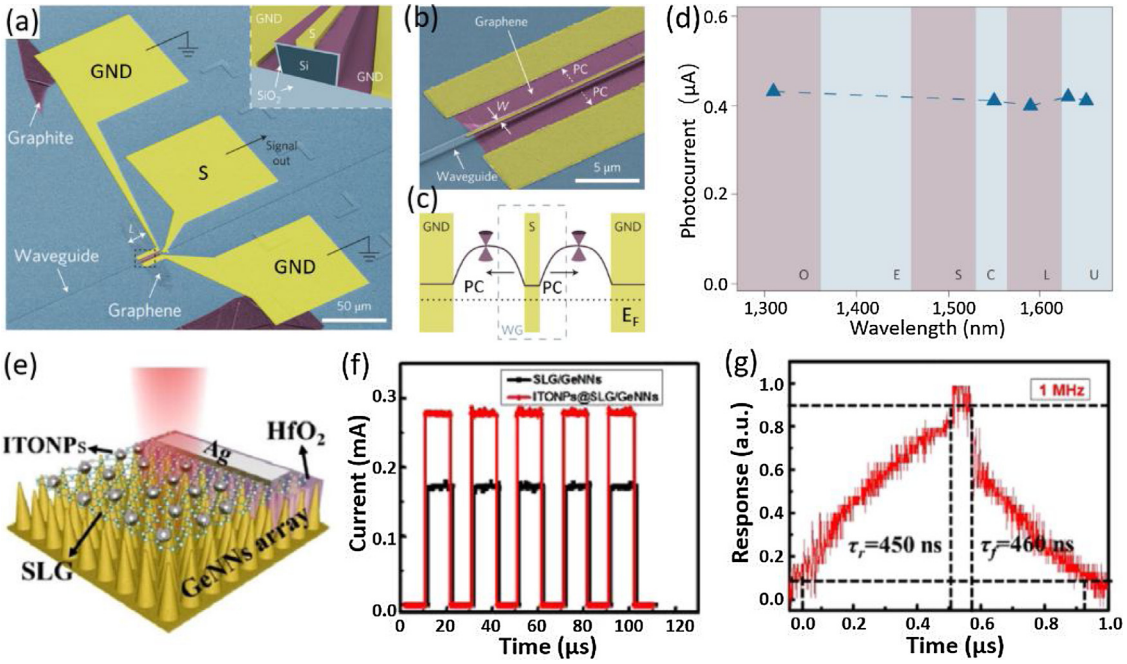

Fig. 15. (a) SEM image of waveguide-integrated Gr photodetector. (b) Enlarged view SEM image of the section. (c) Schematic illustration of the energy band diagram. (d) Photocurrent of the device as a function of light wavelength. Reprinted with permission from Nature Publishing Group. [264] (e) Schematic of ITO NPs decorated Gr/Ge nanoneedles array photodiode. (f) Comparison of photoresponse of the devices with and without ITO NPs. (g) A normalized response cycle for estimating both rise/fall time. Reprinted with permission from Wiley-VCH. [278]

Ge photodetectors limited at 1550 nm [264]. Moreover, high operation rates exceeding 20 GHz have also been demonstrated [262]. Recently, Goykhman et al. reported waveguide-integrated metal/Gr/Si heterostructure photodetectors, which support SPP guiding and benefit from confinement at the heterostructure interface [265]. A responsivity of 85 mAW^{-1} and an IQE value of 7% were achieved at 1 V bias under 1550 nm light. At a reverse bias of 3 V, the authors demonstrated a high responsivity of 0.37 AW^{-1} by employing the avalanche multiplication of the Schottky diode. These results suggest that Gr holds great promise to be chip-integrated with the mature Si technology for high-speed, ultra-broadband CMOS-compatible photodetection.

In addition to being used as solar cells and photodetectors, Gr (rGO)/Si heterostructures have also found applications in liquid and gas sensing, where the molecular absorption on the surface of Gr can directly alter the Gr/Si interface barrier height and thus affect the junction current taking advantage of the atomically thin nature of Gr [266–269]. These devices showed remarkable selectivity to different liquid and gas molecules, which enables them to be used for liquid and gas detection and identification in complicated environments [266,268]. In addition, the Gr/Si heterostructures can usually exhibit several to tens of higher sensitivity compared with conventional Gr sensors while consuming hundreds of times less power [269], suggesting great potential of such heterostructures for low power consumption, high sensitive liquid and gas sensing applications.

Gr/Ge

As a vital group IV semiconductor, Ge holds a lot of distinct properties such as a low bandgap of 0.67 eV, a large absorption coefficient at NIR region (<1.6 μm), low-cost and excellent compatibility of parallel processing with Si technology [270]. These unique features render Ge and Ge-related heterostructures the most central candidates for a variety of optics and electronics applications [271]. To date, a large number of Ge-based NIR photodetectors have been developed, however, based on complicated device configurations of MSM, p-i-n junctions, semiconductot/metal Schottky junctions, and Ge/Si junctions [272–275]. The emergence of Gr/Ge Schottky junctions with potentially strong photovoltaic effect offers the opportunity for realizing NIR photodetectors featuring simple device architecture, easy and low-cost fabrication, low dark current, and fast response speed [276].

Zeng et al. demonstrated a photovoltaic type Gr/Ge Schottky junctions NIR photodetector by transferring PMMA-covered Gr films onto Ge wafers [277]. The PMMA coating also served as an encapsulating layer to avoid additional natural oxidation occurring at Gr/Ge interface, which guarantees a long-term device stability. The detectors were very sensitive to NIR illumination with the peak response at ~1400 nm and a high I_{light}/I_{dark} ratio of 2×10^4 at zero bias. The responsivity and specific detectivity can reach 51.8 mAW^{-1} and 1.38×10^{10} Jones, respectively. In addition, the detectors exhibited a fast response speed with rise/fall times of 23/108 μs. Afterwards, to boost the response performance, NIR photodetectors consisting of Ge nanoneedle arrays and ITO NPs decorated Gr film were designed, which benefited from the synergistic effect of strong light confinement of nanostructure arrays and plasmonic effect of the ITO NPs (Fig. 15e) [278]. The I_{light}/I_{dark} ratio, responsivity and specific detectivity were dramatically improved to 5×10^4, 185 mAW^{-1} and 2.28×10^{13} Jones, respectively (Fig. 15f). Meanwhile, the devices also demonstrated a high-speed response with rise/fall times as low as 450/460 ns (Fig. 15g), which means this device was able to detect optical signal with very high frequency. The generality of these results suggests that the simple Gr/Ge Schottky type NIR photodetectors hold great promise for future NIR optoelectronic devices.

In addition, Gr/Ge hybrid heterostructure phototransistors working on photogating effect have been reported as well [279]. The presence of the Schottky junction effectively facilitates the separation of photocarriers within two materials and therefore leads to suppressed carrier recombination. A distinct photoresponse in a broad spectrum region from the 350 to 1650 nm has been achieved.

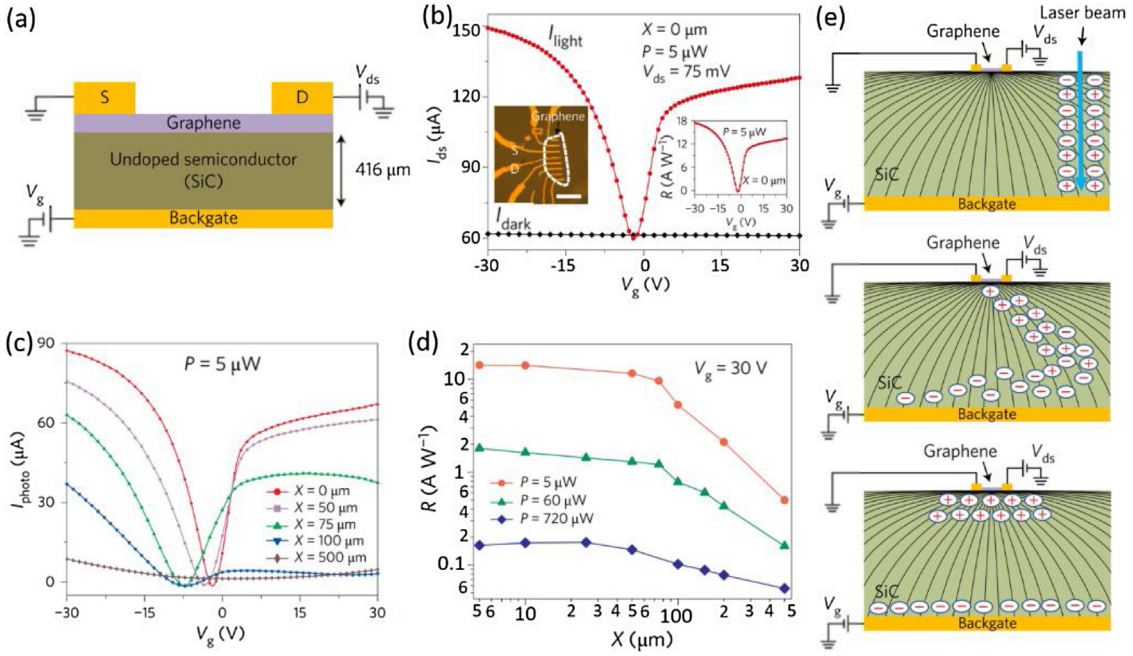

Fig. 16. (a) Schematic illustration of the Gr/SiC heterostructure device. (b) I_{ds}-V_g curves of a device in dark and under light illumination. (c) Photocurrent as a function of gate voltage at different positions. (d) Dependence of responsivity of the device on the illumination position. (e) Numerical model for position-sensitive photoresponse of the Gr/SiC heterostructure. Reprinted with permission from Nature Publishing Group. [289]

Notably, the devices exhibited a high responsivity of 66.2 AW^{-1}, and a gain of 155, which was ~3 orders of magnitude higher than pure Gr photodetectors and ~4 times larger than pure Ge photodetectors.

Gr/SiC

As an important group IV compound semiconductor, SiC is regarded as one of the most promising candidates for UV photodetection due to its wide bandgap ranging from 2.36 to 3.23 eV depending on its structure [280–282]. Recently, besides the wide usage as a substrate for epitaxial growth of high-quality Gr [283–285], SiC has also been integrated with Gr to form heterostructures for photodetection application [286–288]. As an example, Sarker et al. recently demonstrated phototransistors consisting of micrometer-scale exfoliated Gr on undoped SiC substrates (Fig. 16a) [289]. The devices showed a relatively low current with a weak field effect in dark due mainly to the insulating nature of SiC that screens the Gr from experiencing the back-gate voltage V_g (Fig. 16b). Interestingly, a high current with a strong field effect was observed upon illumination shined on Gr, and the current gradually decreased at both positive and negative V_g when the illumination position moved away from Gr (Fig. 16c and d). The responsivity reached up to ~18 AW^{-1} when the illumination was on Gr, and decreased by over one order of magnitude to ~500 mAW^{-1} when the illumination position was 500 μm away from the Gr at a light power of 5 μW. Such striking photoresponse can be well explained by a theoretical model as schematically shown in Fig. 16e. Light illumination on local position of SiC induces photocarriers which transport immediately to beneath the graphene driven by V_g. This would increase the conductivity of SiC substrate at local region and lead to an increase in the electric field at the graphene. The change in the electric field modifies the carrier density and thus the conductivity of graphene, leading to a pronounced photoresponse. However, a fraction of photocarriers are unable to affect the photoresponse since they may be trapped during transport at defect and impurity sites and recombine with their opposite charges. At a larger illumination distance, photocarriers have to travel a longer distance to reach the location under the graphene, and they will suffer from more severe trapping and recombination, which accounts for the weaker photoresponse and is also consistent with the observed longer response time.

In conclusion, Gr/0D carbon nanomaterial heterostructure-based phototransistors can exhibit high responsivities up to 10^9 AW^{-1}, unfortunately, at the expense of response speed, while both Gr/CNTs heterostructure-based phototransistors and photodiodes are very sensitive to a broad region with decent responsivities of ~40 AW^{-1} and 209 mAW^{-1}, respectively, and rapid response rates of less than 100 μs. On the other hand, Gr/Si Schottky junctions have shown great promise as solar cells and photodetectors. The PCE of Gr/Si solar cells increased rapidly from 1.65% to 15.6% within several years *via* various optimization strategies. However, challenges still remain for practical applications. For example, the current studies are almost limited to small device areas (e.g., ~0.1 cm^2) and hence large area solar cells with high PCE should be implemented. The poor air stability is another big problem, and therefore effective and stable Gr doping techniques should be developed. Gr/Si photodiodes normally exhibit high sensitivity in a broad spectrum region across the visible to NIR (<1100 nm) with ultrahigh I_{light}/I_{dark} ratios up to 10^7, responsivities less than 1 AW^{-1}, and fast response speeds (<tens of microseconds) at zero bias. The devices can also work at photoconductor mode with response spectrum extended to 1550 nm by exploiting optical absorption in Gr. The response region can be further extended to MIR (2750 nm) in Gr/Si heterostructure waveguide photodetectors, or even to THz (118.8 μm) in rGO/Si heterostructure photodetectors. Gr/Ge Schottky photodiodes are useful for NIR photodetection with I_{light}/I_{dark} ratios exceeding 10^4, moderate responsivities (51.8 mAW^{-1} to 185 mAW^{-1}) and fast response speeds as low as hundreds of nanoseconds. In addition, Gr/SiC heterostructures exhibited position-sensitive, nonlocal and millimeter-range photodetection property, which may find some specific applications in future optoelectronics. The figure-of-merits of some representative optoelectronic devices based on Gr/group IV semiconductors heterostructures are summarized in Table 1.

Gr/Metal oxides

As the most abundant materials in the Earth's crust, metal oxides exhibit a great deal of remarkable properties, including excellent electron mobility even in the amorphous state, high optical transparency, and large-area electrical uniformity and mechanical flexibility [290]. Furthermore, large-area high-quality electronic-grade metal oxides can be readily prepared *via* vapor- or solution-phase based methods in near-ambient condition. By this token, metal oxides present appealing advantages and hence have been widely explored in various electronic and optoelectronic devices, such as integrated circuits, flexible organic light-emitting diode (OLED) displays and solar cells [290,291]. In particular, these metal oxide semiconductors usually possess wide bandgaps, which render them potentially promising for high-performance UV photodetection. In this section, we are going to review optoelectronic applications of Gr/metal oxide hybrid heterostructures.

Gr/ZnO

ZnO is one of the most pivotal metal oxides and has gained substantial research interest in the past two decades due to its appealing properties such as direct bandgap of ~3.3 eV, large exciton binding energy of ~60 meV, a range of conductivity from metallic to insulating, high transparency, and so on [292,293]. These features, along with the easy fabrication render ZnO a promising material for a variety of photonic and optoelectronic applications in the UV or blue spectral range [294,295]. Recently, Gr/ZnO hybrid heterostructures have been intensively explored for a variety of optoelectronic applications, including solar cells, photodetectors, LEDs and lasers.

Solar cells

As an intrinsic *n*-type inorganic semiconductor, ZnO normally serves as the electron acceptor material or the electrode buffer layer/transparent electrode for efficient electron collection and hole blocking in various solar cells [296]. A photovoltaic device with layered structure of quartz/rGO/ZnO NR array/P3HT/PEDOT:PSS/Au has achieved an PCE of only 0.31%, which is higher than PCE values of other solar cells with Gr electrodes at that time [297]. Later, in order to optimize the PCE, Part et al. prepared uniform ZnO NW arrays for hybrid solar cells, where conductive polymers were used to modify Gr so as to (1) wet the Gr surface, (2) provide a more chemically compatible surface with the subsequent ZnO layer, and (3) enable efficient charge transfer between Gr and ZnO [298]. It was found that ZnO NW arrays grown on modified Gr have similar uniformity and alignment with those on ITO substrates, which is beneficial to photovoltaic applications. Both PbS QDs and P3HT were employed as photoactive materials, and the resultant devices exhibited PCEs of 4.2% and 0.5%, respectively, which are comparable to ITO-based devices with similar architectures. The results suggest that Gr could serve as a viable alternative to conventional transparent conductive electrodes in various photovoltaic device configurations.

In addition, ZnO nanostructure arrays loaded with CdSe QDs on Gr hybrids have also found application in QD sensitized solar cells (QDSSCs), where the hybrids were applied as effective photoanodes to capture and transport photogenerated electrons [299]. With optimization through adjusting the Gr layer thickness, the devices achieved an almost 2-fold improved PCE, compared with devices without Gr layers. Moreover, they have achieved a high *FF* of ~0.618, which is the highest value among all ZnO NRs-based solar cells. Similar geometry has also been adopted in GO based DSSCs, which significantly increased the surface area of the photoanodes, leading to high dye loading as well as high light harvesting efficiency [300]. Eventually, a PCE of ~2.5% was obtained based on this design. Besides ZnO NR arrays on Gr, random Gr/ZnO hybrid composites have been used as photoanodes in DSSCs [301]. Due to decreased internal resistance and reduced electron recombination loss, such a strategy is highly beneficial for electron transfer to the electrode. As a result, the devices with a 9-μm-thick photoanode exhibited an impressive high PCE of 5.86%, which could be the highest value among devices with the same thick photoanodes.

Gr QDs have been combined with ZnO NW arrays for application in solid-state solar cells [302]. In this architecture, Gr QDs act as the light harvesting material while ZnO NW arrays the electron transporting layer. Due to the appropriate band alignment, a favorable charge transfer process (electron injection into the NWs from QDs) can take place at QD/NW interface. On this account, the devices demonstrated an obvious photovoltaic effect with a large V_{OC} of ~0.8 V. However, the PCE is low due to the inefficient photogenerated hole collection as hole transporting layer only contacts with Gr QDs layer at its top surface, and inferior absorption of the entire incident light resulting from the narrow absorption spectrum region of Gr QDs.

Photodetectors

In recent years, Gr/ZnO hybrid heterostructures have also been widely studied for photodetector application. Depending on their working mechanisms, photodetectors based on Gr/ZnO heterostructures can be divided into two general categories: phototransistors and photodiodes. Totally, three types of devices have been involved in Gr/ZnO heterostructure-based phototransistors determined by their device configurations. The first kind of phototransistor is characterized by using ZnO nanostructure as the light absorbing material, and Gr as an electrode [303–306]. Fu et al. demonstrated vertical UV photodetectors consisting of individual ZnO NW sandwiched between two Gr layers [303]. Under UV illumination, the effective separation of photogenerated electron-holes pairs by the local electric field suppressed the carrier recombination rates and increased the carrier lifetime, leading to an increased free carrier density. This in turn can reduce Schottky barrier between Gr and ZnO, and therefore facilitate the transport and collection of photocarriers. As a result, a high I_{light}/I_{dark} ratio of 8×10^2 was achieved, much higher than conventional ZnO NWs photodetectors. Furthermore, a seedless solution process has been developed for controllable growth of crystalline ZnO NW arrays on Gr sheets for UV photodetectors [304]. Such Gr/ZnO heterostructure-based devices were sensitive to UV illumination with a maximum responsivity of 1.62 AW^{-1} per volt, superior to those achieved for other UV detectors made of epitaxial ZnO or ZnO NPs. In another work, Zhang and colleagues demonstrated visible-blind UV photodetectors composed of vertical ZnO NW arrays with Gr [305]. A high responsivity exceeding 10^4 AW^{-1} in near UV region was achieved thanks to modulation of the conducting surface, however, at the cost of response speed. In addition, 20 μm-thick ZnO QDs/Gr heterostructures were also explored for UV photodetection [306]. The devices were found to be very sensitive to UV illumination with good wavelength selectivity and reproducibility. The potential barrier formed between adjacent QDs and Schottky barrier between Gr and QDs can reduce the dark current, while direct transport of photocarriers from QDs to Gr decreases their recombination activity. Due to the significantly higher carrier mobility of Gr than the QDs, the photocurrent is thus remarkably amplified.

The second kind of phototransistors involves ZnO nanostructures as the light harvesting media and Gr as the conducting channel for carrier transport and circulation [307–315]. In 2013, Guo *et al.* have observed an efficient charge transfer between ZnO QDs and Gr, which was assisted by an oxygen molecule absorption and desorption process (Fig. 17a and b) [307]. As depicted in Fig. 17d–g, when shined by UV illumination, photoexcited holes are separated from photoexcited electrons and trapped by the surface

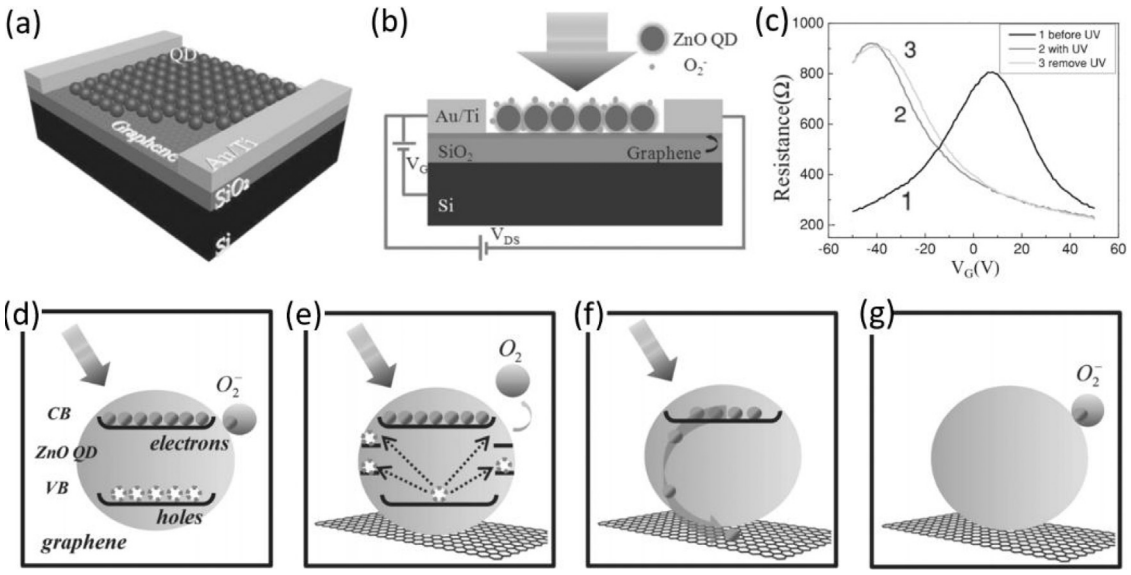

Fig. 17. (a) Schematic of the Gr/ZnO QDs hybrid phototransistor. (b) Side view of the device, which interprets the working mechanism of the device. (c) Transfer curves of Gr, Gr/ZnO QDs hybrid with and without 325 nm illumination. Schematic illustration of the mechanism of the oxygen-assisted charge transfer process (d) with irradiation of photon energy larger than bandgap, (e) with hole trapped at the surface states, (f) the transfer of electron from QDs to the Gr, and (g) without light illumination. Reprinted with permission from Nature Publishing Group. [307]

states, which discharge the oxygen ions absorbed on the surface of the ZnO QDs. Meanwhile, the unpaired electrons with a relatively long lifetime drift to the Gr and continue to transport in the Gr channel, leading to modulation of Gr's transport properties (Fig. 17c). This photogating effect can lead to a photoconductive gain as high as 10^7, which can be further improved by 2-3 orders with further device optimization. Afterwards, ZnO NW (NR) arrays have been combined with various Gr films (e.g., CVD-Gr, Gr foam and rGO) on rigid or flexible substrates to achieve UV phototransistors [308–313]. These detectors exhibited high responsivities with a maximum value of 2.5×10^6 AW^{-1}, corresponding to a photoconductive gain of 8.3×10^6, but a slow response speed (tens of to hundreds of seconds). As an example, Dang and co-workers demonstrated the growth of ZnO NR arrays on the channel of CVD-Gr FETs *via* a hydrothermal method [308]. This device exhibited a high sensitivity and wavelength selectivity to UV illumination. The responsivity and corresponding gain are 3×10^5 AW^{-1} and 10^6, respectively, much higher than that of Gr/ZnO NP heterostructures. As discussed above [307], the photoresponse was also assisted by an oxygen molecule absorption/desorption process.

Further performance improvement has been achieved by assembling Gr/ZnO QD heterostructures on an organic self-assembled monolayer (SAM) modified SiO_2 substrate, where the SAM acts as a spacer to physically separate and electrically decouple the Gr from substrate [314]. This approach led to one order of magnitude increase in mobility for reduced carrier scattering. Therefore, the photogenerated electrons transferred to Gr from the QDs can recirculate multiple cycles before their recombination, which is beneficial for photoconductive gain. Optoelectronic characterization revealed that this device had an ultrahigh responsivity of $\sim 10^8$ AW^{-1} and a corresponding gain of $\sim 3 \times 10^9$, with a UV/visible rejection ratio of $\sim 10^3$ and a specific detectivity of $\sim 5.1 \times 10^{13}$ Jones. Most recently, Gong et al. have developed a phototransistor composed of Gr FET and ZnO QDs, whose surface was treated to exhaust the zinc acetate dihydrate (Zn(Ac)) shell, often formed at ZnO QDs surface as an insulting layer to block electron transfer [315]. Owing to efficient charge transfer from ZnO QDs to Gr, the detectors showed an extraordinary high responsivity of 9.9×10^8 AW^{-1}, which corresponds to a gain of 3.6×10^9, and a maximum specific detectivity as high as 7.5×10^{14} Jones, respectively. The photoresponse parameters are several orders of magnitude higher than devices made of ZnO QDs with insulating shell. This study manifests the critical role of the van der Waals interface in affecting the optoelectronic process in heterostructure photodetectors. Overall, as the responsivities of such phototransistors are already very high, further efforts should be focused on improving the response speeds towards practical applications.

The last device architecture is based on Gr (rGO)/ZnO nanostructure composites that has a working mechanism similar to the second types [316–325]. The composites are usually prepared *via* solvothermal method [316–319], or ultrasonication [323–325]. In general, the detectors displayed not only obvious sensitivity to visible-blind UV illumination, but also tunable wavelength selectivity [317,324]. Compared with the second device architecture, these devices exhibited fast response speed, but a relatively lower responsivities with the maximum value reported to be ~640 AW^{-1} [319], presumably due to the presence of a large number of defect/trap states within the composites. For example, Shao et al. have developed an efficient and versatile solution-based method to wrap Gr onto ZnO NPs to form core-shell heterostructures for UV photodetection [319]. The as-fabricated detectors exhibited a high sensitivity to UV light with rapid rise/fall times of 9/11 ms. The appropriate band alignment between Gr and ZnO is energetically favorable for photogenerated electrons to transfer towards Gr. On the other hand, the carrier transfer is believed to be fast in light of the high carrier mobility of Gr and the unique core-shell structure.

Photodiodes based on Gr/ZnO heterostructures usually exploit the Schottky junction formed between Gr and ZnO [326–335]. The formed built-in potential can separate photogenerated electron-hole pairs at zero bias condition, which can potentially reduce dark current and thus bring about an improved specific detectivity [330,333,335]. In addition, under moderate reverse bias, the separation efficiency of photocarriers will be improved as the built-in electric field are further strengthened, resulting in response speeds much faster than that of Gr/ZnO heterostructures phototransistor [326,328,329,331,332]. Furthermore, a large internal current gain is possible due to the impact ionization of photocarriers with enough energy [23]. In general, these devices exhibited responsivities in the range of tens of to hundreds of mAW^{-1} at zero bias, and the values can be improved to tens of to thousands of AW^{-1} at reverse

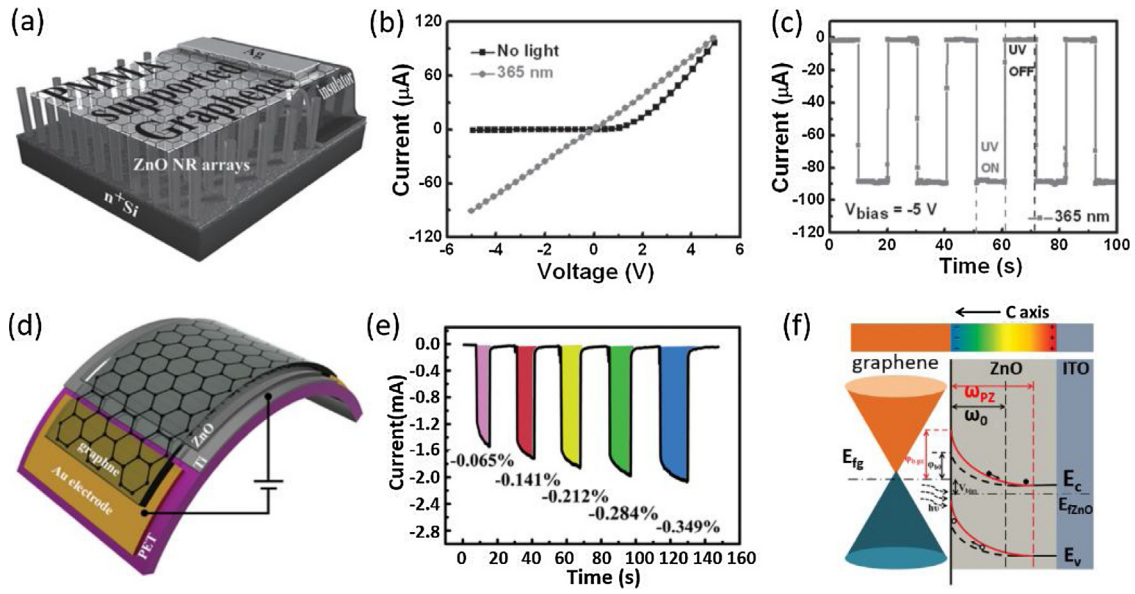

Fig. 18. (a) Device geometry of the Gr/ZnO NW array photodiode. (b) *I-V* curves of the device with and without UV illumination. (c) Photoresponse of the device when the UV was turned on and off repeatedly. Reprinted with permission from Wiley-VCH. [326] (d) Schematic of the flexible Gr/ZnO photodiode on PET substrate. (e) Photoresponse of the flexible device under different straines. (f) Energy band diagram of the heterojunction with and without strain under light illumination. Reprinted with permission from Wiley-VCH. [329]

bias with a maximum responsivity of 3×10^4 AW^{-1} [331]. In 2013, Nie et al. firstly reported a sensitive UV photodetectors made of Gr/ZnO NR arrays Schottky junction with a barrier height of ~0.8 eV (Fig. 18a) [326]. The devices were very sensitive to UV illumination with good operation stability and reproducibility (Fig. 18b and c). The responsivity and gain reached 113 AW^{-1} and 385 at -1 V bias voltage, respectively. What is more, the devices exhibited fast rise/fall times of 0.7/3.6 ms. The excellent response properties can be attributed to the strong UV light trapping capability of the ZnO NR arrays as well as the large built-in electric field formed by the Schottky junction.

Further optimization in device performance is achievable through introduction of a charge tunneling/blocking interlayer [328], or modulation of the Schottky barrier *via* back-gate voltage [327] or external strain [329,334]. For example, Wu and co-workers presented novel UV photodetectors with a responsivity of up to 1350 AW^{-1} at - 5 V, by inserting an h-BN layer in a Gr/ZnO Schottky junction [328], In this structure, the presence of *h*-BN interfacial layer not only reduces the dark current by suppressing the transfer of electrons from Gr to ZnO, but also increases the photocurrent through confining photogenerated electrons within ZnO to reduce carrier recombination. On the other hand, photogenerated holes can easily tunnel through the *h*-BN and then inject into Gr under external reverse bias. Recently, the effect of strain modulation on device performance of flexible Gr/ZnO nanostructure photodetectors has been studied by two groups respectively (Fig. 18d) [329,334]. In the first study, a 17% increase in photocurrent was achieved by applying a -0.349% compressive strain and the corresponding responsivity increased from 71.61 to 84.94 AW^{-1}, representing a 4.8% increase per 0.1% strain (Fig. 18e) [329]. The authors in the second work increase the responsivity by 87% by increasing the applied external strain to 30% [334]. Such a remarkable improvement can be ascribed to the increased Schottky barrier height and widened depletion region regulated by the strain-induced pizeopotential in ZnO (Fig. 18f). What is more, according to a theoretical simulation, the pizeopotential was mainly distributed at the tips of ZnO nanostructures, which is beneficial for the effective modulation of the Schottky junction at Gr/ZnO interface.

The response spectrum can be readily extended to the NIR region by exploiting rGO/ZnO heterostructures or Gr/ZnO/Si triple junctions [330,332]. It has been reported that rGO/ZnO heterostructures photodetector exhibited significantly enhanced photovoltage in a wide wavelength spectrum from visible to NIR region, compared to that of ZnO NW arrays or pure rGO film [332]. Such photovoltage to broadband illumination was associated with the following two origins. First, electron excitation from the valence band to the defect energy levels gives a photoresponse under visible illumination, whereas trapped electrons at the NWs surface due to absorption of oxygen and moisture molecules can be excited under NIR light and subsequently drift to ZnO, resulting in a photoresponse at NIR region. In addition, photocarriers generated within rGO due to strong optical absorption in visible to NIR spectrum also contribute to enhancement of the photovoltaic response. Cheng et al. have fabricated photodetectors based on Gr/ZnO/Si triple junctions, which displayed a broadband photoresponse from 400 to 1000 nm [330]. The incorporation of ZnO layer could enhance the separation of photocarriers by built-in electric fields formed at both Gr/ZnO and ZnO/Si interfaces. In addition, the ZnO layer can serve as an antireflection layer to trap incident light and enhance optical absorption. For these advantages, the devices exhibited a much enhanced responsivity, especially at near-UV to visible region. Moreover, the response speed can also be greatly reduced by an order of magnitude with rise/fall times as low as 280/540 μs.

Ultraviolet laser

Ultraviolet lasing of ZnO has been achieved in varied resonance cavities of Fabry-Perot (F-P), random, and whispering-gallery mode (WGM). Nevertheless, owing to cavity losses and diffraction limit, it is highly challenging to achieve miniaturized lasers with high efficiency. Xu's group observed single-mode lasing resonance in a ZnO microrod by serially adjusting the size of the WGM cavities (Fig. 19a). It was found that the lasing intensity and lasing quality factor were substantially increased by transferring a layer of monolayer Gr on the submicron ZnO cavity (Fig. 19b–d). Further experimental results analysis showed that such an increase in lasing performance was related to the confined optical field

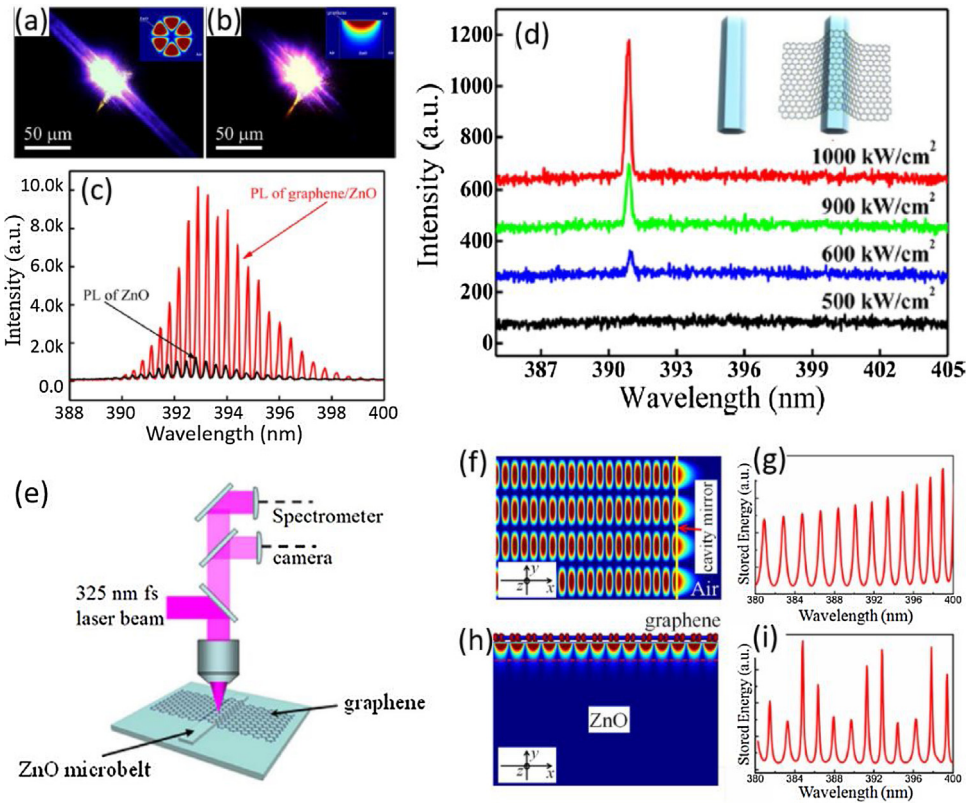

Fig. 19. Dark field optical images of a single ZnO microrod before (a) and after covering with Gr (b). (c) Comparison of the PL spectra. (d) PL spectra of the hybrid microcavity under excitation with different power intensities. Reprinted with permission from American Chemical Society. [336] (e) Schematic diagram for the measured setup. (g) Gr SP excited at the Gr/ZnO interface. The resonance spectrum of the stored energy for (f) the bare ZnO, and (g) hybrid microcavity. Reprinted with permission from Nature Publishing Group. [337]

and enhanced optical gain of the cavity due to the coupling ZnO exciton emission and between Gr SP [336]. By exploiting the coupling between Gr SP modes and conventional optical microcavity modes of ZnO microbelt (Fig. 19e), this group later successfully demonstrated an F-P Laser with enhanced lasing quality and lasing intensity, and reduced lasing threshold. According to their theoretical simulation, the observed optimization in lasing performance can be ascribed to the coupling interaction between the ZnO-FP modes and Gr SP modes (Fig. 19e–g). This new laser based on Gr/ZnO hybrid structure will open up new opportunities for designing other Gr-based optoelectronic and optic devices [337].

Gr/TiO_2

TiO_2 is one of the most studied metal oxides in material science and has been extensively used in a variety of fields including catalysis and photocatalysis, biomedicine, and energy conversion and storage, due to its unique physical and chemical properties [338,339]. It possesses a distinctive electronic structure with a large bandgap (anatase: 3.2 eV, rutile: 3.0 eV) and suitable band-edge position for many redox reactions, a comparably high lifetime of photoexcited electrons, and an exceptional photocorrosion resistance, which enable the wide application of TiO_2 in DSSCs [340]. Recently, TiO_2 and Gr/TiO_2 hybrid heterostructures have attracted considerable attention in optoelectronic applications, including solar cells and photodetectors [341,342]. Since there have been many review papers dedicated to the application of Gr/TiO_2 hybrid heterostructures in solar cells including DSSCs and QDSSCs [165,343], the discussion of this topic will be left aside in this part and we only focus on study of Gr/TiO_2 hybrid heterostructures for photodetector application.

Like Gr/ZnO hybrid structures, Gr/TiO_2 heterostructures have been used as UV light photodetectors in the form of either phototransistors or photodiodes. Manga et al. have developed a solution-processable route to produce a rGO/TiO_2 hybrid phototransistor that is printable and spin-castable [344]. The as-prepared hybrids devices exhibited distinct photoresponse at the UV-visible wavelength region with peak sensitivity at ~320 nm, while virtually no photoresponse was observed in pure rGO or TiO_2. Under UV illumination, photogenerated electrons in TiO_2 were injected into rGO due to appropriate band alignment, whereas photogenerated holes are driven to the surface of TiO_2 by band bending as a result of the presence of oxygen absorption and then are trapped. On the other hand, the photocurrent in the visible region can be explained by the photoinjection of electrons from rGO into the unfilled states of TiO_2, and rapid transport of unpaired holes in rGO. The specific detectivity can reach 2.3×10^{12} and 9.4×10^{11} Jones at UV and visible regions, respectively. What is more, the devices exhibited a fast response speed with ~100 ms rise and fall times. The great advantages held by this technique such as easy chemical manipulation, aqueous-based solution-processability and printability for large-scale screen printing, signify its considerable innovation potential for printable optoelectronic devices. To improve the visible photoresponse and extend the response region to IR wavelength, a Gr/PbSe QDs/TiO_2 hybrid photodetector was fabricated *via* a solution-based process [345]. The devices exhibited an I_{light}/I_{dark} ratio of 10^4, which outperforms devices made of Gr/PbSe (10^2), Gr/TiO_2 (10^2) composites and PbSe QDs (10). The photoresponse was attributed to efficient electron injection from the photoexcited PbSe QDs to TiO_2 or Gr. Thanks to the strong optical absorption across UV-visible to IR region and the efficient carrier separation and transport, the multicomponent composite-based devices

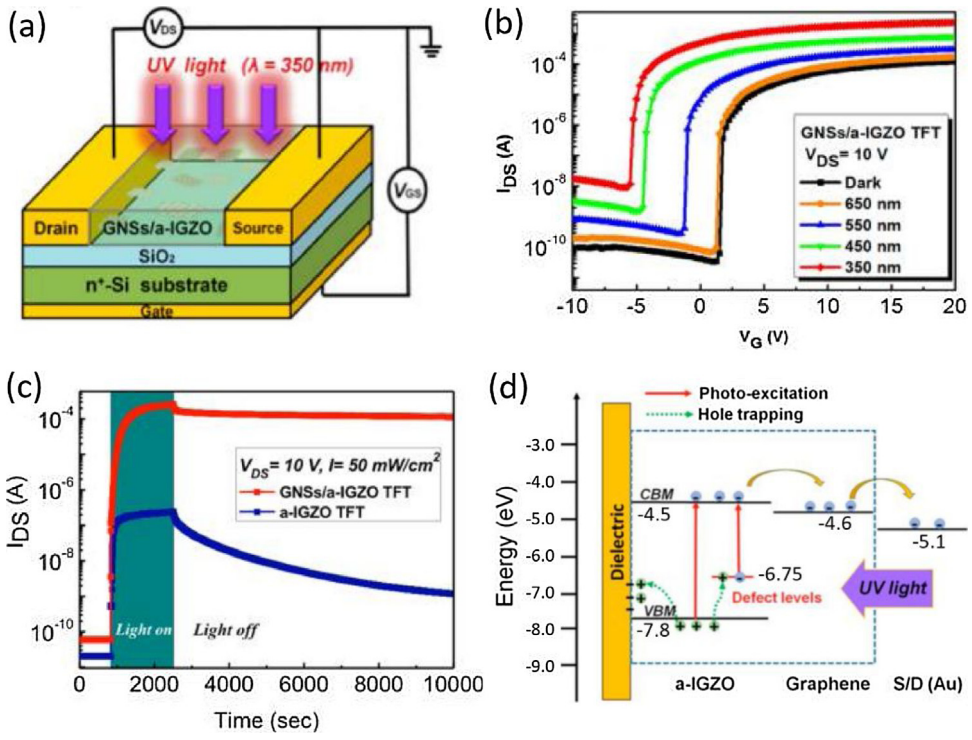

Fig. 20. (a) Device geometry of the Gr/IGZO hybrid phototransistor. (b) Transfer characteristics of the device with and without light illumination. (c) Time response of the I_{ds} of IGZO and Gr/IGZO devices. (d) Band diagram of a Gr/IGZO device under light illumination, which explains the mechanism for the long-lasting persistent photoconductivity. Reprinted with permission from American Chemical Society. [353]

demonstrated much improved specific detectivity of 3×10^{13} and 5.7×10^{12} Jones at visible and IR regions, respectively.

Afterwards, Zheng and co-workers have studied the optoelectronic properties of chemically exfoliated Gr/TiO_2 NPs heterostructures and found a reversible photoresponse in the visible spectrum region [346]. In the device, negatively charged oxygen anions were formed as a result of the reaction between active electrons and oxygen molecules absorption at TiO_2 surface. The resultant reduce in scattering sites and release of holes into the Gr channel caused a low conductance of the *n*-type Gr in dark. On contrary, under light illumination, the desorption of oxygen molecules released the electrons back to the Gr channel and therefore formed the photocurrent.

Photodiodes based on Gr/TiO_2 Schottky junction have also been reported recently [347–349]. CVD-Gr on single-crystal TiO_2 wafer heterostructures exhibited an obvious current rectifying behavior in dark. Interestingly, the devices were highly sensitive to UV light at both reverse and forward bias voltages, with peak sensitivity at 410 nm and excellent reproducibility and air stability. A high I_{light}/I_{dark} ratio of 6.8×10^4 along with a fast response rate of 0.74/1.18 ms (rise/fall time) was achieved at -10 V reverse bias. In addition, the responsivity and specific detectivity were calculated to be 1.63 mAW^{-1} and 7.29×10^{10} Jones, respectively. Further performance improvement can be achieved by employing TiO_2 nanotube (NT) arrays with strong UV light trapping capability as the light harvesting media [348,349]. UV detectors based on Gr/TiO_2 NT array Schottky junctions exhibited an enhanced responsivity and specific detectivity of 15 AW^{-1} and 1.5×10^{12} Jones at -5 V bias, respectively [348]. In addition to improved UV light absorption, other three factors have contributed to the improved sensitivity. First, the reduced Schottky barrier upon UV light due to oxygen absorption/desorption at the surface of TiO_2 NTs with high surface area to volume ratio can facilitate transport of electrons through the barrier. In addition, the presence of huge amount of oxygen vacancy within TiO_2 NTs which serve as efficient carrier trapping centers can remarkably extend the carrier lifetime. Furthermore, oxygen absorption induced trapping of free electrons leads to the formation of a low-conductivity depletion region, which facilitates efficient separation of photogenerated electrons and holes, and reduces carrier recombination. These results suggest the potential of such Schottky UV photodiodes for future high-speed, high-sensitivity optoelectronic devices and systems.

Gr/Other metal oxides

Apart from ZnO and TiO_2, other semiconductor metal oxides including NiO [350], MoO_3 [351], WO_3 [352], InGaZnO [353–356], SnO_2 [357], ZrO_2 [358], Ga_2O_3 [359,360] have been integrated with Gr to form heterostructures for optoelectronic applications. Various studies have shown that DSSCs with a *p*-type semiconductor photoelectrode usually exhibit much poorer photovoltaic performance than *n*-DSSCs due to the intrinsically low hole transfer rate. To this end, Yang et al. developed a *p*-DSSCs that used Gr/NiO composites as photoelectrodes [350]. By virtue of the larger surface area and higher conductivity than the pristine NiO photoelectrodes, the charge recombination of the composite-based DSSCs was remarkably suppressed. These beneficial factors contribute to 2 times improvement in PCEs. In fact, the Gr/metal oxide hybrid has also be used as sensitive phototransistors [351–358]. These devices exhibited positive or negative photoresponses depending on the type of both Gr doping and photocarriers. The maximum responsivities achieved in these devices are tens of AW^{-1}. For example, a high I_{light}/I_{dark} ratio of up to 10^7 and long-lasting persistent photoconductivity with enduring lifetime up to years have been observed in Gr/amorphous IGZO hybrid (Fig. 20a–c) [353]. Fig. 20d shows the band alignment with IGZO. It is obvious that the presence of Gr sheets could facilitate the dissociation of photoexcited electron-hole pairs generated within IGZO and the migration of the electrons from IGZO to Gr, thus reducing the carrier recombination. The fast transport of electrons through the Gr channel due to its high carrier

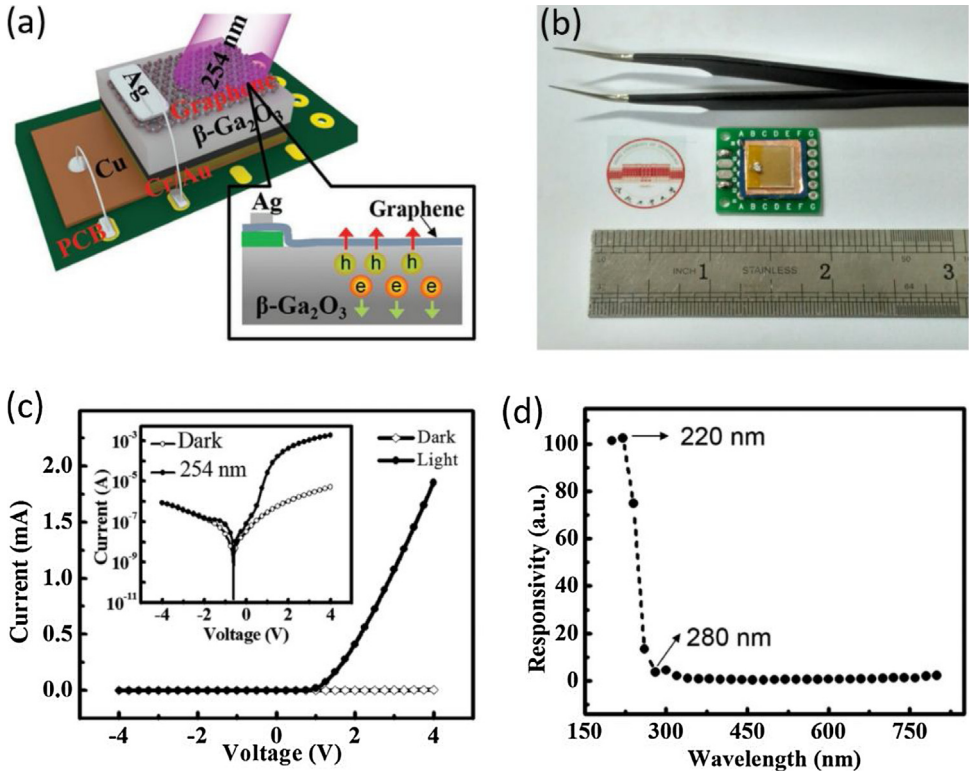

Fig. 21. (a) Schematic of Gr/β-Ga_2O_3 deep UV photodiode. (b) Photograph of the device. (c) *I-V* curves of the photodiode under 254 nm illumination. (d) Responsivity of the device as a function of incident light wavelength. Reprinted with permission from Wiley-VCH. [359]

mobility is helpful to achieve a large photocurrent. Not only that, holes have a great probability to be trapped and localized at deep-level and/or defect trap centers, which prevents the recombination of holes with free electrons, and cause an ultra-long recovery time of photocurrent. In addition, Gr QDs have been incorporated into IGZO-based phototransistors, which had a maximum responsivity of 897 AW^{-1} and a high I_{light}/I_{dark} ratio of up to 10^6 [355,356]. Under illumination, the photogenerated electrons in the QDs can easily transfer to the underlying IGZO and transport through the channel, leaving photogenerated holes trapped inside the QDs. These trapped holes can act as effective gate to cause the negative shift of the threshold voltage of the IGZO-phototransistor [355].

Sensitive deep UV photodetectors with similar device geometry has been achieved by coating Gr on wide bandgap semiconductor surface [359,360]. For example, Kong et al. demonstrated a deep UV photodiode based on multilayer Gr/*n*-type β-Ga_2O_3 substrate (Fig. 21a and b) [359]. The devices exhibited dramatically increased current at forward bias voltage upon 254 nm UV illumination under reverse bias (Fig. 21c). The responsivity and specific detectivity were as high as 39.3 AW^{-1} and 5.92×10^{13} Jones at 20 V, respectively, which are comparable to or even better than reported Ga_2O_3 nanostructure-based photodetectors. In addition, the devices can operate well under periodically repeated UV illumination with outstanding reproducibility and stability. Furthermore, it is worth noting that the photodiodes demonstrated a high deep UV selectivity: the devices showed a peak sensitivity at ~220 nm, but were nearly blind to light with wavelength longer than 280 nm (Fig. 21d). These results along with the easy fabrication process signify that such heterostructure-based deep UV photodetectors might hold great opportunities for future optoelectronic applications.

In summary, Gr/ZnO nanostructure array heterostructures have found application in hybrid solar cells, where Gr was used as a transparent electrode and ZnO served as the electron acceptor. For photodetector applications, Gr/ZnO heterostructure-based phototransistors exhibited high responsivities (as high as 9.9×10^8 AW^{-1}), yet, slow response speeds usually in the order of tens of seconds at UV region. The oxygen molecule absorption/desorption process and Gr/ZnO van der Waals interface are critical issues that determine the photoresponse performance. In addition, Gr/IGZO hybrid composites showed a unique semiconductor-conductor transition, i.e., a long-lasting persistent photoconductivity, which might be useful in a variety of optoelectronic devices. On the other hand, Gr/metal oxide (ZnO, TiO_2, Ga_2O_3) Schottky photodiodes were highly sensitive to UV illumination with a highest responsivity reaching 3×10^4 AW^{-1} at moderate reverse bias. In particular, Gr/Ga_2O_3 Schottky junctions have shown grand promise for DUV photodetection. Table 2 summarized the performance parameters of some typical Gr/metal oxide heterostructures-based photodetectors.

Gr/Other semiconductors

In the previous sections, we have introduced the development of various optoelectronic device applications based on Gr/group II-VI nanostructures, /group III-V semiconductors, /group IV semiconductors, /metal oxides hybrid heterostructures. In this part, we will summarize the recent advances in optoelectronic devices based on Gr/other semiconductors, including 2D layered semiconductors, organic semiconductors, perovskite materials, and so on.

Gr/2D layered semiconductors

2D layered materials (e.g., MoS_2, $MoSe_2$ and WS_2) refer to a group of materials derived from layered van der Waals solids, where atomic layers are formed by atoms that are arranged into planes and held together with strong covalent or ionic bonds [14,23,361]. This unique structure allows the cleavage of bulk

Table 2
Summary of performance parameters of some representative Gr/metal oxide and Gr/other semiconductors hybrid heterostructure optoelectronic devices.

Devices	Geometry	Mode	Wavelength	On/Off	*R*(A/W)/*G*/*EQE*	Speed/frequency	Ref.
	Gr/ZnO NW/Gr	Photoconductor	325 nm	8×10^2	/	0.7/0.5 s	[303]
	Gr/ZnO NW/Au	Photoconductor	357 nm	/	*R*: 10^4	> 10 s	[305]
	Gr/ZnO QDs/Gr	Photoconductor	365 nm	/	/	0.29/0.285 s	[306]
	Gr/ZnO QDs	Phototransistor	325 nm	/	*G*: 10^7	> 1 s	[307]
	Gr/ZnO NRs	Phototransistor	365 nm	/	*R*: 3×10^5	> 10 s	[308]
	Gr/ZnO QDs	Phototransistor	335 nm	/	*R*: $\sim 10^8$	> 1 s	[314]
	Gr/ZnO QDs	Phototransistor	330 nm	/	*R*: 9.9×10^8	5/85.1 s	[315]
	Gr/ZnO QDs core-shell	Phototransistors	335 nm	~600	*R*: ~*640*	9/11 ms	[319]
	Gr/ZnO NRs	Photodiode	365 nm	> 10^3	*R*: *113*	0.7/3.6 ms	[326]
	Gr/h-BN/bulk ZnO	Photodiode	365 nm	~10^3	*R*: *1350*	> 1 s	[328]
	Gr/ZnO NRs	Photodiode	325 nm	/	*R*: ~*85*	0.3/0.5 s	[329]
	rGO/TiO2 matrix	Photoconductor	320 nm	/	*G*: ~*0.85*	100 ms	[344]
	Gr/PbSe/TiO2 NPs	Phototransistor	350 nm	104	*G*: ~*1.4*	50/750 ns	[345]
	Gr/TiO2 wafer	Photodiode	405 nm	6.8×10^4	*R*: *0.0016*	0.74/1.18 ms	[347]
	Gr/TiO_2 NT	Photodiode	365 nm	/	*R*: 15	> 10 s	[348]
	Gr/IGZO film	Phototransistor	350 nm	2.0×10^7	*R*: 22.8	/	[353]
PDs	Gr/β-Ga_2O_3 wafer	Photodiode	254 nm	~10^3	*R*: 39.3	~95/~220 s	[359]
	Gr/InSe/Gr	Photoconductor	633 nm	/	*R*: 4×10^3	~1/~10 ms	[371]
	Gr/MoS_2	Phototransistor	635 nm	/	*R*: 5×10^8	> 1 min	[30]
	Gr/MoS_2	Phototransistor	650 nm	/	*R*: $\sim 1.2 \times 10^7$	> 1 min	[374]
	Gr/$MoTe_2$	Phototransistor	1064 nm	/	*R*: ~970	78 ms	[378]
	Gr/GaSe	Phototransistor	532 nm	/	*R*: $\sim 3.5 \times 10^5$	~10/~10 ms	[380]
	Gr/Bi_2Te_3	Phototransistor	532 nm	/	*R*: 35	8.7 ms	[381]
	Gr/WS_2/Gr	Photodiode	633 nm	/	*EQE:* >30%	/	[367]
	Gr/MoS_2/Gr	Photodiode	514 nm	/	*EQE:* 27%	0.05 ms	[384]
	Gr/InSe/Gr	Photodiode	633 nm	/	*R*: $\sim 10^5$	/	[371]
	Gr/MoS_2	Photodiode	1440 nm	/	*R*: 1.26	/	[387]
	Gr/WSe_2	Photodiode	532 nm	/	*R*: 350 (1 V)	50/30 μs	[390]
	WSe_2/Gr/MoS_2	Photodiode	400/2400nm	/	*R*: >10^4/~0.1	53.6/30.3 μs	[392]
	Gr/P3HT	Phototransistor	325 nm	/	*G*: ~100	/	[395]
	Gr/C_8-BTBT	Phototransistor	355 nm	/	*R*: 4.76×10^5	~830 ms	[400]
	Gr/$CH_3NH_3PbI_3$ film	Phototransistor	532 nm	/	*R*: 180	87/540 ms	[410]
	Gr/$CH_3NH_3PbI_3$ film	Phototransistor	450 nm	/	*R*: 1.73×10^7	> 1 s	[413]
	Gr/P3HT/$CH_3NH_3PbI_{3-x}Cl_x$ film	Phototransistor	598 nm	/	*R*: $\sim 4.3 \times 10^9$	> 10 s	[414]
	Gr/$CH_3NH_3PbI_3$ NWs	Phototransistor	633 nm	/	*R*: $\sim 2.6 \times 10^6$	> 10 s	[415]
	Gr/ $(C_4H_9NH_3)_2PbBr_4$/Gr	Photoconductor	470 nm	10^3	*R*: ~2100	< 1 s	[421]
	Gr/$CH_3NH_3PbI_3$/Gr	Phototransistor	532 nm	/	*R*: ~950	22/37 ms	[422]
	Gr/PbS QDs	Phototransistor	532 nm	/	*R*: $\sim 10^7$	> 1 s	[29]
	Gr/ruthenium complex	Phototransistor	450 nm	/	*R*: $\sim 10^5$	> 10 s	[426]

crystals into individual freestanding few-atom thick or even single-atom thick layers *via* mechanical or liquid phase exfoliation methods [362,363]. Due to the dimensionality confinement effect and modulation in their band structures, 2D layered materials usually exhibit a broad range of fascinating electrical, optical, thermal and mechanical characteristics that can hardly be found in their 3D bulk counterparts [364]. In particular, their tunable bandgaps by varying the number of layers provide possibility of photodetection at different wavelengths [365]. On the other hand, the increased light absorption efficiency induced by the quantum confinement effect [366] and strong light-2D layered semiconductor interaction due to the existence of Van Hove singularities in the electronic density of states [367] also lead to enhanced photon absorption and photoinduced charge carrier creation. The van der Waals interactions between neighboring layers without dangling bonds, together with the rapid advancement in isolation and deterministic transfer of various 2D layered semiconductors allow the integration of them with other materials including Gr to form a variety of planar or vertical functional heterostructures with fundamentally different properties. In the following, we are going to introduce optoelectronic applications based on Gr/2D layered semiconductor van der Waals heterostructures.

Solar cells

Transition metal dichalcogenide (TMD, e.g., MoS_2, $MoSe_2$ and WS_2) monolayers with thickness of smaller than 1 nm can absorb up to 5-10% of incident sunlight, which surpasses the sunlight absorption of Si or GaAs by 1 order of magnitude [368]. Benefiting from the strong light absorption, Schottky barrier solar cells based on a bilayer of Gr/MoS_2 heterostructure can exhibit a theoretical PCE range of 0.1-1.0%. In this geometry, there exists a large Schottky barrier as high as 1.2 eV. Therefore, photogenerated electrons can be easily injected from the conduction band of MoS_2 to Gr, while photogenerated holes in the valence band of the MoS_2 are confined. Although the absolute PCE value is not high, it is approximately 1-3 orders of magnitude higher than the value for the best reported ultrathin solar cells. Afterwards, a higher PCE has been achieved in Schottky junction solar cells composed of Gr/WS_2 heterostructures (Fig. 22a) [369]. The authors in this work found that both the characteristics of the Schottky junction and the photovoltaic performance depend significantly on the layer number of Gr (Fig. 22b). The device reaches a maximum PCE of 3.3% with multilayer Gr as the Schottky contact, as multilayer Gr possesses higher electrical conductivity that can control the trap-assisted recombination process in WS_2 and provide better capability to suppress dark current (Fig. 22c). Further photovoltaic performance improvement can be conceivable *via* designing light-trapping structures such as integrating the Gr/TMD heterostructure solar cells in a wedge-shaped microcavity with a spectrum-splitting structure [370].

Photodetectors

Gr/TMD heterostructures have demonstrated great promise in phototransistors or photodiodes, depending on their working principles. In general, two types of devices have been involved in Gr/TMD phototransistors according to their difference in device configuration. In the first geometry, 2D layered semiconductors such

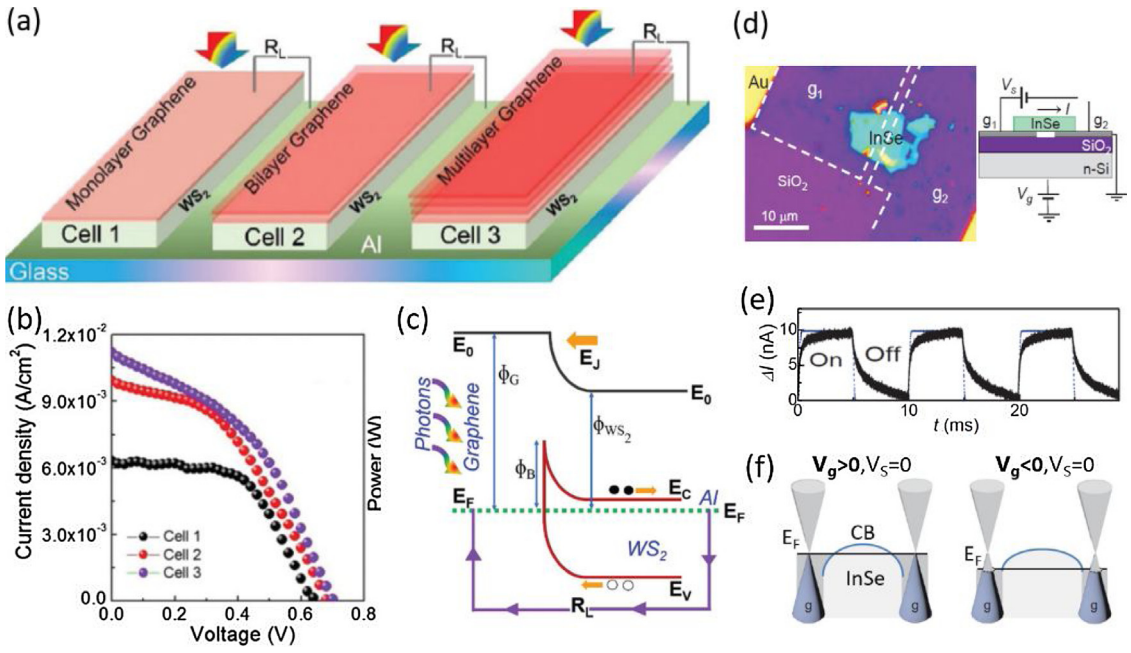

Fig. 22. (a) Schematic illustration of three Gr/WS_2 Schottky junction solar cells in which monolayer, bilayer, and multiplayer Gr were used. (b) *J-V* curves of the three solar cells under AM 1.5G illumination. (c) Energy band diagram of the Gr/WS_2 heterojunction under illumination. Reprinted with permission from the Royal Society of Chemistry. [369] (d) SEM image and schematic illustration of the Gr/InSe heterostructure. (e) Transient response of the Gr/InSe heterostructure device. (f) Energy band diagram of the device at both forward and reverse bias voltage. Reprinted with permission from Wiley-VCH. [371]

as InSe [371], WS_2 [372], and $MoTe_2$ [373] are used as light absorbing media, while two separated Gr layers serve as electrodes to form planar MSM-like phototransistors. The major advantage of Gr electrodes over traditional metallic electrodes relies on the strong Fermi level tunability of Gr that can modulate the Schottky barrier between Gr and the semiconductors, due to the finite density of states from the Dirac cones of the valence and conduction bands of Gr, as well as the feature of van der Waals interfaces that is free of Fermi level pinning effect. These thus allow the photoresponse characteristics to be adjusted by electrostatic gating or light input control. Through tuning the Schottky barrier, ideal Ohmic contacts between Gr and 2D layered semiconductors can be easily obtained. For example, Mudd et al. demonstrated a sensitive planar Gr/n-InSe/Gr heterostructures device with a responsivity as high as 4×10^3 AW^{-1} (Fig. 22d) [371]. The devices also showed a fast response speed with rise/fall time of ~1/10 ms (Fig. 22e). In this study, due to the higher work function of Gr than InSe, electrons tend to transfer from Gr to *n*-InSe to form an accumulation layer at the interface with Gr at an equilibrium condition over a wide range of applied gate voltages (Fig. 22f). The resultant Ohmic contact is important to high responsivity and rapid response rate. In another work, Tan and co-workers observed an abnormal dependence of responsivity on incident light power in Gr/WS_2/Gr heterostructure device [372]. The responsivity increased with increasing light power at "OFF" state (V_g = 0 V), but decreased with increasing light power at "ON" state (V_g = 30 V), which is completely different from what was observed in Au/WS_2/Au device. The increase in responsivity with increasing light power can be attributed to the efficient light induced charge transfer process in which the electrons reside in Gr while holes are located in WS_2. This photo-gating effect can result in increase in Fermi level and reduce in contact resistance. Once the phototransistor is switched to "ON" state, the influence of illumination on the Fermi level of Gr is reduced and thus result in a different power dependence of responsivity.

In the second photo-gating effect dominated device architecture, the 2D layered semiconductors including MoS_2 [30,374–377], $MoTe_2$ [378], InSe [379], GaSe [380], Bi_2Te_3 [381], $Bi_2Se_{1.5}Te_{1.5}$ [382] and g-C_3N_4 [383] often function as the light harvesting media, whereas the Gr serves as the conducting channel for carrier transport and circulation. For instance, phototransistors based on hybrid heterostructures of mechanically exfoliated Gr and MoS_2 exhibited a very high responsivity of 5×10^8 AW^{-1} at room temperature, which increased to 1×10^{10} AW^{-1} at 130 K, however, at the sacrifice of response speed (~tens of seconds) [30]. Such an exceptionally high responsivity can be ascribed to the following processes. Under illumination, photogenerated holes are trapped inside the MoS_2 by local states, while photogenerated electrons are transferred to the Gr with the assistance of a gate electric field. The electrons will recombine with holes induced by the negative gate bias in the channel, which reduces the channel conductance and leads to a sizeable net photocurrent. Meanwhile, the trapped holes act as a local gate, giving rise to a pronounced photogating effect on the Gr *via* capacitive coupling. The long lifetimes of the trapped holes also explained the slow response rate. Li et al reported a similar phototransistor by using CVD derived Gr and MoS_2 (Fig. 23a) [374]. The photogating effect induced working mechanism was confirmed by the transfer curves shift horizontally with increasing illumination power, as shown in Fig. 23b. In addition, the responsivity decreased remarkably with increasing light power (Fig. 23c), suggesting that charge trapping in MoS_2 and/or at Gr/MoS_2 interface plays a key role in the sensing process. Even though this hybrid heterostructure demonstrated a relatively lower responsivity of ~1.2×10^7 AW^{-1} due to lower carrier mobility of CVD-Gr, and very slow response times (hundreds of seconds). Nonetheless, this device is more suitable for practical applications for their convenient preparation in large area.

The combination of Gr with other 2D layered semiconductors could exhibit similar photogating effect. Compared with devices composed of Gr/MoS_2 heterostructures, these phototransistors displayed much lower responsivities (tens of to ~10^5 AW^{-1}), however, normally with fast response speed [378–383]. The extension of response spectrum to the NIR can be achieved by utilizing $MoTe_2$ and Bi_2Te_3 with small bandgap [378,381]. By eliminating possible deep charge traps that are probably present at the Gr/GaSe inter-

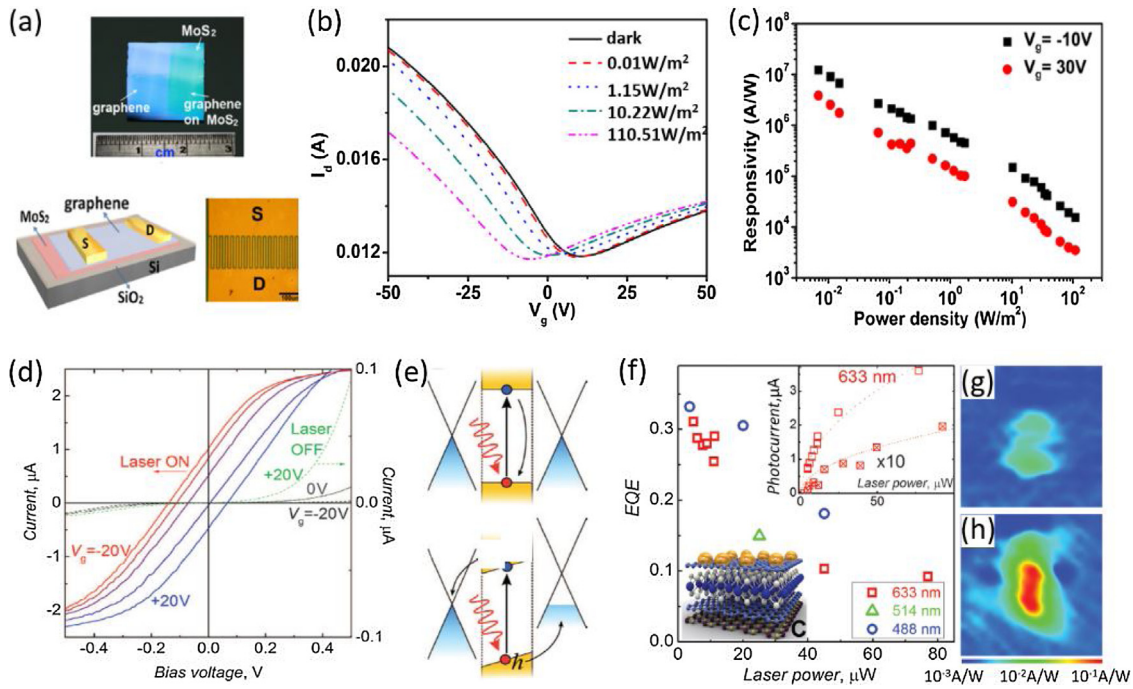

Fig. 23. (a) Photograph, schematic illustration and SEM image of the Gr/MoS_2 hybrid phototransistor. (b) Transfer curves of the device under light illumination with different powers. (c) Responsivity of the device as a function of incident light intensity. Reprinted with permission from Nature Publishing Group. [374] (d) Gate voltage dependent *I-V* curves of Gr/WS_2/Gr heterostructure. (e) Energy band diagram of the heterostructure with and without built-in electric field. (f) Quantum efficiency under different light intensity. (g and h) Photocurrent mapping of the device without and with Au NPs. Reprinted with permission from American Association for the Advancement of Science. [367]

face, Lu et al. have achieved a high responsivity of ~3.5×10^5 AW^{-1} and a fast response speed of ~10 ms simultaneously in a Gr/GaSe hybrid phototransistor [380]. The robust and low-cost fabrication of such phototransistors suggests great promise for large-scale device fabrication with compatibility to existing microfabrication procedures and on-chip integration with Si-based readout circuits.

Gr/2D layered semiconductor heterostructures have found equally important promise in three types of photodiodes. The first structure exploits Gr/2D layered semiconductor/Gr vertically stacked heterostructures, in which the facile modulation of Fermi level of Gr and Schottky barrier height could allow the tuning of photocarrier generation, separation and transport processes within the heterostructure. Hitherto, a variety of 2D layered semiconductors including WS_2 [367], MoS_2 [384], WSe_2 [385], $MoTe_2$ [386] and InSe [371] have been integrated with Gr to form heterojunction devices that exhibited photovoltaic characteristics with maximum EQE values of 25-53.8% and fast response speed. For example, a vertically stacked heterostructure of Gr/WS_2/Gr can act as a tunneling transistor where the current is adjustable by the gate bias in the dark, while the device demonstrates a pronounced photoresponse with obvious gate-modulated photocurrent upon illumination (Fig. 23d) [367]. The *I-V* characteristics are linear at low bias and become non-linear (current saturation) at high bias due to the limited number of available charge carriers in the photoactive region. In the idealized case, no photocurrent was formed as the electrons/holes generated in the WS_2 have no preferred diffusion direction considering the symmetric band alignment between the top Gr/WS_2 and bottom Gr/WS_2 (Fig. 23e). However, once a built-in electric field across the WS_2 was formed, the photogenerated carriers will be efficiently separated, forming sizeable photocurrent in the circuit (Fig. 23f). Scanning photocurrent microscopy (SPCM) photocurrent mapping also confirms the photocurrent generation primarily at the regions of the heterostructures with asymmetrical potentials (Fig. 23g and h). Further photoresponse improvement by ~10-fold (the responsivity increases from ~10^{-2} AW^{-1} to ~10^{-1} AW^{-1}) has been obtained by integrating the heterostructures with plasmonic metallic nanostructures for optical absorption enhancement. It is worth noting that the polarity and amplitude of photocurrent can be modulated by tuning the direction and strength of the built-in electric field through designing a dual-gated Gr/2D layered semiconductor/Gr heterostructure [384]. Time-resolved photocurrent analysis revealed that such vertical heterostructures had a response time as low as ~5.5 ps in heterostructures based on mono- or tri-layer WSe_2, and several nanoseconds for ~40 nm thick WSe_2-based heterostructure [385]. Remarkably, the heterostructure consisting of ~10 nm thick WSe_2 exhibited a real-time response time less than ~1.6 ns due to limitation by the instruments and their resistance-capacitance (RC) time. In addition, such heterostructures also exhibited a high responsivity at forward bias. A heterostructure composed of Gr/InSe/Gr showed a maximum responsivity of ~10^5 AW^{-1} and a specific detectivity of ~10^{15} Jones at low incident power [371].

The second kind of photodiode that is characterized by relatively low responsivity has been fabricated by integrating Gr with 2D layered semiconductors such as MoS_2 [387,388], $MoTe_2$ [389] and WSe_2 [390]. The gate-tunable mismatch of Fermi levels of Gr and the semiconductor enables the adjustable Schottky junction, allowing tunable rectification behavior and photovoltaic response characteristics. Importantly, the detection range of such heterostructures can be extended to overcome the band-edge absorption limit of the semiconductor exploiting the internal photo emission in Gr. Dai et al has reported a Gr/MoS_2 Schottky junctions photodiode with a distinctive photoresponse in a wide spectral range from 400 to 1500 nm (Fig. 24a) [387]. The responsivity reaches a maximum value of 0.52 AW^{-1} at 590 nm when the device operates in energy gap excitation mode, while the value reaches a maximum of 1.26 AW^{-1} at 1440 nm when the internal photo emission in Gr dominates the photocurrent generation (Fig. 24b). Moreover, a metal-insulator-semiconductor (MIS)-like photodiode with an insulating layer inserted between Gr and the

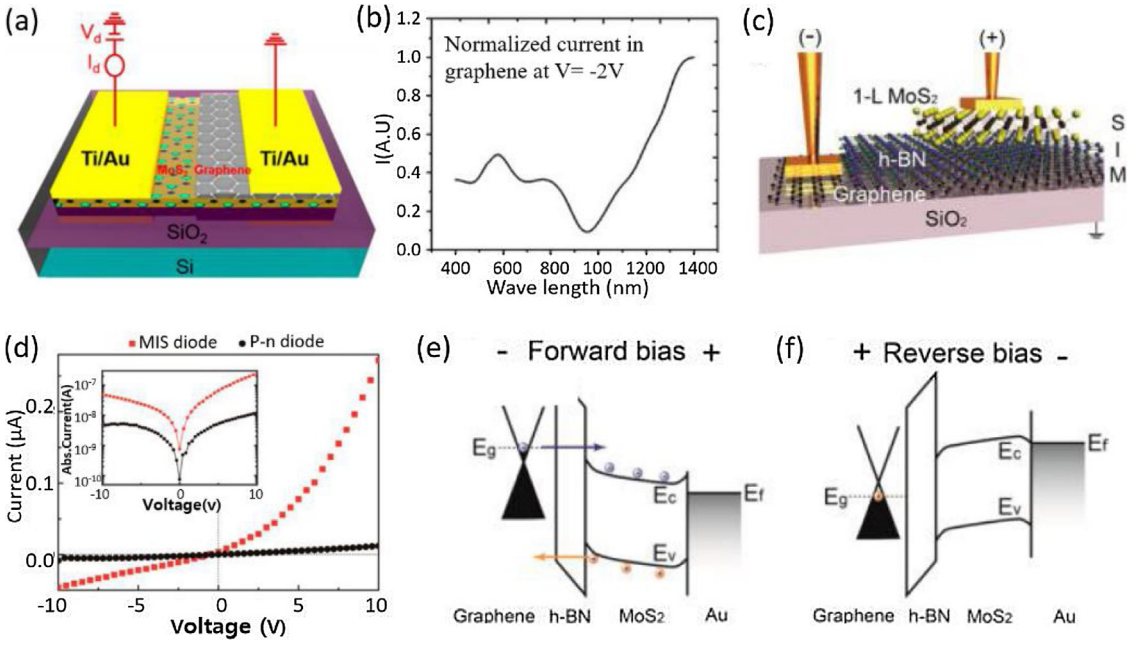

Fig. 24. (a) Schematic of the Gr/MoS_2 Schottky photodiode. (b) Spectral response of the device. Reprinted with permission from American Chemical Society. [387] (c) Schematic illustration of the Gr/*h*-BN/MoS_2 MIS diode. (d) *I-V* curves of the MIS and p-n diode. Energy band diagram of the heterojunction (e) under forward, and (f) reverse bias. Reprinted with permission from American Chemical Society. [388]

MoS_2 has demonstrated improved current rectification and much higher current flow over a metal-semiconductor (MS) diode and a PN junction based on 2D layered semiconductors (Fig. 24c), owing to carrier tunneling at forward bias and depressed carrier tunneling at reverse bias (Fig. 24e and f). This device also exhibited a obvious photoresponse to 532 nm with a responsivity of 0.3 mAW^{-1} [388].

Wi et al. demonstrated Gr/*n*-MoS_2/*p*-MoS_2/Au vertical heterostructures which represent the last architecture of photodiode [391]. It was revealed that the heterostructures doped with fluorine-contained plasmas exhibited higher degree of current rectification and higher *EQE* values in both photovoltaic (zero bias) and photoconductive (negative bias) modes, while the CHF_3 plasma-doped heterostructures showed a much higher *EQE* as high as 80% at violet-near UV region due to a low density of interfacial recombination centers. In addition, a vertical heterostructure of WSe_2/Gr/MoS_2 exhibiting a gate-tunable rectifying behavior and broadband photodetection with the response range up to 2400 nm has been reported [392]. The device exhibited a high responsivity of up to 10^4 AW^{-1} at visible region, which decreases drastically to 10^{-1} AW^{-1} at 2400 nm IR wavelength. Such distinct responsivity to different wavelengths can be understood as follows: In the visible range where incident photon energy is larger than the bandgap of the TMDs, the incident light could be absorbed by all three layered materials (WSe_2, Gr and MoS_2), which generates a large number of photocarriers and contributes to a sizeable photocurrent. Nonetheless, when the device was shined by IR illumination with energy smaller than the bandgap of WSe_2, only Gr can absorb light and hence form very low photocurrent.

Gr/Organic semiconductors

Organic semiconductors including small molecules and polymers are appealing materials for electronics and optoelectronics [393]. Organic thin films can be facilely assembled on a variety of substrates *via* solution-based processing techniques, such as spin-coating, spray-coating, dip-coating and ink-jet printing, *etc.*, towards large-area, flexible and light-weight electronic and optoelectronic applications. In addition, it is feasible to tune the optoelectronic properties of organic semiconductors, both at a material and device level, through adjusting their molecular structures, which provides the possibility to optimize photocarrier generation, charge transport, and radiative recombination processes determined by the targeted application [394]. In this section, we will review the recent achievement in optoelectronic applications of Gr/organic semiconductors-based hybrid heterostructures.

The most important optoelectronic application of Gr/organic semiconductors heterojunction lies in phototransistors in which the organic semiconductors function as appropriate light harvesting sensitizers, while Gr serves as the conducting channel for carrier transport and circulation. The organic semiconductors involved include poly(3-hexylthiophene) (P3HT) [395,396], bulk heterojunction of polymer and fullerene [395], dye molecules (e.g., rhodamine 6G) [397], tetraphenyl-porphyrin (H2TPP) [398], metalloporphyrins [398], pentacene [399] and dioctylbenzothienobenzothiophene (C_8-BTBT) [400]. In these devices, the appropriate band alignment between Gr and the organic semiconductors can induce the transfer of photocarriers from the semiconductors to Gr and significantly enhance the photoresponse. These hybrid phototransistors usually exhibit responsivities from tens of to larger than 10^5 AW^{-1}. For example, a Gr/P3HT hybrid heterostructure on a piezoelectric substrate has demonstrated a ~10-fold enhanced responsivity than a control device on a SiO_2 substrate [395]. The improved photoresponse is interpreted by a vertical electric field of the polarization of piezoelectric substrate, that facilitates the spatial separation of photogenerated electrons and holes and promotes the hole doping of Gr.

Gr/pentacene heterostructure has been reported to act as a multifunctional photodetector with a nonvolatile memory function for storing photonic signal [399]. The device displayed an evident photoresponse from 400 to 800 nm, with a peak responsivity and specific detectivity of 700 AW^{-1} and 10^{13} Jones, respectively. Notably, the transfer characteristics showed a large hysteresis behavior with the Dirac point voltage shifted towards positive gate voltage both in dark and under illumination, which conveys a nonvolatile memory functionality to the photodetector. Such a hysteresis behavior originates from the trapping-detrapping of charge

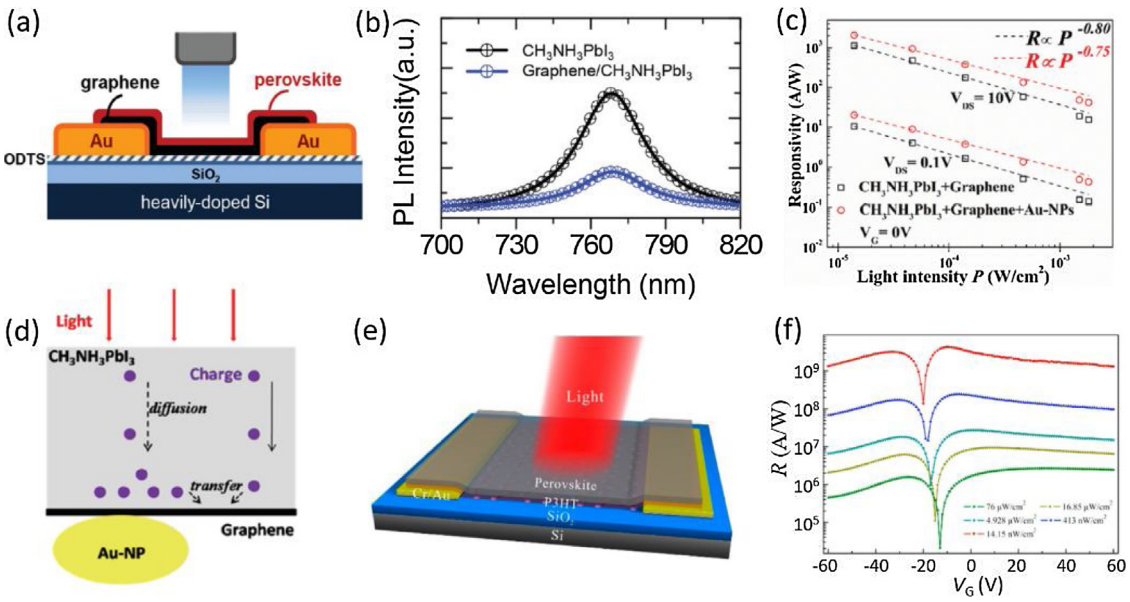

Fig. 25. (a) Schematic of the Gr/$CH_3NH_3PbI_3$ hybrid phototransistor. (b) PL spectra of $CH_3NH_3PbI_3$ and Gr/$CH_3NH_3PbI_3$ hybrid. Reprinted with permission from Wiley–VCH. [410] (c) Responsivity of a Gr/$CH_3NH_3PbI_3$ phototransistor modified with Au NPs as a function of light intensity. (d) Schematic of the generation, diffusion and transfer of photo-induced carriers in the perovskite layer with and without Au NPs. Reprinted with permission from the Royal Society of Chemistry. [412] (e) Schematic illustration of the $CH_3NH_3PbI_{3-x}Cl_x$/P3HT/Gr hybrid phototransistor. (f) Responsivity as a function of gate voltage at different light intensities. Reprinted with permission from American Chemical Society. [414]

carriers in the Au NPs as a result of tunneling through the dielectric layer. The device can possess an excellent retention characteristics of the stored light information with a retention time exceeding 10^4 s and the photocurrent remaining invariant over 200 cycles. It was also found that the photocurrent increases stepwise with increasing optical power, which may enable the realization of multibit memory storage. Recently, Liu et al. demonstrated van der Waals epitaxy of ultrathin organic C_8-BTBT crystals on Gr for sensitive photodetector applications [400]. Ultrathin phototransistors with even monolayer organic semiconductors exhibited a responsivity higher than 10^4 AW^{-1}, while thicker multilayer C_8-BTBT devices afforded an enhanced responsivity as high as 4.76×10^5 AW^{-1}, which is the best result for organic UV photodetectors thus far. Such a prominent photoresponse can be attributed to the ultrahigh photoconductive gain and efficient interfacial charge transfer efficiency, which stems from the high quality of C_8-BTBT layers the Gr/C_8-BTBT interface. Even so, the response speed degraded by more than 30 times from ~25 ms for monolayer C_8-BTBT device to ~830 ms for thicker one, due to greater energy barrier hopping of trapped carriers between C_8-BTBT layers. In view of the diversity of organic molecules, the epitaxial ultrathin organic crystals on Gr may potentially serve as a versatile platform for high-performance, broadband phototransistors application.

Gr/organic semiconductors heterostructure has found application in transparent conductive electrodes as well. Large-area Gr films with tailored thickness from 10 to 20 nm can be facilely prepared by spray-coating of a hybrid ink of electrochemically exfoliated Gr and poly(3,4-ethylenedioxythiophene):poly(styrenesulfonate) (PEDOT:PSS) [401]. The as-prepared Gr films exhibited a high conductivity of 1000 Scm^{-1} with a transmittance of 80% at 500 nm, which is superior to other solution-processed Gr films and can avoid the drawbacks of CVD process, offering the possibility to be scaled up. The as-fabricated Gr films proved to be ideal transparent electrodes for organic photodiodes with P3HT:PCBM blend as photoactive layer, which exhibited remarkable photoresponse with a specific detectivity of 1.33×10^{12} Jones at 500 nm illumination.

Gr/Perovskite materials

In the past several years, organic-inorganic halide perovskites have drawn significant attention and emerged as one of the most exploited candidate materials for cost-effective and high-performance photovoltaics and optoelectronics [402–405]. This group of materials have a generalized formula of ABX_3, where A is an organic cation, methylammonium (CH_3NH_3) or formamidinium ($NH{=}CHNH_3$) ion, B is a metal cation (e.g. Pb^{2+}, Sn^{2+}, Cs^{2+} or Cd^{2+}), and X is a halide anion (I-, Cl- or Cl-) [406]. Their great promise in optoelectronics originates from the appealing electrical and optical properties, including long carrier lifetime (~270 ns) and carrier diffusion length (up to ~175 μm in single-crystals), high carrier mobility (~10-2320 $cm^2V^{-1}s^{-1}$), low exciton binding energy (~2 meV), tunable direct bandgaps, high light absorption coefficient as well as wide optical absorption across the UV-visible to NIR spectrum [407–409]. A variety of study has shown that when Gr is combined with perovskite materials, the resultant Gr/perovskite hybrid structure can take advantage of the synergistic benefit of both materials, and hence bring about novel functionality and property to the device. Here, we are going to focus on the recent research on the optoelectronic application of Gr/perovskite materials-based hybrid heterostructures.

Thus far, a number of perovskite thin films such as $CH_3NH_3PbI_3$ [410–413] or $CH_3NH_3PbI_{3-x}Cl_x$ [414] and perovskite nanostructures including $CH_3NH_3PbI_3$ NWs [415], $CH_3NH_3PbBr_2I$ NCs [416] and $CsPbBr_{3-x}I_x$ NCs [417] have been integrated with Gr to form sensitive Gr/perovskite phototransistors. In early studies, devices composed Gr/$CH_3NH_3PbI_3$ thin films hybrid usually exhibited responsivities of hundreds of AW^{-1} and relatively rapid response speeds faster than 1 s, with a broad response spectral across the UV-visible range [410,411]. Fig. 25a shows an example of a representative Gr/$CH_3NH_3PbI_3$ hybrid phototransistor. The device performance of these phototransistors is not comparable to the state-of-the-art Gr-based hybrid phototransistors with the similar working mechanism [29,30,418], however it is several orders of magnitude higher than those of pure Gr device [419]. The enhanced

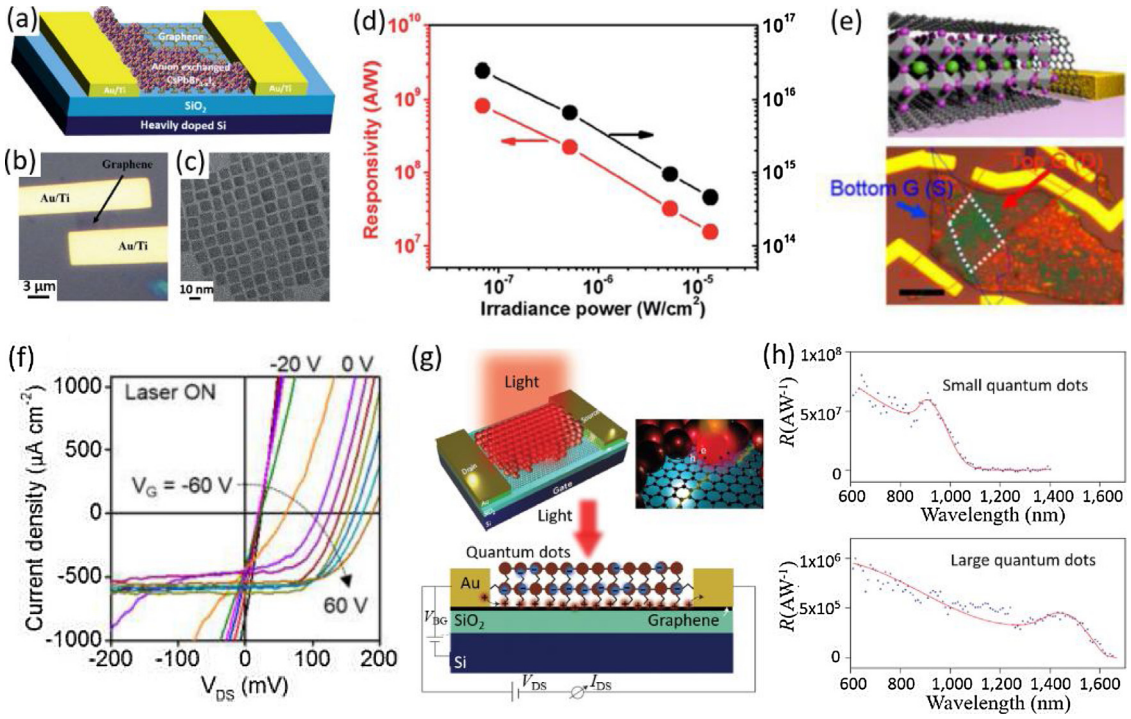

Fig. 26. (a) Schematic of the Gr/CsPbBr$_{3-x}$I$_x$ NCs hybrid phototransistor. (b) Optical photograph of the device. (c) HRTEM image of the CsPbBr$_{3-x}$I$_x$ NCs. (d) Responsivity and specific detectivity of the photodetector under different irradiance power. Reprinted with permission from the Royal Society of Chemistry. [417] (e) Schematic and SEM image of the Gr/perovskite/Gr vertically stacked heterostructure. (f) I_{ds}-V_{ds} at varied V_g under 532 nm illumination. Reprinted with permission from American Chemical Society. [422] (g) Schematic illustration of Gr/PbS QDs hybrid phototransistor. (h) Spectral selectivity of the two devices with single layer and bilayer Gr. Reprinted with permission from Nature Publishing Group. [29]

photoresponse performance can be attributed to the transfer of electrons from the Gr to the proximal perovskite layer, which fill the empty states in the valence band of the perovskite and therefore reduce the recombination of photocarriers in the perovskite. As a result, the photogenerated electrons remained in the conduction band of the perovskite, which produce an effective photogating effect and alter the conductivity of Gr channel through capacitive coupling. The process of electron trapping was evidenced by a dramatic quenching of the PL intensity of the Gr/perovskite system (Fig. 25b).

The photosensitivity can be optimized by using plasmonic metallic NPs [412], improving the quality of the perovskite films [413], and suppressing recombination of photocarriers *via* selective charge transfer [414]. For example, integration of Au NPs with SPR peak located at ~530 nm into Gr/$CH_3NH_3PbI_3$ hybrid phototransistors has increased the responsivity from ~1143 to ~2067 AW^{-1}, and achieved much faster response speed (Fig. 25c) [412]. The higher responsivity is attributed to the improved light harvesting due to enhanced near-field of the perovskite as a result of the plasmonic effect of Au NPs. Since the enhanced light harvesting takes place very close to the Gr/perovskite interface, therefore the diffusion paths for photocarriers towards Gr are very short, contributing to a rapid photoresponse (Fig. 25d). Afterwards, a sequential vapor deposition technique has been developed to grow ultraflat $CH_3NH_3PbI_3$ perovskite films on Gr, so as to provide compact heterostructures for efficient light harvesting and exciton separation [413]. The as-fabricated hybrid phototransistor achieved an ultrahigh responsivity of 1.73×10^7 AW^{-1} and specific detectivity of 2×10^{15} Jones, respectively, which are several orders of magnitude higher than those composed of $CH_3NH_3PbI_3$ films from spin-coating method. Very recently, Xie et al. tried to insert a P3HT thin layer as hole transporting layer between $CH_3NH_3PbI_{3-x}Cl_x$ perovskite and Gr for high-performance phototransistors (Fig. 25e) [414]. On account of the effective separation of photogenerated electrons and holes, the recombination of photocarriers is greatly prohibited and high density electrons are trapped in the perovskite layer. In addition, $CH_3NH_3PbI_{3-x}Cl_x$ perovskite possesses much longer carrier diffusion length than $CH_3NH_3PbI_3$ perovskite, which enables more efficient transfer of photogenerated holes towards Gr. Benefiting from these factors, this multi-heterojunction phototransistor exhibited an unprecedented ultrahigh responsivity of ~4.3×10^9 AW^{-1} and a gain approaching 10^{10}, respectively. The performance values are at least one order of magnitude higher than other devices without P3HT layer and outperform those of the state-of-the-art Gr-based hybrid phototransistors [29,30,418].

Compared with thin film, perovskite nanostructures with higher crystallinity usually possess much lower bulk recombination rate of photogenerated carriers, and therefore is beneficial for photodetection application. Phototransistors based on hybrid heterostructures of Gr and perovskite nanostructures such as $CH_3NH_3PbI_3$ NWs, $CH_3NH_3PbBr_2I$ NCs and CsPbBr$_{3-x}$I$_x$ NCs exhibited responsivities from ~ 6.0×10^5 AW^{-1} to as high as 8.2×10^8 AW^{-1} [415–417]. Spina et al. developed a sensitive Gr/$MAPbI_3$ NWs hybrid phototransistor that had responsivity as high as 2.6×10^6 AW^{-1} [415]. Such a good device performance is mainly due to the perovskite morphology. Later on, by hybridizing Gr with CsPbBr$_{3-x}$I$_x$ NCs, Lee's group achieved a more sensitive phototransistor (Fig. 26a–c) [417]. Due to superb carrier transport of the Gr, the hybrid devices exhibited an ultrahigh responsivity of 8.2×10^8 AW^{-1} and specific detectivity of 2.4×10^{16} Jones (Fig. 26d), suggesting great promise of perovskite NCs in next-generation high-performance photodetector application. In a recent work, Qian and co-workers reported a phototransistor comprising a heterostructure of a nitrogen-doped Gr QDs/perovskite composite layer and a rGO layer [420]. This design could improve the photocurrent and photoswitching characteristics in that the Gr QDs can function as an effective and fast pathway for transfer of photogenerated electrons from the perovskite to the rGO layer. As a consequence, the hybrid phototransistor exhibited

a prominent photoresponse with a responsivity of 1.92×10^4 AW^{-1} and rapid response speed of ~10 ms in a wide spectrum range from 365 to 940 nm. The NIR response beyond the intrinsic bandgap of the perovskite is related to the photocarrier generation in rGO and PbI_2 species.

Another architecture is structurally characterized by using 2D perovskite crystals as light sensitizer, and two separated Gr layers as conducting electrodes. For example, Tan et al. have reported a photodetector based on 2D $(C_4H_9NH_3)_2PbBr_4$ with domain size of several to tens of micrometers and thickness of several to tens of nanometers [421]. The phototransistors with the protection and top contact of Gr electrodes showed pronounced optoelectronic property with low dark current (~10^{-10} A) and high current on/off ratio (up to 10^3). More importantly, the devices achieved a high responsivity of up to ~2100 AW^{-1} through the design of Gr interdigital electrodes to enlarge the effective absorption cross section. The remarkable photoresponse is ascribed to both the strong optical absorption of 2D perovskite crystals and effective charge collection by Gr electrodes. By sandwiching two Gr layers together with 2D $CH_3NH_3PbI_3$ layers which were converted from ultrathin PbI_2 layers exfoliated from a PbI_2 crystal, Cheng et al achieved a sensitive vertically stacked phototransistor [422]. In virtue of the extremely short vertical carrier transit path and consequently a small carrier transit time, the devices reached a maximum responsivity of ~950 AW^{-1}, a photoconductive gain of ~2200 and fast response speed on the order of several millisecond, which are superior to other devices with lateral configurations. Furthermore, Gr/WSe_2/$CH_3NH_3PbI_3$/Gr vertical photodiodes have been realized, which exhibited diode-like rectifying behavior within the positive V_g range, while nearly symmetric *I-V* characteristics within the negative V_g range. This phenomenon is related to the transition from the PN to PP junctions at the $CH_3NH_3PbI_3$/WSe_2 interface due to the ambipolar nature of WSe_2 under different gate voltages.

Gr/Group IV-VI semiconductors

Aside from the above materials, other semiconductors including PbS QDs [29,418,423], PbSe QDs [424] and coordination compounds [425,426] have been employed as light sensitizers and integrated with Gr to form hybrid heterostructure phototransistors. These devices also work on the photogating effect (Fig. 26g). As a result of the strong and tunable IR light absorption in the QD layer, phototransistors based on Gr/PbS QDs hybrid heterostructures can exhibit maximum responsivities as high as ~10^7 AW^{-1} and a photoconductive gain of 10^8 in IR wavelength region (Fig. 26h), however, at the expense of response speeds (several to tens of seconds) [29,418]. The responsivity values are several orders of magnitude higher than that of pure PbS QDs photodetectors and can be attributed to the following processes. Light absorption in QDs produces electron and hole pairs, and holes tend to transfer to Gr due to decreased energy. These holes recirculate many times and contribute to the photocurrent in the channel before they recombine with electrons trapped in the QDs, while the trapped electrons act as an effective gate to modulate the conductivity of Gr. It was also revealed that the slow photocurrent decay process can be accelerated by the application of an electric pulse at the gate of the devices. In this case, the as-generated electric field can reduce the potential barrier, and keeps electrons trapped in the QDs at Gr/QDs interface [29]. Note that the ligand capped on the surface of the QDs is critical to the photoresponse characteristics in terms of photocurrent and response speed because the ligand can greatly influence the charge transfer between the Gr and QDs [418]. Flexible phototransistors on plastic substrates also showed similar photo responsivity with excellent flexibility and bending stability. Afterwards, multi-heterojunction phototransistors consisting of layer-by-layer Gr/PbSe QDs hybrids have been fabricated and studied [424]. The devices with Gr at the bottom layer can exhibited a responsivity of ~10^6 AW^{-1} under 808 nm illumination. These results suggest that phototransistors comprising Gr and PbS (PbSe) QDs hybrid heterostructures are suitable for high-performance IR photodetection and may hold great promise in some emerging fields such as wearable and stretchable electronics/optoelectronics. Gr/coordination compound hybrid phototransistors with chlorophyll molecules or ultrathin ruthenium complex as light absorbing media also shown a remarkable photoresponse [425,426]. The responsivities achieved in the two devices are ~10^6 and 10^5 AW^{-1}, respectively, which can be explained by the efficient separation and transfer of photogenerated carriers at the Gr/light sensitizers interface and the pronounced photogating effect.

To conclude, Gr/2D TMDs heterostructures can enable the realization of ultrathin solar cells with very high power densities, whose performance are greatly affected by the thickness of the Gr and TMDs and can be further promoted by designing light-trapping structure. Gr/2D layered semiconductor heterostructures-based phototransistors with MSM-like architecture exhibit high responsivities of 4×10^3 AW^{-1} with fast response speeds of ~1/~10 ms, while their hybrid phototransistors working on photogating effect can demonstrate ultrahigh responsivities of up to 5×10^8 AW^{-1}, unfortunately at the sacrifice of response speed (tens of seconds). On the other hand, various Gr/2D layered semiconductors heterostructures-based photodiodes have been realized, including Gr/2D layered semiconductors/Gr, Gr/2D layered semiconductors Schottky junctions and some other artificial heterostructures, which usually exhibit tunable photovoltaic response characteristics. These devices normally demonstrate responsivities less than 1 AW^{-1} at zero bias condition, however, much higher values as high as ~10^5 AW^{-1} at forward bias. In particular, a WSe_2/Gr/MoS_2 heterostructure can exhibit a broadband photoresponse with detection wavelength as long as 2400 nm. Normally, Gr/organic semiconductors hybrid phototransistors show responsivities from tens of to 10^5 AW^{-1} and performance improvement can be realized through employing piezoelectric substrates or using organic bulk heterojunctions as photoactive layers. Especially, a Gr/pentacene heterostructure can work as both a photodetector and a nonvolatile memory device for storing photonic signal with excellent retention time. Ultrathin phototransistors composed of heterostructures of Gr and epitaxial-grown monolayer organic crystals exhibit responsivities of 10^4 AW^{-1} with rapid response speeds of ~25 ms and both performance values are related to the thickness of the organic crystals. In addition, Gr/perovskite hybrid phototransistors can exhibit record responsivities higher than 10^9 AW^{-1} upon a variety of optimization including light absorption enhancement, optimizing the quality of the perovskite films, photocarrier recombination suppression through interface energy engineering and using perovskite nanostructures with higher crystalline quality. Gr/2D perovskite crystals/Gr planar or vertical phototransistors demonstrate higher responsivities of ~2100 or ~950 AW^{-1} with fast response speeds due to enhanced effective absorption cross section or ultra-short carrier transit path. Gr/PbS QDs hybrid phototransistors show maximum reponsivities as high as 10^7 AW^{-1} at IR wavelength region. What is more, the photoresponse parameters in terms of photocurrent and response speed are highly influenced by the ligand capped on the surface of the QDs. Gr phototransistors hybridized with other photosensitizers also shown great promise in ultrasensitive photodetection with maximum responsivities reaching ~10^6 AW^{-1}. The figure-of-merits of some representative photodetectors based on Gr/other semiconductors heterostructures are summarized in Table 2.

Conclusions and outlook

Gr/semiconductor hybrid heterostructures have shown huge potential in a great variety of optoelectronic device applications, such as solar cells, photodetectors, LEDs and lasers, *etc*. In this article, we have presented a comprehensive overview of the research achievements in optoelectronic devices based on various Gr/semiconductors heterostructures, including /group II-VI nanostructures, /group III-V semiconductors, /group IV semiconductors, /metal oxides and /other semiconductors. Particular attention has been given to some critical issues pertaining to the device design, device performance and physics, and processing techniques for performance improvement. Through optimization *via* various approaches, these devices normally demonstrate not only enhanced optoelectronic performance, but also some novel functionalities, which paves the way for them towards many practical applications.

For photovoltaic applications, solar cells composed of Gr/semiconductors hybrid heterostructures normally exploit the Schottky junction between Gr and the semiconductors, where light absorption mainly takes place in the semiconductors, while Gr acts as not only an active layer for photocarrier separation but also a transparent electrode for carrier collection. Their photovoltaic performance are primarily determined by the processes of light absorption as well as generation, separation, transport and collection of photocarriers. Therefore, various techniques have been developed to optimize the device performance. The work function, sheet resistance and optical transparency of Gr can be greatly adjusted *via* layer number tuning, chemical doping, photo-induced doping or electric field gating doping, therefore the carrier concentration, barrier height, series resistance and optical absorption of the devices can be optimized. The barrier height of the devices and recombination rate of the photocarriers can be improved through interface band engineering to tune band alignment and interface passivation to saturate the dangling bonds and reduce interface defects. Light absorption enhancement can be realized by introducing semiconductor nano/microstructure arrays, antireflective layer coating, or exploiting plasmonic effect of metallic nanostructures. Solar cells based on Gr/semiconductors hybrid heterostructures usually exhibit pronounced photovoltaic performance. The PCEs of Gr/group II-VI nanostructures hybrids are not very high currently due to the insufficient light absorption over the whole solar energy spectrum. On the other hand, high PCEs of 15.6% and 18.5% have been achieved for Gr/Si and Gr/GaAs Schottky junctions within a short period of time, respectively, which signifies bright future for this kind of solar cells. However, the PCEs are still lower than that of currently commercial Si-based photovoltaic devices and there are a number of challenges that need to be tackled in future work. For practical applications, the efficiency, cost and lifetime of the devices are some of the most critical issues. To further improve the efficiency, more attention should be paid to the properties of the materials and rational device design. For example, production of large-scale Gr films with higher intrinsic sheet conductivity are needed. Novel Gr doping techniques that can further tune its work function and enhance its sheet conductivity can be developed. Also, new interface passivation and modification methods can be introduced to effectively optimize the band alignment and suppress photocarrier recombination. Introducing other optoelectronic materials and structures may be helpful for further improving device performance. In addition, large-area production of solar cells with high PCEs is urgently needed as well. As the fabrication of such Schottky type solar cells is free of complicated manufacturing processes and expensive equipment, the cost is primarily limited by the material usage, namely the semiconductors such as Si and GaAs. An alternative route is to use semiconductor nanostructure arrays that can not only use less materials but also guarantee efficient optical absorption. Additionally, using polycrystalline semiconductors (solar-grade) to replace single-crystalline ones that normally used in current studies can be considered as well. To improve the lifetime of the devices, several critical issues should be tackled. Development of efficient and stable Gr doping techniques is in demand to overcome the poor air stability of the devices. Also, effective device packing is useful to avoid interface oxidation for long-term operation.

For photodetecting applications, hybrid phototransistors composed of Gr and semiconductors usually work on the photogating effect, where the semiconductors are used as the light absorbing media and Gr functions as the conducting channel for carrier transport and circulation. These devices can exhibit remarkable photoresponse characteristics with ultrahigh responsivities exceeding 10^9 AW^{-1}, yet, normally with very slow response speeds. So they are more suitable for some special applications where fast response is not a necessity. In the case of photodiodes which also exploit the Schottky junction between Gr and the semiconductors, devices usually display very fast response speeds. Nevertheless, the responsivities are low at zero bias, which could be improved at moderate reverse bias. To meet the requirement for many applications, the performance of these photodetectors should be further optimized. First, the properties of some sensing materials can be optimized. For example, as the heterogeneity of nanostructured materials (NWs, QDs, 2D semiconductors, *etc*.) can greatly affect the uniformity of the device performance, more precise control of not only the morphology, hierarchical, crystallinity, and orientation assembly, but also physical and chemical properties especially carrier transport characteristics is highly demanding. In the case of thin films, the crystalline quality and charge carrier mobility, as well as thermal stability should be improved as well. Second, the performance could be improved with the aid of novel device design. Some emerging methods such as plasmonic techniques, integration of optical waveguide and microcavities are helpful approaches to enhance light-matter interaction for optical absorption improvement. Importantly, particular efforts should be devoted to enhancing the response speed of hybrid phototransistors. Optimizing the charge carrier mobility of the sensing materials and introducing a vertical electric field are effective approaches that can optimize the transfer and separation of photocarriers. The study of Gr/semiconductor solar cells can also afford some useful experiences for further improving the performance of Gr/semiconductor photodiodes. In addition, broadband or spectrum-selective photodetection should be developed for some specific applications. Therefore, selection of appropriate sensing materials and introducing new materials should be taken into consideration. Also, for some novel device concepts such as bendable, stretchable and wearable device applications, development of flexible photodetectors and solar cells is much needed. In addition to performance improvement, long-term stability and durability, environmental-friendly and cost-effective processing techniques, as well as large-scale production and integration are critical issues that need more efforts in future work towards real applications. However, the path to commercialization is still very tough, for which a great number of new technology and structural design are needed to put a step further. Given the simple device architecture and cost-effective manufacturing process, and high device performance, Gr/semiconductor hybrid heterostructures are very promising for new generation optoelectronic device applications.

Acknowledgement

This work was supported by the National Natural Science Foundation of China (NSFC), (Nos. 61675062, 61575059, 21501038),

the Natural Science Foundation of Anhui Province of China (Nos. 1408085MB31, J2014AKZR0036), and the Fundamental Research Funds for the Central Universities (2013HGCH0012, 2014HGCH0005).

References

[1] K.S. Novoselov, Science 306 (2004) 666–669.
[2] Y.M. Lin, C. Dimitrakopoulos, K.A. Jenkins, D.B. Farmer, H.Y. Chiu, A. Grill, et al., Science 327 (2010) 662.
[3] M. Liu, X. Yin, E. Ulin-Avila, B. Geng, T. Zentgraf, L. Ju, et al., Nature 474 (2011) 64–67.
[4] K.S. Kim, Y. Zhao, H. Jang, S.Y. Lee, J.M. Kim, K.S. Kim, et al., Nature 457 (2009) 706–710.
[5] Y.W. Zhu, S. Murali, M.D. Stoller, K.J. Ganesh, W.W. Cai, P.J. Ferreira, et al., Science 332 (2011) 1537–1541.
[6] F. Xia, T. Mueller, Y. Lin, A. Valdes-Garcia, P. Avouris, Nat. Nanotechnol. 4 (2009) 839–843.
[7] T.H. Han, Y. Lee, M.R. Choi, S.H. Woo, S.H. Bae, B.H. Hong, et al., Nat. Photonics 6 (2012) 105–110.
[8] M.F. El-Kady, V. Strong, S. Dubin, R.B. Kaner, Science 335 (2012) 1326–1330.
[9] A.K. Geim, K.S. Novoselov, Nat. Mater. 6 (2007) 183–191.
[10] K.S. Novoselov, V.I. Fal'ko, L. Colombo, P.R. Gellert, M.G. Schwab, K. Kim, Nature 490 (2012) 192–200.
[11] M.H. Rümmeli, C.G. Rocha, F. Ortmann, I. Ibrahim, H. Sevincli, F. Börrnert, et al., Adv. Mater. 23 (2011) 4471–4490.
[12] Z.Y. Yin, J.X. Zhu, Q.Y. He, X.H. Cao, C.L. Tan, H.Y. Chen, et al.,Adv. Energy Mater. 4 (2014), 1300574.
[13] Z. Liu, S.P. Lau, F. Yan, Chem. Soc. Rev. 44 (2015) 5638–5679.
[14] F.H.L. Koppens, T. Mueller, P. Avouris, A.C. Ferrari, M.S. Vitiello, M. Polini, Nat. Nanotechnol. 9 (2014) 780–793.
[15] J. Li, L. Niu, Z. Zheng, F. Yan, Adv. Mater. 26 (2014) 5239–5273.
[16] Z. Sun, H. Chang, ACS Nano 8 (2014) 4133–4156.
[17] L. Wang, W. Liu, Y. Zhang, Z.H. Zhang, S. Tiam Tan, X. Yi, et al., Nano Energy 12 (2015) 419–436.
[18] F. Bonaccorso, Z. Sun, T. Hasan, A.C. Ferrari, Nat. Photonics 4 (2010) 611–622.
[19] Y. Song, W. Fang, R. Brenes, J. Kong, Nano Today 10 (2015) 681–700.
[20] C. Lee, X. Wei, J.W. Kysar, J. Hone, Science 321 (2008) 385–388.
[21] F. Wang, Y. Zhang, C. Tian, C. Girit, A. Zettl, M. Crommie, et al., Science 320 (2008) 206–209.
[22] H. Liu, Y. Liu, D. Zhu, J. Mater. Chem. 21 (2011) 3335–3345.
[23] C. Xie, C. Mak, X. Tao, F. Yan,Adv. Funct. Mater. 27 (2017), 1603886.
[24] W. Bao, L. Jing, J. Velasco, Y. Lee, G. Liu, D. Tran, B. Standley, et al., Nat. Phys. 7 (2011) 948–952.
[25] L. Lin, L. Liao, J. Yin, H. Peng, Z. Liu, Nano Today 10 (2015) 701–716.
[26] S. Sonde, F. Giannazzo, V. Raineri, R. Yakimova, J.R. Huntzinger, A. Tiberj, et al.,Phys. Rev. B. 80 (2009), 241406.
[27] X. Li, H. Zhu, K. Wang, A. Cao, J. Wei, C. Li, et al., Adv. Mater. 22 (2010) 2743–2748.
[28] Y. Song, X. Li, C. Mackin, X. Zhang, W. Fang, T. Palacios, et al., Nano Lett. 15 (2015) 2104–2110.
[29] G. Konstantatos, M. Badioli, L. Gaudreau, J. Osmond, M. Bernechea, F.P.G. de Arquer, et al., Nat. Nanotechnol. 7 (2012) 363–368.
[30] K. Roy, M. Padmanabhan, S. Goswami, T.P. Sai, G. Ramalingam, S. Raghavan, et al., Nat. Nanotechnol. 8 (2013) 826–830.
[31] X. Li, W. Chen, S. Zhang, Z. Wu, P. Wang, Z. Xu, et al., Nano Energy 16 (2015) 310–319.
[32] A. Di Bartolomeo, Phys. Rep. 606 (2016) 1–58.
[33] X.M. Li, H.W. Zhu, Phys. Today 69 (2016) 46–51.
[34] X. Li, L. Tao, Z. Chen, H. Fang, X. Li, X. Wang, et al.,Appl. Phys. Rev. 4 (2017), 21306.
[35] W.J. Jie, J.H. Hao, Nanoscale 6 (2014) 6346–6362.
[36] P. Avouris, C. Dimitrakopoulos, Mater, Today 15 (2012) 86–97.
[37] Y.W. Zhu, S. Murali, W. Cai, X. Li, J.W. Suk, J.R. Potts, et al., Adv. Mater. 22 (2010) 3906–3924.
[38] X. Huang, Z. Yin, S. Wu, X. Qi, Q. He, Q. Zhang, et al., Small 7 (2011) 1876–1902.
[39] X. Huang, X. Qi, F. Boey, H. Zhang, Chem. Soc. Rev. 41 (2012) 666–686.
[40] C. Soldano, A. Mahmood, E. Dujardin, Carbon 48 (2010) 2127–2150.
[41] V. Singh, D. Joung, L. Zhai, S. Das, S.I. Khondaker, S. Seal, Prog. Mater. Sci. 56 (2011) 1178–1271.
[42] A.H. Castro Neto, N.M.R. Peres, K.S. Novoselov, A.K. Geim, F. Guinea, Rev. Mod. Phys. 81 (2009) 109–162.
[43] L.A. Falkovsky, J. Phys,Conf. Ser. 129 (2008), 12004.
[44] K.I. Bolotin, K.J. Sikes, Z. Jiang, M. Klima, G. Fudenberg, J. Hone, et al., Solid State Commun. 146 (2008) 351–355.
[45] K. Chen, X. Wan, D. Liu, Z. Kang, W. Xie, J. Chen, et al., Nanoscale 5 (2013) 5784–5793.
[46] J.H. Chen, W.G. Cullen, C. Jang, M.S. Fuhrer, E.D. Williams,Phys. Rev. Lett. 102 (2009), 236805.
[47] T.O. Wehling, S. Yuan, A.I. Lichtenstein, A.K. Geim, M.I. Katsnelson,Phys. Rev. Lett. 105 (2010), 56802.
[48] C.H. Lui, L. Liu, K.F. Mak, G.W. Flynn, T.F. Heinz, Nature 462 (2009) 339–341.
[49] J.H. Chen, C. Jang, S. Xiao, M. Ishigami, M.S. Fuhrer, Nat. Nanotechnol. 3 (2008) 206–209.
[50] W. Zhu, T. Low, V. Perebeinos, A. a Bol, Y. Zhu, H. Yan, et al., Nano Lett. 12 (2012) 3431–3436.
[51] Y.W. Son, M.L. Cohen, S.G. Louie,Phys. Rev. Lett. 97 (2006), 216803.
[52] B. Trauzettel, D.V. Bulaev, D. Loss, G. Burkard, Nat. Phys. 3 (2007) 192–196.
[53] Y. Zhang, T.T. Tang, C. Girit, Z. Hao, M.C. Martin, A. Zettl, et al., Nature 459 (2009) 820–823.
[54] J.B. Oostinga, H.B. Heersche, X. Liu, A.F. Morpurgo, L.M.K. Vandersypen, Nat. Mater. 7 (2008) 151–157.
[55] K.F. Mak, L. Ju, F. Wang, T.F. Heinz, Solid State Commun. 152 (2012) 1341–1349.
[56] R.R. Nair, P. Blake, A.N. Grigorenko, K.S. Novoselov, T.J. Booth, T. Stauber, et al., Science. 320 (2008) 1308.
[57] V.G. Kravets, A.N. Grigorenko, R.R. Nair, P. Blake, S. Anissimova, K.S. Novoselov, et al.,Phys. Rev. B 81 (2010), 155413.
[58] F. Rana, P.A. George, J.H. Strait, J. Dawlaty, S. Shivaraman, M. Chandrashekhar, et al.,Phys. Rev. B 79 (2009), 115447.
[59] F. Xia, T. Mueller, R. Golizadeh-Mojarad, M. Freitage, Y.M. Lin, J. Tsang, et al., Nano Lett. 9 (2009) 1039–1044.
[60] S. Park, R.S. Ruoff, Nat. Nanotechnol. 4 (2009) 217–224.
[61] D.C. Elias, R.R. Nair, T.M.G. Mohiuddin, S.V. Morozov, P. Blake, M.P. Halsall, et al., Science 323 (2009) 610–613.
[62] Z. Luo, P.M. Vora, E.J. Mele, A.T.C. Johnson, J.M. Kikkawa,Appl. Phys. Lett. 94 (2009), 111909.
[63] S.M. Sze, K.K. Ng, Physics of Semiconductor Devices, John Wiley & Sons, Inc., Hoboken, NJ, USA, 2006.
[64] C. Xie, F. Yan,Small 13 (2017), 1701822.
[65] S. Iijima, Nature 354 (1991) 56–58.
[66] S. Iijima, T. Ichihashi, Nature 363 (1993) 603–605.
[67] J.S. Jie, W.J. Zhang, I. Bello, C.S. Lee, S.T. Lee, Nano Today 5 (2010) 313–336.
[68] M.I.B. Utama, J. Zhang, R. Chen, X.L. Xu, D.H. Li, H.D. Sun, et al., Nanoscale 4 (2012) 1422–1435.
[69] W.U. Huynh, Science 295 (2002) 2425–2427.
[70] C. Xie, L.B. Luo, L.H. Zeng, L. Zhu, J.J. Chen, B. Nie, et al., CrystEngComm 14 (2012) 7222–7228.
[71] Y. Huang, X. Duan, C.M. Lieber, Small 1 (2005) 142–147.
[72] X. Duan, Y. Huang, R. Agarwal, C.M. Lieber, Nature 421 (2003) 241–245.
[73] H. Li, X. Wang, J. Xu, Q. Zhang, Y. Bando, D. Golberg, et al., Adv. Mater. 25 (2013) 3017–3037.
[74] L. Zhao, L. Hu, X. Fang, Adv. Funct. Mater. 22 (2012) 1551–1566.
[75] T.Y. Zhai, X.S. Fang, L. Li, Y. Bando, D. Golberg, Nanoscale 2 (2010) 168–187.
[76] K. Deng, L. Li, Adv. Mater. 26 (2014) 2619–2635.
[77] A. Cao, Z. Liu, S. Chu, M. Wu, Z. Ye, Z. Cai, et al., Adv. Mater. 22 (2010) 103–106.
[78] P. Wang, T. Jiang, C. Zhu, Y. Zhai, D. Wang, S. Dong, Nano Res. 3 (2010) 794–799.
[79] C.X. Guo, H. Bin Yang, Z.M. Sheng, Z.S. Lu, Q.L. Song, C.M. Li, Angew. Chem. Int. Ed. 49 (2010) 3014–3017.
[80] T. Dufaux, J. Boettcher, M. Burghard, K. Kern, Small 6 (2010) 1868–1872.
[81] Y. Ye, Y. Dai, L. Dai, Z. Shi, N. Liu, F. Wang, et al., ACS Appl. Mater. Interf. 2 (2010) 3406–3410.
[82] D. Spirito, S. Kudera, V. Miseikis, C. Giansante, C. Coletti, R. Krahne, J. Phys. Chem. C 119 (2015) 23859–23864.
[83] H. Lee, K. Heo, J. Park, Y. Park, S. Noh, K.S. Kim, et al., J. Mater. Chem. 22 (2012) 8372–8376.
[84] Y. Jiang, W.J. Zhang, J.S. Jie, X.M. Meng, X. Fan, S.T. Lee, Adv. Funct. Mater. 17 (2007) 1795–1800.
[85] Y. Ye, L. Gan, L. Dai, Y. Dai, X. Guo, H. Meng, et al., Nanoscale 3 (2011) 1477–1481.
[86] L. Zhang, L. Fan, Z. Li, E. Shi, X.M. Li, H.B. Li, et al., Nano Res. 4 (2011) 891–900.
[87] Z. Gao, W. Jin, Y. Li, Q. Song, Y. Wang, K. Zhang, et al., J. Mater. Chem. C 3 (2015) 4511–4514.
[88] W.F. Jin, Y. Ye, L. Gan, B. Yu, P.C. Wu, Y. Dai, et al., J. Mater. Chem. 22 (2012) 2863–2867.
[89] Z.W. Gao, W.F. Jin, Y. Zhou, Y. Dai, B. Yu, C. Liu, et al., Nanoscale 5 (2013) 5576–5581.
[90] Y. Zhang, L. Du, Y. Lei, H. Zhao, Mater. Lett. 131 (2014) 288–291.
[91] X. Geng, L. Niu, Z. Xing, R. Song, G. Liu, M. Sun, et al., Adv. Mater. 22 (2010) 638–642.
[92] Y. Lin, K. Zhang, W. Chen, Y. Liu, Z. Geng, J. Zeng, et al., ACS Nano 4 (2010) 3033–3038.
[93] S. Lin, X. Li, S. Zhang, P. Wang, Z. Xu, H. Zhong, et al.,Appl. Phys. Lett. 107 (2015), 191106.
[94] G. Yang, D. Kim, J. Kim, Opt. Express 23 (2015) A1081–A1086.
[95] X. Fang, T. Zhai, U.K. Gautam, L. Li, L. Wu, Y. Bando, et al., Prog. Mater. Sci. 56 (2011) 175–287.
[96] X. Fang, S. Xiong, T. Zhai, Y. Bando, M. Liao, U.K. Gautam, et al., Adv. Mater. 21 (2009) 5016–5021.
[97] L. Li, Y. Yang, X. Huang, G. Li, L. Zhang, J. Phys. Chem. B. 109 (2005) 12394–12398.
[98] M. Sookhakian, Y.M. Amin, R. Zakaria, W.J. Basirun, M.R. Mahmoudian, B. Nasiri-Tabrizi, et al., J. Alloys Compd. 632 (2015) 201–207.
[99] Y. Kim, S.J. Kim, S. Cho, B.H. Hong, D. Jang,Sci. Rep. 5 (2015), 12345.
[100] F. Huang, F. Jia, C. Cai, Z. Xu, C. Wu, Y. Ma, et al.,Sci. Rep. 6 (2016), 28943.

[101] F. Jia, F. Huang, S. Ouyang, C. Cai, Z. Xu, C. Wu, et al., J. Mater. Chem. C. 4 (2016) 10797–10803.
[102] Y. Wang, C.W. Ge, Y.F. Zou, R. Lu, K. Zheng, T.F. Zhang, et al., Adv. Opt. Mater. 4 (2016) 291–296.
[103] L.B. Luo, S.H. Zhang, R. Lu, W. Sun, Q.L. Fang, C.Y. Wu, et al., RSC Adv. 5 (2015) 13324–13330.
[104] A. Robin, E. Lhuillier, X.Z. Xu, S. Ithurria, H. Aubin, A. Ouerghi, et al.,Sci. Rep. 6 (2016), 24909.
[105] S. Mokkapati, C. Jagadish, Mater. Today 12 (2009) 22–32.
[106] H.J. Joyce, Q. Gao, H. Hoe Tan, C. Jagadish, Y. Kim, J. Zou, et al., Prog. Quantum Electron. 35 (2011) 23–75.
[107] Y. Zhang, J. Wu, M. Aagesen, H. Liu,J. Phys. D. Appl. Phys. 48 (2015), 463001.
[108] H. Morko, Handbook of Nitride Semiconductors and Devices, Wiley-VCH Verlag GmbH & Co. KGaA, Weinheim, Germany, 2008.
[109] T. Zdanowicz, T. Rodziewicz, M. Zabkowska-Waclawek, Sol. Energy Mater. Sol. Cells 87 (2005) 757–769.
[110] G. Jo, M. Choe, C.Y. Cho, J.H. Kim, W. Park, S. Lee, et al.,Nanotechnology 21 (2010), 175201.
[111] B.J. Kim, C. Lee, Y. Jung, K. Hyeon Baik, M.A. Mastro, J.K. Hite, et al.,Appl. Phys. Lett. 99 (2011), 143101.
[112] S. Tongay, M. Lemaitre, T. Schumann, K. Berke, B.R. Appleton, B. Gila, et al.,Appl. Phys. Lett. 99 (2011), 102102.
[113] H. Zhong, Z. Liu, L. Shi, G. Xu, Y. Fan, Z. Huang, et al.,Appl. Phys. Lett. 104 (2014), 212101.
[114] S. Kim, T.H. Seo, M.J. Kim, K.M. Song, E.K. Suh, H. Kim, Nano Res. 8 (2015) 1327–1338.
[115] L. Wang, Y. Zhang, X. Li, E. Guo, Z. Liu, X. Yi, et al., RSC Adv. 3 (2013) 3359–3364.
[116] C.W. Chang, W.C. Tan, M.L. Lu, T.C. Pan, Y.J. Yang, Y.F. Chen, Adv. Funct. Mater. 23 (2013) 4043–4048.
[117] A.V. Babichev, H. Zhang, P. Lavenus, F.H. Julien, A.Y. Egorov, Y.T. Lin, et al.,Appl. Phys. Lett. 103 (2013), 201103.
[118] C. Lee, S. Kang, H. Cha, C. Won, S. Hong, B.J. Cho, et al.,Jpn. J. Appl. Phys. 54 (2015), 06FF08.
[119] F. Lin, S.W. Chen, J. Meng, G. Tse, X.W. Fu, F.J. Xu, et al.,Appl. Phys. Lett. 105 (2014), 73103.
[120] M. Choe, C.Y. Cho, J.P. Shim, W. Park, S.K. Lim, W.K. Hong, et al.,Appl. Phys. Lett. 101 (2012), 31115.
[121] D. Tomer, S. Rajput, L.J. Hudy, C.H. Li, L. Li,Nanotechnology 26 (2015), 215702.
[122] W. Jie, F. Zheng, J. Hao,Appl. Phys. Lett. 103 (2013), 233111.
[123] W. Chen, X. Li, W.Y. Yin, S. Lin, Z. Zhao, E. Li, et al., IEEE T. Electron Dev. 62 (2015) 3760–3766.
[124] H. He, X. Yu, Y. Wu, X. Mu, H. Zhu, S. Yuan, et al., Nano Energy 16 (2015) 91–98.
[125] S.S. Lin, Z.Q. Wu, X.Q. Li, Y.J. Zhang, S.J. Zhang, P. Wang, et al.,Adv. Energy Mater. 6 (2016), 1600822.
[126] S.J. Zhang, S.S. Lin, X.Q. Li, X.Y. Liu, H.A. Wu, W.L. Xu, et al., Nanoscale 8 (2016) 226–232.
[127] X.Q. Li, S.S. Lin, X. Lin, Z.J. Xu, P. Wang, S.J. Zhang, et al., Opt. Express 24 (2016) 134–145.
[128] L.B. Luo, J.J. Chen, M.Z. Wang, H. Hu, C.Y. Wu, Q. Li, et al., Adv. Funct. Mater. 24 (2014) 2794–2800.
[129] L.B. Luo, H. Hu, X.H. Wang, R. Lu, Y.F. Zou, Y.Q. Yu, et al., J. Mater. Chem. C 3 (2015) 4723–4728.
[130] Y. Wu, X. Yan, X. Zhang, X. Ren,Appl. Phys. Lett. 109 (2016), 183101.
[131] J. Wallentin, N. Anttu, D. Asoli, M. Huffman, I. Aberg, M.H. Magnusson, et al., Science 339 (2013) 1057–1060.
[132] A. Yamamoto, M. Yamaguchi, C. Uemura, Appl. Phys. Lett. 44 (1984) 611–613.
[133] P. Wang, X. Li, Z. Xu, Z. Wu, S. Zhang, W. Xu, et al., Nano Energy 13 (2015) 509–517.
[134] L.B. Luo, Y.F. Zou, C.W. Ge, K. Zheng, D.D. Wang, R. Lu, et al., Adv. Opt. Mater. 4 (2016) 763–771.
[135] G. Niu, G. Capellini, F. Hatami, A. Di Bartolomeo, T. Niermann, E.H. Hussein, et al., ACS Appl. Mater. Interf. 8 (2016) 26948–26955.
[136] D.E. Aspnes, A.A. Studna, Phys. Rev. B. 27 (1983) 985–1009.
[137] J.S. Miao, W.D. Hu, N. Guo, Z. Lu, X. Liu, L. Liao, et al., Small 11 (2015) 936–942.
[138] R.F. Davis, Proc. IEEE. 79 (1991) 702–712.
[139] K. Qian, R.Y. Tay, V.C. Nguyen, J. Wang, G. Cai, T. Chen, et al., Adv. Funct. Mater. 26 (2016) 2176–2184.
[140] G. Cassabois, P. Valvin, B. Gil, Nat. Photonics 10 (2016) 262–266.
[141] Q. Li, M. Liu, Y. Zhang, Z. Liu, Small 12 (2016) 32–50.
[142] K.K. Kim, A. Hsu, X. Jia, S.M. Kim, Y. Shi, M. Hofmann, et al., Nano Lett. 12 (2012) 161–166.
[143] C.R. Dean, A.F. Young, I. Meric, C. Lee, L. Wang, S. Sorgenfrei, et al., Nat. Nanotechnol. 5 (2010) 722–726.
[144] L. Ju, J. Velasco, E. Huang, S. Kahn, C. Nosiglia, H.Z. Tsai, et al., Nat. Nanotechnol. 9 (2014) 348–352.
[145] C.C. Chen, Z. Li, L. Shi, S.B. Cronin, Nano Res. 8 (2015) 666–672.
[146] R.J. Shiue, Y. Gao, Y. Wang, C. Peng, A.D. Robertson, D.K. Efetov, et al., Nano Lett. 15 (2015) 7288–7293.
[147] L.M. Peng, Z. Zhang, S. Wang, Mater. Today 17 (2014) 433–442.
[148] D. Jariwala, V.K. Sangwan, L.J. Lauhon, T.J. Marks, M.C. Hersam, Chem. Soc. Rev. 42 (2013) 2824–2860.
[149] L. Dai, D.W. Chang, J.B. Baek, W. Lu, Small 8 (2012) 1130–1166.
[150] P. Avouris, Z. Chen, V. Perebeinos, Nat. Nanotechnol. 2 (2007) 605–615.
[151] C.J. Shearer, A. Cherevan, D. Eder, Adv. Mater. 26 (2014) 2295–2318.
[152] S.H. Cheng, T.M. Weng, M.L. Lu, W.C. Tan, J.Y. Chen, Y.F. Chen,Sci. Rep. 3 (2013), 2694.
[153] C.W. Chiang, G. Haider, W.C. Tan, Y.R. Liou, Y.C. Lai, R. Ravindranath, et al., ACS Appl. Mater. Interf. 8 (2016) 466–471.
[154] G. Haider, P. Roy, C.W. Chiang, W.C. Tan, Y.R. Liou, H.T. Chang, et al., Adv. Funct. Mater. 26 (2016) 620–628.
[155] X.C. Yu, Z.G. Dong, J.K.W. Yang, Q.J. Wang, Optica 3 (2016) 979–984.
[156] C.O. Kim, S.W. Hwang, S. Kim, D.H. Shin, S.S. Kang, J.M. Kim, et al.,Sci. Rep. 4 (2015), 5603.
[157] H. Dai, Acc. Chem. Res. 35 (2002) 1035–1044.
[158] V.N. Popov, Mater. Sci. Eng. R 43 (2004) 61–102.
[159] A. Jorio, G. Dresselhaus, G. Dresselhaus, Carbon nanotubes: Advanced topics in the synthesis, structure, in: properties and applications, Springer-Verlag, Berlin, Heidelberg, Germany, 2008.
[160] X. Dong, B. Li, A. Wei, X. Cao, M.B. Chan-Park, H. Zhang, et al., Carbon 49 (2011) 2944–2949.
[161] D. Yu, L. Dai, J. Phys. Chem. Lett. 1 (2010) 467–470.
[162] V.C. Tung, L.M. Chen, M.J. Allen, J.K. Wassei, K. Nelson, R.B. Kaner, et al., Nano Lett. 9 (2009) 1949–1955.
[163] M.Y. Yen, M.C. Hsiao, S.H. Liao, P.I. Liu, H.M. Tsai, C.C.M. Ma, et al., Carbon 49 (2011) 3597–3606.
[164] B.G. Cook, W.R. French, K. Varga,Appl. Phys. Lett. 101 (2012), 153501.
[165] J.D. Roy Mayhew, I.A. Aksay, Chem. Rev. 114 (2014) 6323–6348.
[166] D.S. Hecht, L. Hu, G. Irvin, Adv. Mater. 23 (2011) 1482–1513.
[167] E.J.H. Lee, L. Zhi, M. Burghard, K. Mullen, K. Kern, Adv. Mater. 22 (2010) 1854–1857.
[168] R. Lu, C. Christianson, B. Weintrub, J.Z. Wu, ACS Appl. Mater. Interf. 5 (2013) 11703–11707.
[169] Y. Liu, F. Wang, X. Wang, X. Wang, E. Flahaut, X. Liu, et al.,Nat. Commun. 6 (2015), 8589.
[170] T.F. Zhang, Z.P. Li, J.Z. Wang, W.Y. Kong, G.A. Wu, Y.Z. Zheng, et al.,Sci. Rep. 6 (2016), 38569.
[171] S. Du, W. Lu, A. Ali, P. Zhao, K. Shehzad, H. Guo, et al.,Adv. Mater. 29 (2017), 1700463.
[172] K.Q. Peng, S.T. Lee, Adv. Mater. 23 (2011) 198–215.
[173] Z. Huang, J.E. Carey, M. Liu, X. Guo, E. Mazur, J.C. Campbell,Appl. Phys. Lett. 89 (2006), 33506.
[174] Y. Wang, T. Wang, P. Da, M. Xu, H. Wu, G. Zheng, Adv. Mater. 25 (2013) 5177–5195.
[175] J. Jean, P.R. Brown, R.L. Jaffe, T. Buonassisi, V. Bulović, Energy Environ. Sci. 8 (2015) 1200–1219.
[176] M.A. Green, Y. Hishikawa, W. Warta, E.D. Dunlop, D.H. Levi, J. Hohl-Ebinger, et al., Prog. Photovoltaics Res. Appl. 25 (2017) 668–676.
[177] X.M. Li, Z. Lv, H.W. Zhu, Adv. Mater. 27 (2015) 6549–6574.
[178] Y. Wang, K. Ding, B.Q. Sun, S.T. Lee, J.S. Jie, Nano Res. 9 (2016) 72–93.
[179] Y.I. Zhang, L. Zhang, C. Zhou, Acc. Chem. Res. 46 (2013) 2329–2339.
[180] S. Zhuiykov, Nanostructured Semiconductor Oxides for the Next Generation of Electronics and Functional Devices, Elsevier, Cambridge, UK, 2014.
[181] Y.J. Yu, Y. Zhao, S. Ryu, L.E. Brus, K.S. Kim, P. Kim, Nano Lett. 9 (2009) 3430–3434.
[182] C. Mattevi, H. Kim, M. Chhowalla, J. Mater. Chem. 21 (2011) 3324–3334.
[183] X.W. Zhang, C. Xie, J.S. Jie, X. Zhang, Y.M. Wu, W.J. Zhang, J. Mater. Chem. A 1 (2013) 6593–6601.
[184] Y.M. Wu, X.W. Zhang, J.S. Jie, C. Xie, X.J. Zhang, B.Q. Sun, et al., J. Phys. Chem. C 117 (2013) 11968–11976.
[185] C. Xie, X.Z. Zhang, Y.M. Wu, X.J. Zhang, X.W. Zhang, Y. Wang, et al., J. Mater. Chem. A1 (2013) 8567–8574.
[186] Y.F. Li, W. Yang, Z.Q. Tu, Z.C. Liu, F. Yang, L.Q. Zhang, et al.,Appl. Phys. Lett. 104 (2014), 43903.
[187] T. Feng, D. Xie, Y. Lin, Y. Zang, T. Ren, R. Song, et al.,Appl. Phys. Lett. 99 (2011), 233505.
[188] C. Xie, P. Lv, B. Nie, J. Jie, X. Zhang, Z. Wang, et al.,Appl. Phys. Lett. 99 (2011), 133113.
[189] X.M. Li, D. Xie, H. Park, M. Zhu, T.H. Zeng, K.L. Wang, et al., Nanoscale 5 (2013) 1945–1948.
[190] T.T. Feng, D. Xie, Y.X. Lin, H.M. Zhao, Y. Chen, H. Tian, et al., Nanoscale 4 (2012) 2130–2133.
[191] X. Li, D. Xie, H. Park, T.H. Zeng, K. Wang, J. Wei, et al., Adv. Energy Mater. 3 (2013) 1029–1034.
[192] Y. Lin, X. Li, D. Xie, T. Feng, Y. Chen, R. Song, et al., Energy Environ. Sci. 6 (2013) 108–115.
[193] T.X. Cui, R.T. Lv, Z.H. Huang, S.X. Chen, Z.X. Zhang, X. Gan, et al., J. Mater. Chem. A 1 (2013) 5736–5740.
[194] E. Shi, H. Li, L. Yang, L. Zhang, Z. Li, P. Li, et al., Nano Lett. 13 (2013) 1776–1781.
[195] K.J. Jiao, X.L. Wang, Y. Wang, Y.F. Chen, J. Mater. Chem. C 2 (2014) 7715–7721.
[196] K.Q. Ruan, K. Ding, Y.M. Wang, S.L. Diao, Z.B. Shao, X.J. Zhang, et al., J. Mater. Chem. A 3 (2015) 14370–14377.
[197] X. Miao, S. Tongay, M.K. Petterson, K. Berke, A.G. Rinzler, B.R. Appleton, et al., Nano Lett. 12 (2012) 2745–2750.
[198] X. Liu, X.W. Zhang, Z.G. Yin, J.H. Meng, H.L. Gao, L.Q. Zhang, et al.,Appl. Phys. Lett. 105 (2014), 183901.

[199] C. Xie, X.J. Zhang, K.Q. Ruan, Z.B. Shao, S.S. Dhaliwal, L. Wang, et al., J. Mater. Chem. A 1 (2013) 15348–15354.
[200] X. An, F. Liu, S. Kar, Carbon 57 (2013) 329–337.
[201] P.H. Ho, Y.T. Liou, C.H. Chuang, S.W. Lin, C.Y. Tseng, D.Y. Wang, et al., Adv. Mater. 27 (2015) 1724–1729.
[202] L. Yang, X. Yu, W. Hu, X. Wu, Y. Zhao, D. Yang, ACS Appl. Mater. Interf. 7 (2015) 4135–4141.
[203] J.M. Kim, S.W. Seo, D.H. Shin, H.S. Lee, J.H. Kim, C.W. Jang, et al., Curr. Appl. Phys. 17 (2017) 1136–1141.
[204] L.B. Luo, C. Xie, X.H. Wang, Y.Q. Yu, C.Y. Wu, H. Hu, et al., Nano Energy 9 (2014) 112–120.
[205] G. Fan, H. Zhu, K. Wang, J. Wei, X. Li, Q. Shu, et al., ACS Appl. Mater. Interf. 3 (2011) 721–725.
[206] X. Li, L. Fan, Z. Li, K. Wang, M. Zhong, J. Wei, et al., Adv. Energy Mater. 2 (2012) 425–429.
[207] X. Li, X. Zang, X. Li, M. Zhu, Q. Chen, K. Wang, et al.,Adv. Energy Mater. 4 (2014), 1400224.
[208] C. Kuru, S. Yavuz, A. Kargar, D. Choi, C. Choi, C. Rustomji, et al., J. Nanosci. Nanotechnol. 16 (2016) 1190–1193.
[209] P.H. Ho, W.C. Lee, Y.T. Liou, Y.P. Chiu, Y.S. Shih, C.C. Chen, et al., Energy Environ. Sci. 8 (2015) 2085–2092.
[210] X. Yu, L. Yang, Q. Lv, M. Xu, H. Chen, D. Yang, Nanoscale 7 (2015) 7072–7077.
[211] A.G. Aberle, Prog, Photovoltaics Res. Appl. 8 (2000) 473–487.
[212] T. Jiao, D. Wei, X. Song, T. Sun, J. Yang, L. Yu, et al., RSC Adv. 6 (2016) 10175–10179.
[213] L. Yang, X. Yu, M. Xu, H. Chen, D. Yang, J. Mater. Chem. A 2 (2014) 16877–16883.
[214] Y. Tsuboi, F. Wang, D. Kozawa, K. Funahashi, S. Mouri, Y. Miyauchi, et al., Nanoscale 7 (2015) 14476–14482.
[215] J.H. Meng, X. Liu, X.W. Zhang, Y. Zhang, H.L. Wang, Z.G. Yin, et al., Nano Energy 28 (2016) 44–50.
[216] J.R. Wallbank, M. Mucha-Kruczyński, X. Chen, V.I. Fal'ko, Ann. Phys. 527 (2015) 359–376.
[217] Y. Liu, N.O. Weiss, X. Duan, H.C. Cheng, Y. Huang, X.F. Duan,Nat. Rev. Mater. 1 (2016), 16042.
[218] K. Ding, X.W. Zhang, F. Xia, R. Wang, Y. Kuang, S. Duhm, et al., J. Mater. Chem. A 5 (2017) 285–291.
[219] C. Xie, B. Nie, L.H. Zeng, F.X. Liang, M.Z. Wang, L.B. Luo, et al., ACS Nano 8 (2014) 4015–4022.
[220] E. Garnett, P. Yang, Nano Lett. 10 (2010) 1082–1087.
[221] H. Yu, S. Chen, X. Fan, X. Quan, H. Zhao, X. Li, et al., Angew. Chem. Int. Ed. 49 (2010) 5106–5109.
[222] W.C. Tu, C.Y. Huang, C.W. Fang, M.Y. Lin, W.C. Lee, X.S. Liu, et al.,J. Phys. D. Appl. Phys. 49 (2016), 49LT02.
[223] W.C. Lee, M.L. Tsai, Y.L. Chen, W.C. Tu,Sci. Rep. 7 (2017), 46478.
[224] R. Kumar, B.R. Mehta, M. Bhatnagar, R.S.S. Mahapatra, S. Salkalachen, P. Jhawar, Nanoscale Res. Lett. 9 (2014) 349.
[225] C. Xie, J.S. Jie, B. Nie, T.X. Yan, Q. Li, P. Lv, et al.,Appl. Phys. Lett. 100 (2012), 193103.
[226] C. Battaglia, A. Cuevas, S. De Wolf, Energy Environ. Sci. 9 (2016) 1552–1576.
[227] X. Gan, R. Lv, H. Zhu, L.P. Ma, X. Wang, Z. Zhang, et al., J. Mater. Chem. A 4 (2016) 13795–13802.
[228] H.A. Atwater, A. Polman, Nat. Mater. 9 (2010) 865.
[229] Y.S. Rim, S.H. Bae, H. Chen, N. De Marco, Y. Yang, Adv. Mater. 28 (2016) 4415–4440.
[230] T. Jiao, D. Wei, J. Liu, W. Sun, S. Jia, W. Zhang, et al., RSC Adv. 5 (2015) 73202–73206.
[231] J. Ahn, H. Chou, S.K. Banerjee,J. Appl. Phys. 121 (2017), 163105.
[232] F. Xia, T. Mueller, Y. Lin, A. Valdes-Garcia, P. Avouris, Nat. Nanotechnol. 4 (2009) 839–843.
[233] Z. Zhang, J. Zhang, N. Chen, L. Qu, Energy Environ. Sci. 5 (2012) 8869–8890.
[234] K.J. Williams, C.A. Nelson, X. Yan, L.S. Li, X. Zhu, ACS Nano 7 (2013) 1388–1394.
[235] P. Gao, K. Ding, Y. Wang, K. Ruan, S. Diao, Q. Zhang, et al., J. Phys. Chem. C 118 (2014) 5164–5171.
[236] S. Diao, X. Zhang, Z. Shao, K. Ding, J. Jie, X. Zhang, Nano Energy 31 (2016) 359–366.
[237] T.X. Cui, R.T. Lv, Z.H. Huang, X. Gan, K.L. Wang, D.H. Wu, et al., RSC Adv. 3 (2013) 22295–22300.
[238] W. Xu, B. Deng, E. Shi, S. Wu, M. Zou, L. Yang, et al., ACS Appl. Mater. Interf. 7 (2015) 17088–17094.
[239] E. Shi, H. Li, W. Xu, S. Wu, J. Wei, Y. Fang, et al., Nano Energy 17 (2015) 216–223.
[240] X. An, F. Liu, Y.J. Jung, S. Kar, Nano Lett. 13 (2013) 909–916.
[241] Y. An, A. Behnam, E. Pop, A. Ural,Appl. Phys. Lett. 102 (2013), 13110.
[242] P. Lv, X.J. Zhang, X.W. Zhang, W. Deng, J.S. Jie, IEEE Electron Device L. 34 (2013) 1337–1339.
[243] M. Amirmazlaghani, F. Raissi, O. Habibpour, J. Vukusic, J. Stake, IEEE J. Quantum Electron. 49 (2013) 589–594.
[244] L.B. Luo, L.H. Zeng, C. Xie, Y.Q. Yu, F.X. Liang, C.Y. Wu, et al.,Sci. Rep. 4 (2015), 3914.
[245] L.H. Zeng, C. Xie, L.L. Tao, H. Long, C.Y. Tang, Y.H. Tsang, et al., Opt. Express 23 (2015) 4839–4846.
[246] F.X. Liang, D.Y. Zhang, Y.F. Zou, H. Hu, T.F. Zhang, Y.C. Wu, et al., RSC Adv. 5 (2015) 19020–19026.
[247] M.E. Ayhan, G. Kalita, M. Kondo, M. Tanemura, RSC Adv. 4 (2014) 26866–26871.
[248] D. Xiang, C. Han, Z. Hu, B. Lei, Y. Liu, L. Wang, et al., Small 11 (2015) 4829–4836.
[249] X. Li, M. Zhu, M. Du, Z. Lv, L. Zhang, Y. Li, et al., Small 12 (2016) 595–601.
[250] M. Zhu, L. Zhang, X.M. Li, Y.J. He, X. Li, F.M. Guo, et al., J. Mater. Chem. A 3 (2015) 8133–8138.
[251] X. Wan, Y. Xu, H. Guo, K. Shehzad, A. Ali, Y. Liu, et al., Npj 2D Mater. Appl. 1 (2017) 4.
[252] F. Liu, S. Kar, ACS Nano 8 (2014) 10270–10279.
[253] Z. Chen, Z. Cheng, J. Wang, X. Wan, C. Shu, H.K. Tsang, et al., Adv. Opt. Mater. 3 (2015) 1207–1214.
[254] Z. Chen, X. Li, J. Wang, L. Tao, M. Long, S.J. Liang, et al., ACS Nano 11 (2017) 430–437.
[255] L. Tao, Z. Chen, X. Li, K. Yan, J.B. Xu, Npj 2D Mater. Appl. 1 (2017) 19.
[256] Q. Zhang, X. Wang, D. Li, Z. Zhang, Adv. Funct. Mater. 24 (2014) 7613–7618.
[257] J. Shen, X. Liu, X. Song, X. Li, J. Wang, Q. Zhou, et al., Nanoscale (2017) 6020–6025.
[258] M. Zhu, X. Li, Y. Guo, X. Li, P. Sun, X. Zang, et al., Nanoscale 6 (2014) 4909–4914.
[259] Y. Cao, J. Zhu, J. Xu, J. He, J.L. Sun, Y. Wang, et al., Small 10 (2014) 2345–2351.
[260] G. Li, L. Liu, G. Wu, W. Chen, S. Qin, Y. Wang, T. Zhang, Small 12 (2016) 5019–5026.
[261] G. Eda, M. Chhowalla, Adv. Mater. 22 (2010) 2392–2415.
[262] X. Gan, R.J. Shiue, Y. Gao, I. Meric, T.F. Heinz, K. Shepard, et al., Nat. Photonics 7 (2013) 883–887.
[263] X. Wang, Z. Cheng, K. Xu, H.K. Tsang, J.B. Xu, Nat. Photonics 7 (2013) 888–891.
[264] A. Pospischil, M. Humer, M.M. Furchi, D. Bachmann, R. Guider, T. Fromherz, et al., Nat. Photonics 7 (2013) 892–896.
[265] I. Goykhman, U. Sassi, B. Desiatov, N. Mazurski, S. Milana, D. de Fazio, et al., Nano Lett. 16 (2016) 3005–3013.
[266] H.Y. Kim, K. Lee, N. McEvoy, C. Yim, G.S. Duesberg, Nano Lett. 13 (2013) 2182–2188.
[267] A. Fattah, S. Khatami, C.C. Mayorga-Martinez, M. Medina-Sánchez, L. Baptista-Pires, A. Merkoçi, Small 10 (2014) 4193–4199.
[268] M. Zhu, X. Li, S. Chung, L. Zhao, X. Li, X. Zang, et al., Carbon 84 (2015) 138–145.
[269] A. Singh, M.A. Uddin, T. Sudarshan, G. Koley, Small 10 (2014) 1555–1565.
[270] J. Michel, J. Liu, L.C. Kimerling, Nat. Photonics 4 (2010) 527–534.
[271] R. Höll, M. Kling, E. Schroll, Ore Geol. Rev. 30 (2007) 145–180.
[272] L. Colace, G. Masini, F. Galluzzi, G. Assanto, G. Capellini, L. Di Gaspare, et al., Appl. Phys. Lett. 72 (1998) 3175–3177.
[273] L. Vivien, J. Osmond, J.M. Fédéli, D. Marris-Morini, P. Crozat, J.F. Damlencourt, et al., Opt. Express 17 (2009) 6252–6257.
[274] L. Cao, J.S. Park, P. Fan, B. Clemens, M.L. Brongersma, Nano Lett. 10 (2010) 1229–1233.
[275] S. Sahni, X. Luo, J. Liu, Y. Xie, E. Yablonovitch, Opt. Lett. 33 (2008) 1138–1140.
[276] L. Lancellotti, T. Polichetti, F. Ricciardella, O. Tari, S. Gnanapragasam, S. Daliento, et al., Thin Solid Films 522 (2012) 390–394.
[277] L.H. Zeng, M.Z. Wang, H. Hu, B. Nie, Y.Q. Yu, C.Y. Wu, et al., ACS Appl. Mater. Interf. 5 (2013) 9362–9366.
[278] R. Lu, C.W. Ge, Y.F. Zou, K. Zheng, D.D. Wang, T.F. Zhang, et al., Laser Photon. Rev. 10 (2016) 595–602.
[279] F. Yang, H. Cong, K. Yu, L. Zhou, N. Wang, Z. Liu, et al., ACS Appl. Mater. Interf. 9 (2017) 13422–13429.
[280] S.A. Kukushkin, A.V. Osipov,J. Phys. D. Appl. Phys. 47 (2014), 313001.
[281] A. Sciuto, F. Roccaforte, S. Di Franco, V. Raineri, G. Bonanno,Appl. Phys. Lett. 89 (2006), 81111.
[282] X. Chen, H. Zhu, J. Cai, Z. Wu,J. Appl. Phys. 102 (2007), 24505.
[283] W. Strupinski, K. Grodecki, A. Wysmolek, R. Stepniewski, T. Szkopek, P.E. Gaskell, et al., Nano Lett. 11 (2011) 1786–1791.
[284] J. Röhrl, M. Hundhausen, K.V. Emtsev, T. Seyller, R. Graupner, et al.,Appl. Phys. Lett. 92 (2008), 201918.
[285] R. Sun, Y. Zhang, K. Li, C. Hui, K. He, X. Ma, et al.,Appl. Phys. Lett. 103 (2013), 13106.
[286] E. Cazalas, I. Childres, A. Majcher, T.F. Chung, Y.P. Chen, I. Jovanovic,Appl. Phys. Lett. 103 (2013), 53123.
[287] E. Kuşdemir, D. Özkendir, V. Fırat, C. Çelebi,J. Phys. D. Appl. Phys. 48 (2015), 95104.
[288] J. Huang, L.W. Guo, W. Lu, Y.H. Zhang, Z. Shi, Y.P. Jia, et al.,Chinese Phys. B 25 (2016), 67205.
[289] B.K. Sarker, E. Cazalas, T.F. Chung, I. Childres, I. Jovanovic, Y.P. Chen, Nat. Nanotechnol. (2017) 1–8.
[290] X. Yu, T.J. Marks, A. Facchetti, Nat. Mater. 15 (2016) 383–396.
[291] J. Meyer, S. Hamwi, M. Kroger, W. Kowalsky, T. Riedl, A. Kahn, Adv. Mater. 24 (2012) 5408–5427.
[292] D.C. Look, Mater. Sci. Eng. B Solid State Mater. Adv. Technol. 80 (2001) 383–387.
[293] Ü. Özgür, Y.I. Alivov, C. Liu, A. Teke, M.A. Reshchikov, S. Doğan, et al.,J. Appl. Phys. 98 (2005), 41301.
[294] A.B. Djurišić, Y.H. Leung, Small 2 (2006) 944–961.
[295] L. Schmidt-Mende, J.L. MacManus-Driscoll, Mater. Today 10 (2007) 40–48.
[296] J. Huang, Z.G. Yin, Q.D. Zheng, Energy Environ. Sci. 4 (2011) 3861–3877.
[297] Z. Yin, S. Wu, X. Zhou, X. Huang, Q. Zhang, F. Boey, et al., Small 6 (2010) 307–312.

[298] H. Park, S. Chang, J. Jean, J.J. Cheng, P.T. Araujo, M. Wang, et al., Nano Lett. 13 (2013) 233–239.
[299] J. Chen, C. Li, G. Eda, Y. Zhang, W. Lei, M. Chhowalla, et al., Chem. Commun. 47 (2011) 6084–6086.
[300] S. Ameen, M.S. Akhtar, M. Song, H.S. Shin, ACS Appl Mater Interf. 4 (2012) 4405–4412.
[301] F. Xu, J. Chen, X. Wu, Y. Zhang, Y. Wang, J. Sun, et al., J. Phys. Chem. C 117 (2013) 8619–8627.
[302] M. Dutta, S. Sarkar, T. Ghosh, D. Basak, J. Phys. Chem. C 116 (2012) 20127–20131.
[303] X.W. Fu, Z.M. Liao, Y.B. Zhou, H.C. Wu, Y.Q. Bie, et al.,Appl. Phys. Lett. 100 (2012), 223114.
[304] J. Liu, R. Lu, G. Xu, J. Wu, P. Thapa, D. Moore, Adv. Funct. Mater. 23 (2013) 4941–4948.
[305] H. Zhang, A.V. Babichev, G. Jacopin, P. Lavenus, F.H. Julien, A.Y. Egorov, et al.,J. Appl. Phys. 114 (2013), 234505.
[306] B.D. Boruah, A. Misra, RSC Adv. 5 (2015) 90838–90846.
[307] W. Guo, S. Xu, Z. Wu, N. Wang, M.M.T. Loy, S. Du, Small 9 (2013) 3031–3036.
[308] V.Q. Dang, T.Q. Trung, D.I. Kim, L.T. Duy, B.U. Hwang, D.W. Lee, et al., Small 11 (2015) 3054–3065.
[309] V.Q. Dang, T.Q. Trung, L.T. Duy, B.Y. Kim, S. Siddiqui, W. Lee, et al., ACS Appl. Mater. Interf. 7 (2015) 11032–11040.
[310] B.D. Boruah, A. Mukherjee, S. Sridhar, A. Misra, ACS Appl. Mater. Interf. 7 (2015) 10606–10611.
[311] R.K. Biroju, N. Tilak, G. Rajender, S. Dhara, P.K. Giri,Nanotechnology 26 (2015), 145601.
[312] H. Yang, J. Li, D. Yu, L. Li, Cryst. Growth Des. 16 (2016) 4831–4838.
[313] B.D. Boruah, D.B. Ferry, A. Mukherjee, A. Misra,Nanotechnology 26 (2015), 235703.
[314] D. Shao, J. Gao, P. Chow, H. Sun, G. Xin, P. Sharma, et al., Nano Lett. 15 (2015) 3787–3792.
[315] M. Gong, Q. Liu, B. Cook, B. Kattel, T. Wang, W.L. Chan, et al., ACS Nano 11 (2017) 4114–4123.
[316] H. Chang, Z. Sun, K.Y.F. Ho, X. Tao, F. Yan, W.M. Kwok, et al., Nanoscale 3 (2011) 258–264.
[317] Z. Zhan, L. Zheng, Y. Pan, G. Sun, L. Li, J. Mater. Chem. 22 (2012) 2589–2595.
[318] P. Sahatiya, S. Badhulika, RSC Adv. 5 (2015) 82481–82487.
[319] D. Shao, M. Yu, H. Sun, T. Hu, J. lian, S. Sawyer, Nanoscale 5 (2013) 3664–3667.
[320] D.I. Son, H.Y. Yang, T.W. Kim, W.I. Park,Appl. Phys. Lett. 102 (2013), 21105.
[321] S. Darbari, V. Ahmadi, P. Afzali, Y. Abdi, M. Feda,J. Nanoparticle Res. 16 (2014), 2798.
[322] D.I. Son, H.Y. Yang, T.W. Kim, W.I. Park, Compos. Part B Eng. 69 (2015) 154–158.
[323] Z. Wang, X. Zhan, Y. Wang, S. Muhammad, Y. Huang, J. He, Nanoscale 4 (2012) 2678–2684.
[324] X.B. Liu, H.J. Du, X.W. Sun, RSC Adv. 4 (2014) 5136–5140.
[325] X. Ye, H. Liu, N. Hu, J. Wang, M. Li, Y. Zhang, Mater. Lett. 150 (2015) 126–129.
[326] B. Nie, J.G. Hu, L.B. Luo, C. Xie, L.H. Zeng, P. Lv, et al., Small 9 (2013) 2872–2879.
[327] S. Lee, Y. Lee, D.Y. Kim, E.B. Song, S.M. Kim,Appl. Phys. Lett. 102 (2013), 242114.
[328] Z. Wu, X. Li, H. Zhong, S. Zhang, P. Wang, T. Kim, et al., Opt. Express 23 (2015) 18864–18871.
[329] S. Liu, Q. Liao, S. Lu, Z. Zhang, G. Zhang, Y. Zhang, Adv. Funct. Mater. 26 (2016) 1347–1353.
[330] C.C. Cheng, J.Y. Zhan, Y.M. Liao, T.Y. Lin, Y.P. Hsieh, Y.F. Chen,Appl. Phys. Lett. 109 (2016), 53501.
[331] T.F. Zhang, G.A. Wu, J.Z. Wang, Y.Q. Yu, D.Y. Zhang, D.D. Wang, et al., Nanophotonics 6 (2017) 1073–1081.
[332] H. Liu, Q. Sun, J. Xing, Z. Zheng, Z. Zhang, Z. Lü, et al., ACS Appl. Mater. Interf. 7 (2015) 6645–6651.
[333] B.D. Boruah, A. Mukherjee, A. Misra,Nanotechnology 27 (2016), 95205.
[334] P. Sahatiya, S. Solomon Jones, P. Thanga Gomathi, S. Badhulika,2D Mater. 4 (2017), 25053.
[335] L. Duan, F. He, Y. Tian, B. Sun, J. Fan, X. Yu, et al., ACS Appl. Mater. Interf. 9 (2017) 8161–8168.
[336] J. Li, Y. Lin, J. Lu, C. Xu, Y. Wang, Z. Shi, et al., ACS Nano 9 (2015) 6794–6800.
[337] J. Li, M. Jiang, C. Xu, Y. Wang, Y. Lin, J. Lu, et al.,Sci. Rep. 5 (2015), 9263.
[338] A.L. Linsebigler, G. Lu, J.T. Yates, Chem. Rev. 95 (1995) 735–758.
[339] S. Liu, J. Yu, M. Jaroniec, Chem. Mater. 23 (2011) 4085–4093.
[340] Y.C. Nah, I. Paramasivam, P. Schmuki, ChemPhysChem 11 (2010) 2698–2713.
[341] M. Ge, C. Cao, J. Huang, S. Li, Z. Chen, K.Q. Zhang, et al., J. Mater. Chem. A 4 (2016) 6772–6801.
[342] P. Roy, S. Berger, P. Schmuki, Angew. Chem. Int. Ed. 50 (2011) 2904–2939.
[343] F.W. Low, C.W. Lai, Renew. Sustain. Energy Rev. 82 (2018) 103–125.
[344] K.K. Manga, S. Wang, M. Jaiswal, Q. Bao, K.P. Loh, Adv. Mater. 22 (2010) 5265–5270.
[345] K.K. Manga, J. Wang, M. Lin, J. Zhang, M. Nesladek, V. Nalla, et al., Adv. Mater. 24 (2012) 1697–1702.
[346] K. Zheng, F. Meng, L. Jiang, Q. Yan, H.H. Hng, X. Chen, Small 9 (2013) 2076–2080.
[347] F.X. Liang, D.Y. Zhang, J.Z. Wang, W.Y. Kong, Z.X. Zhang, Y. Wang, et al., Opt. Express 24 (2016) 25922–25932.
[348] M.Z. Wang, F.X. Liang, B. Nie, L.H. Zeng, L.X. Zheng, P. Lv, et al., Part. Part. Syst. Charact. 30 (2013) 630–636.
[349] D.Y. Zhang, C.W. Ge, J.Z. Wang, T.F. Zhang, Y.C. Wu, F.X. Liang, Appl. Surf. Sci. 387 (2016) 1162–1168.
[350] H.B. Yang, G.H. Guai, C.X. Guo, Q.L. Song, S.P. Jiang, Y.L. Wang, et al., J. Phys. Chem. C 115 (2011) 12209–12215.
[351] J. Yang, R. Li, N. Huo, W.L. Ma, F. Lu, C. Fan, et al., RSC Adv. 4 (2014) 49873–49878.
[352] D. Shao, M. Yu, J. Lian, S. Sawyer,Nanotechnology 24 (2013), 295701.
[353] M.K. Dai, Y.R. Liou, J.T. Lian, T.Y. Lin, Y.F. Chen, ACS Photonics 2 (2015) 1057–1064.
[354] H. Jeong, J. Heo, J. Kyoung, C.W. Baik, S. Park, S.W. Hwang, et al., ECS J. Solid State Sci. Technol. 4 (2015) N131–N136.
[355] Z. Pei, H.C. Lai, J.Y. Wang, W.H. Chiang, C.H. Chen, IEEE Electron Device L. 36 (2015) 44–46.
[356] H. Zhu, A. Liu, F. Shan, W. Yang, W. Zhang, D. Li, et al., Carbon 100 (2016) 201–207.
[357] Y.F. Wang, X. Wang, X.F. Li, D.J. Li, Y.W. Sun, X.X. Zhang, Electrochim. Acta. 182 (2015) 1107–1111.
[358] X.Q. Shi, X.H. Liu, H.B. Zeng, Mater. Res. Bull. 96 (2017) 458–462.
[359] W.Y. Kong, G.A. Wu, K.Y. Wang, T.F. Zhang, Y.F. Zou, D.D. Wang, et al., Adv. Mater. 28 (2016) 10725–10731.
[360] M. Ai, D. Guo, Y. Qu, W. Cui, Z. Wu, P. Li, et al., J. Alloys Compd. 692 (2017) 634–638.
[361] M. Buscema, J.O. Island, D.J. Groenendijk, S.I. Blanter, G.A. Steele, H.S.J. van der Zant, et al., Chem. Soc. Rev. 44 (2015) 3691–3718.
[362] M. Chhowalla, H.S. Shin, G. Eda, L.J. Li, K.P. Loh, H. Zhang, Nat. Chem. 5 (2013) 263–275.
[363] J.N. Coleman, M. Lotya, A. O'Neill, S.D. Bergin, P.J. King, U. Khan, et al., Science 331 (2011) 568–571.
[364] Y. Shi, H. Li, L.J. Li, Chem. Soc. Rev. 44 (2015) 2744–2756.
[365] B. Radisavljevic, A. Radenovic, J. Brivio, V. Giacometti, A. Kis, Nat. Nanotechnol. 6 (2011) 147–150.
[366] K.F. Mak, K. He, C. Lee, G.H. Lee, J. Hone, T.F. Heinz, et al., Nat. Mater. 12 (2012) 207–211.
[367] L. Britnell, R.M. Ribeiro, A. Eckmann, R. Jalil, B.D. Belle, A. Mishchenko, et al., Science 340 (2013) 1311–1314.
[368] M. Bernardi, M. Palummo, J.C. Grossman, Nano Lett. 13 (2013) 3664–3670.
[369] M. Shanmugam, R. Jacobs-Gedrim, E.S. Song, B. Yu, Nanoscale 6 (2014) 12682–12689.
[370] Y.B. Wu, W. Yang, T.B. Wang, X.H. Deng, J.T. Liu,Sci. Rep. 6 (2016), 20955.
[371] G.W. Mudd, S.A. Svatek, L. Hague, O. Makarovsky, Z.R. Kudrynskyi, C.J. Mellor, et al., Adv. Mater. 27 (2015) 3760–3766.
[372] H. Tan, Y. Fan, Y. Zhou, Q. Chen, W. Xu, J.H. Warner, ACS Nano 10 (2016) 7866–7873.
[373] F. Wang, L. Yin, Z. Wang, K. Xu, F. Wang, T.A. Shifa, et al.,Appl. Phys. Lett. 109 (2016), 193111.
[374] W. Zhang, C.P. Chuu, J.K. Huang, C.H. Chen, M.L. Tsai, Y.H. Chang, et al.,Sci. Rep. 4 (2014), 3826.
[375] H. Xu, J. Wu, Q. Feng, N. Mao, C. Wang, J. Zhang, Small 10 (2014) 2300–2306.
[376] D. Ma, J. Shi, Q. Ji, K. Chen, J. Yin, Y. Lin, Y. Zhang, et al., Nano Res. 8 (2015) 3662–3672.
[377] X. Li, J. Wu, N. Mao, J. Zhang, Z. Lei, Z. Liu, et al., Carbon 92 (2015) 126–132.
[378] W.Z. Yu, S.J. Li, Y.P. Zhang, W.L. Ma, T. Sun, J. Yuan, et al.,Small (2017), 1700268.
[379] Z. Chen, J. Biscaras, A. Shukla, Nanoscale 7 (2015) 5981–5986.
[380] R. Lu, J. Liu, H. Luo, V. Chikan, J.Z. Wu,Sci. Rep. 6 (2016), 19161.
[381] H. Qiao, J. Yuan, Z. Xu, C. Chen, S. Lin, Y. Wang, et al., ACS Nano 9 (2015) 1886–1894.
[382] J.C. Song, J. Yuan, F. Xia, J.Y. Liu, Y.P. Zhang, Y.L. Zhong, et al.,Adv. Electron. Mater. 2 (2016), 1600077.
[383] S.K. Lai, C. Xie, K.S. Teng, Y. Li, F. Tan, F. Yan, et al., Adv. Opt. Mater. 4 (2016) 555–561.
[384] W.J. Yu, Y. Liu, H. Zhou, A. Yin, Z. Li, Y. Huang, et al., Nat. Nanotechnol. 8 (2013) 952–958.
[385] M. Massicotte, P. Schmidt, F. Vialla, K.G. Schädler, A. Reserbat-Plantey, K. Watanabe, et al., Nat. Nanotechnol. 11 (2015) 42–46.
[386] K. Zhang, X. Fang, Y. Wang, Y. Wan, Q. Song, W. Zhai, et al., ACS Appl. Mater. Interf. 9 (2017) 5392–5398.
[387] P. Vabbina, N. Choudhary, A.A. Chowdhury, R. Sinha, M. Karabiyik, S. Das, et al., ACS Appl. Mater. Interf. 7 (2015) 15206–15213.
[388] H. Jeong, H.M. Oh, S. Bang, H.J. Jeong, S.J. An, G.H. Han, et al., Nano Lett. 16 (2016) 1858–1862.
[389] M. Kuiri, B. Chakraborty, A. Paul, S. Das, A.K. Sood, A. Das,Appl. Phys. Lett. 108 (2016), 63506.
[390] A. Gao, E. Liu, M. Long, W. Zhou, Y. Wang, T. Xia, et al.,Appl. Phys. Lett. 108 (2016), 223501.
[391] S. Wi, M. Chen, H. Nam, A.C. Liu, E. Meyhofer, X. Liang,Appl. Phys. Lett. 104 (2014), 232103.
[392] M. Long, E. Liu, P. Wang, A. Gao, H. Xia, W. Luo, et al., Nano Lett. 16 (2016) 2254–2259.
[393] K.J. Baeg, M. Binda, D. Natali, M. Caironi, Y.Y. Noh, Adv. Mater. 25 (2013) 4267–4295.
[394] R.D. Jansen-van Vuuren, A. Armin, A.K. Pandey, P.L. Burn, P. Meredith, Adv. Mater. (2016) 4766–4802.
[395] W.C. Tan, W.H. Shih, Y.F. Chen, Adv. Funct. Mater. 24 (2014) 6818–6825.
[396] E.H. Huisman, A.G. Shulga, P.J. Zomer, N. Tombros, D. Bartesaghi, S.Z. Bisri, et al., ACS Appl. Mater. Interf. 7 (2015) 11083–11088.

[397] Y. Lee, S.H. Yu, J. Jeon, H. Kim, J.Y. Lee, H. Kim, et al., Carbon 88 (2015) 165–172.
[398] S.J. Kim, W. Song, S. Kim, M.A. Kang, S. Myung, S.S. Lee, et al.,Nanotechnology 27 (2016), 75709.
[399] S. Jang, E. Hwang, Y. Lee, S. Lee, J.H. Cho, Nano Lett. 15 (2015) 2542–2547.
[400] X. Liu, X. Luo, H. Nan, H. Guo, P. Wang, L. Zhang, et al., Adv. Mater. 28 (2016) 5200–5205.
[401] Z. Liu, K. Parvez, R. Li, R. Dong, X. Feng, K. Müllen, Adv. Mater. 27 (2015) 669–675.
[402] M. Liu, M.B. Johnston, H.J. Snaith, Nature 501 (2013) 395–398.
[403] C. Xie, P. You, Z. Liu, L. Li, F. Yan,Light Sci. Appl. 6 (2017), e17023.
[404] N. Wang, L. Cheng, R. Ge, S. Zhang, Y. Miao, W. Zou, et al., Nat. Photonics 10 (2016) 699–704.
[405] H. Zhu, Y. Fu, F. Meng, X. Wu, Z. Gong, Q. Ding, et al., Nat. Mater. 14 (2015) 636–642.
[406] Z.H. Bakr, Q. Wali, A. Fakharuddin, L. Schmidt-Mende, T.M. Brown, R. Jose, Nano Energy 34 (2017) 271–305.
[407] Y. Zhao, K. Zhu, Chem. Soc. Rev. 45 (2016) 655–689.
[408] Q. Chen, N. De Marco, Y. Yang, T. Bin Song, C.C. Chen, H. Zhao, et al., Nano Today 10 (2015) 355–396.
[409] B. Saparov, D.B. Mitzi, Chem. Rev. 116 (2016) 4558–4596.
[410] Y. Lee, J. Kwon, E. Hwang, C.H. Ra, W.J. Yoo, J.H. Ahn, et al., Adv. Mater. 27 (2015) 41–46.
[411] V.Q. Dang, G.S. Han, T.Q. Trung, L.T. Duy, Y.U. Jin, B.U. Hwang, et al., Carbon 105 (2016) 353–361.
[412] Z. Sun, L. Aigouy, Z. Chen, Nanoscale 8 (2016) 7377–7383.
[413] P.H. Chang, S.Y. Liu, Y.B. Lan, Y.C. Tsai, X.Q. You, C.S. Li, et al.,Sci. Rep. 7 (2017), 46281.
[414] C. Xie, F. Yan, ACS Appl. Mater. Interf. 9 (2017) 1569–1576.
[415] M. Spina, M. Lehmann, B. Náfrádi, L. Bernard, E. Bonvin, R. Gaál, et al., Small 11 (2015) 4824–4828.
[416] Y. Wang, Y. Zhang, Y. Lu, W. Xu, H. Mu, C. Chen, et al., Adv. Opt. Mater. 3 (2015) 1389–1396.
[417] D.H. Kwak, D.H. Lim, H.S. Ra, P. Ramasamy, J.S. Lee, RSC Adv. 6 (2016) 65252–65256.
[418] Z. Sun, Z. Liu, J. Li, G. Tai, S.P. Lau, F. Yan, Adv. Mater. 24 (2012) 5878–5883.
[419] X. Hu, X. Zhang, L. Liang, J. Bao, S. Li, W. Yang, et al., Adv. Funct. Mater. 24 (2014) 7373–7380.
[420] L. Qian, Y. Sun, M. Wu, D. Xie, L. Ding, G. Shi,Adv. Mater. 29 (2017), 1606175.
[421] Z. Tan, Y. Wu, H. Hong, J. Yin, J. Zhang, L. Lin, et al., J. Am. Chem. Soc. 138 (2016) 16612–16615.
[422] H.C. Cheng, G. Wang, D. Li, Q. He, A. Yin, Y. Liu, et al., Nano Lett. 16 (2016) 367–373.
[423] D. Zhang, L. Gan, Y. Cao, Q. Wang, L. Qi, X. Guo, Adv. Mater. 24 (2012) 2715–2720.
[424] Y. Zhang, M. Cao, X. Song, J. Wang, Y. Che, H. Dai, X. Ding, et al., J. Phys. Chem. C 119 (2015) 21739–21743.
[425] S.Y. Chen, Y.Y. Lu, F.Y. Shih, P.H. Ho, Y.F. Chen, C.W. Chen, et al., Carbon 63 (2013) 23–29.
[426] X. Liu, E.K. Lee, J.H. Oh, Small 10 (2014) 3700–3706.

Chao Xie obtained his B.S. and Ph.D. degrees from Hefei University of Technology in 2009 and 2014, respectively. He then worked as a postdoctoral research fellow at The Hong Kong Polytechnic University and Hanyang University, respectively, for the subsequent three years. He is currently an associate professor at School of Electronic Science and Applied Physics, Hefei University of Technology. He is the author or co-author of nearly 40 papers in peer reviewed journals with a total citation over 1000 and an h-index of 19. His research interests mainly focus on the fabrication and development of high-performance electronic/optoelectronic devices based on novel functional materials, including 1D nanostructures, graphene, other 2D materials and perovskite materials, etc.

Yi Wang received his B.S. degree in Electronics and Communication Engineering in 2015 from Hefei Normal University. He is currently a master student under the tutelage of Prof. Linbao Luo at Hefei University of Technology. His research interests focus on fabrication of high-performance optoelectronic devices based on perovskite and fluorinated graphene.

Zhi-Xiang Zhang was born in Wuhu, Anhui, China in 1994, and received his B.S. degree in Microelectronics from Hefei University of Technology. He is currently a doctoral candidate under the supervision of Prof. Linbao Luo at Hefei University of Technology. His research interests include preparation of low-dimensional semiconductor nanostructures, two dimensional materials and their optoelectronic device applications.

Di Wang is currently a graduate student under the supervision of Prof. Linbao Luo in School of Electronic Science and Applied Physics, Hefei University of Technology. He received his B.S. degree in Electronic Science and Technology from Weifang University in 2015. His research interests focus on the synthesis and optoelectronic device applications of two-dimensional nanostructures.

Lin-Bao Luo received M.Sc in inorganic chemistry at Department at Chemistry, University of Science and Technology of China under the supervision of Prof. Shu-Hong Yu in 2006, and Ph. D. Degree from Department of Physics and Materials Sciences, City University of Hong Kong under the guidance of Prof. Shuit-Tong Lee in 2009. After spending one and half years at the same group as a research associate, he joined the School of Electronic Sciences and Applied Physics, Hefei University of Technology, where he is now a full professor of applied physics. He has published more than 100 peer referred journals (e.g. Adv. Mater. Laser & Photonics Rev., Opt. Express, ACS Nano etc), with a total citation of 3300 and an h-index of 29. His research interest mainly focuses on controlled fabrication of graphene and low-dimensional semiconductor nanostructures for high-performance optoelectronic and electronic devices application including photodetectors, photovoltaic devices, and non-volatile memory devices etc.